Ultra-Wideband Antenna in Coplanar Technology

by

Hung-Jui Lam
B.Eng., University of Victoria, 2005

A Thesis Submitted in Partial Fulfillment of the
Requirements for the Degree of

MASTER OF APPLIED SCIENCE

In the Department of Electrical and Computer Engineering

Ultra-Wideband Antenna in Coplanar Technology

by

Hung-Jui Lam
B.Eng., University of Victoria, 2005

Supervisory Committee

Dr. Jens Bornemann

Supervisor, Department of Electrical and Computer Engineering

Dr. Thomas E. Darcie

Departmental Member, Department of Electrical and Computer Engineering

Dr. Edward J. Park

Outside Member, Department of Mechanical Engineering

Dr. Zuomin Dong

External Examiner, Department of Mechanical Engineering

ABSTRACT

Ultra-wideband (UWB) antennas are one of the most important elements for UWB systems. With the release of the 3.1 - 10.6 GHz band, applications for short-range and high-bandwidth handheld devices are primary research areas in UWB systems. Therefore, the realization of UWB antennas in printed-circuit technologies within relatively small substrate areas is of primary importance.

This thesis focuses on the design of a new UWB antenna based on coplanar technology. Compared with microstrip circuitry, coplanar technology achieves easier fabrication and wider antenna bandwidth. Two professional full-wave field solver software packages, HFSS and MEFiSTo-3D, are used as analysis tools to obtain antenna performances.

A new printed-circuit antenna in coplanar technology for UWB systems is introduced. The frequency of operation is 3.1 GHz to 10.6 GHz with a VSWR < 2. Nearly omni-directional characteristics in vertical polarization are demonstrated at selected frequencies. Relatively good group delay characteristics are obtained and compare well with other published UWB antenna designs.

Table of Contents

List of Tables

List of Figures

Acknowledgments

I would like to express my sincere thanks and deepest gratitude to all of the people who have helped me to complete this thesis.

I wish to express my gratitude to my supervisor, Prof. Jens Bornemann, for his tireless guidance, support and thoughtful advice throughout these years. I am grateful for his assistant through out the revisions and reviews of the thesis.

I would like to thank Dr. Huilian Du for her help on modeling of the proposed UWB antenna under the MEFiSTo-3D simulating environment. My sincere thanks go to Ms. Yingying Lu for her simulation results on the planar triangular monopole antenna using MEFiSTo-3D. I would also like to thank Mr. Ian Wood for using CST Microwave Studio to perform some result confirmations on the planar triangular monopole antenna. Many thanks go to my friends for their help and support.

Last, but not least, my heartfelt appreciation goes to my family and my girlfriend for their love, understanding and encouragement throughout my research.

Dedication

To my mother, father, sister and girlfriend

1.0 Introduction

The rapid development of components and systems for future ultra-wideband (UWB) technology has significantly increased measurement efforts within the electromagnetic compatibility community. Therefore, frequency- and time-domain testing capability for UWB compliance is at the forefront of research and development in this area, e.g. [1] - [4]. Within such testing systems, the UWB antenna is a specific component whose transmitting and receiving properties differ from those for conventional narrowband operation. Several antennas have been developed. For localized equipment as, e.g., in chamber measurement setups, TEM horns can be used [1], [5]. For mobile testing, though, printed-circuit antennas are more appropriate.

Also, with the release of the 3.1 - 10.6 GHz band for ultra-wideband (UWB) operation, a variety of typical UWB applications evolved; examples are indoor/outdoor communication systems, ground-penetrating and vehicular radars, wall and through-wall imaging, medical imaging and surveillance, e.g. [6], [7]. Many future systems will utilize handheld devices for such short-range and high bandwidth applications. Therefore, the realization of UWB antennas in printed-circuit technologies within relatively small substrate areas is of primary importance. And a number of such antennas with either

microstrip, e.g. [8] - [18] or coplanar waveguide feeds, e.g. [19] - [33], and in combined technologies, e.g. [34] - [36], have been presented recently, mostly for the 3.1 - 10.6 GHz band, but also for higher frequency ranges, e.g. [37] and lower frequency ranges, e.g. [38].

1.1 Purpose of Thesis

Coplanar technology offers a number of advantages for the fabrication of printed-circuit UWB antennas. With microstrip technology applied to those planar UWB antennas, fabrication on both sides of the substrate is required. However, by applying coplanar technology, easier fabrication and wider antenna bandwidth can be achieved. By introducing the stepped configuration in the design, multiple field interactions can be produced, thus improving the antenna bandwidth. This method follows principles similar to those outlined in [37].

The purpose of this thesis is the design of a planar UWB antenna in coplanar technology and using commercially available electromagnetic field solvers. During the design process, the finite-element full-field solver software HFSS® is used for analysis purposes and for fine optimization with respect to the voltage-standing wave ratio

(VSWR) and radiation pattern performances. To validate the obtained results, simulations with HFSS are compared with existing measurements of another UWB antenna. It is found that the simulated and measured results agree well. A different professional software, which is a time-domain field solver, MEFiSTo-3D®, is used to simulate VSWR performances, amplitude responses and group delay characteristics over a wide frequency range.

1.2 Organization of Thesis

Chapter 2 of the thesis provides an overview over UWB concepts and is mainly a summary taken from related publications. Each sub-section of Chapter 2 contains information largely based on one or two references. The basic content is very similar to such references, with changes only in wordings and phrases. Chapter 2 discusses history and fundamentals of UWB technology. It is provided as background information and follows a few well written papers on exactly this topic.

Chapter 3 of the thesis gives a brief introduction to printed-circuit-board (PCB) UWB antennas. Different design parameters of UWB antennas are also discussed. Different examples of existing microstrip and coplanar-waveguide (CPW) UWB antennas

from several published designs are illustrated. Comparisons based on different design parameters of those UWB antenna examples are discussed.

Chapter 4 of the thesis presents a new printed-circuit UWB antenna design in CPW technology. The first part talks about the process and transitions between the initial and final design stages. Next, simulated results of different design parameters from both HFSS and MEFiSTo-3D are presented. Simulation models and settings from both softwares are illustrated and explained. Also, the method used to obtain the group delay characteristics in MEFiSTo-3D is introduced and performed. The size of the absorbing boundary for the simulation model in MEFiSTo-3D is limited by the available computer memory (RAM – Random Access Memory). This setup parameter has great effect on the group delay result. Finally, an improved design of the proposed UWB antenna is presented and its performance parameters illustrated.

The last section (Chapter 5) summarizes the most important accomplishments throughout the thesis. Some future works such as a dual-polarization omni-directional UWB antenna in CPW technology and UWB antennas with notch characteristics are also briefly discussed here.

1.3 Contributions

The contributions of this research are twofold:

First, a new printed-circuit UWB antenna in coplanar technology is presented and its performance demonstrated to be superior to other designs published so far. Moreover, an improved version is presented which uses smaller slots in the coplanar feed, but increases the computational resources required for its reliable analysis.

Secondly, a stepped rather than a continuous metallization profile is introduced in order to reduce the size of the printed-circuit area. Moreover, this profile is quasi-conical in shape which provides a better impedance match over a wide bandwidth.

Thirdly, a method for the group delay computation of UWB antennas is presented. It is based on time-domain analysis and has not been used before in connection with electromagnetic field solvers.

2.0 Fundamentals of Ultra-Wideband Technology

2.1 General Overview

Consider the term "ultra wideband" (UWB) as a relatively new term to describe a technology, which had been known since the early 1960's. The old definition was referring to "carrier-free", "baseband", or "impulse" technology. The fundamental concept is to develop, transmit and receive an extremely short duration burst of radio frequency (RF) energy, like a short pulse. The pulse typically has a duration of a few tens of picoseconds to a few nanoseconds. These pulses represent one to only a few cycles of an RF carrier wave; therefore, as for resultant waveforms, extremely broadband signals can be achieved. Often it is difficult to determine the actual RF center frequency for an extremely short pulse; thus, the term "carrier-free" comes in [39]. The amount of power transmitted is a few milliwatts, which, when coupled with the spectral spread, produces very low spectral power densities. The Federal Communication Commission (FCC) specifies that between 3.1 and 10.6 GHz, the emission limits should be less than -41.3 dBm/MHz, or 75 nW/MHz. The total power between these limits is a mere 0.5 mW. These spectral power densities reside well below a receiver noise level [40]. Typical UWB signals, which cover significant frequency spectra, are presented in [41].

Advantages of UWB technology are listed as:

1) UWB waveforms have large bandwidths due to their short time pulse duration. For example, as in communication technology, like in multi-user network applications, extremely high data rate performance can be provided by UWB pulses. As for radar applications, very fine range resolution and precision distance and/or positioning measurement capabilities can be achieved by those same pulses [39].

2) Short duration waveforms have relatively good immunity to multi-path cancellation effects as observed in mobile and in-building environments. Multi-path cancellation is the effect happening when a strong reflected wave (e.g., off of a wall, ceiling, vehicle, or building, etc.) cancels the direct path signal. The reflected wave arrives partially or totally out of phase with respect to the direct path signal, thus causing a reduced amplitude response in the receiver. Due to the very short pulse property of the UWB signal, no cancellation will occur because the direct path signal has passed before the reflected path signal arrives. Therefore, high-speed, mobile wireless applications are particularly well suited for UWB system implementation [39].

3) Extremely short pulse duration in the time domain is equivalent to extremely large

bandwidth in the frequency domain. Due to the large bandwidth, energy densities (i.e., transmitted Watts of power per Hertz of bandwidth) can be quite low. This low energy density can be translated into a low probability of detection (LPD) RF signature. An LPD signature is particularly useful for military applications (e.g., for covert communications and radar). Also, a LPD signature generates minimal interference to proximity systems and minimal RF health hazards. The UWB signal is noise-like due to its low energy density and the pseudo-random (PR) characteristics of the transmitted signal. This feature might enable the UWB system to avoid interference to existing radio systems, one of the most important topics in UWB research. Those characteristics are very significant for both military and commercial applications [39], [42].

4) Low system complexity and low cost are the most important advantages of UWB technology. Those advantages arise from the essentially baseband nature of the signal transmission. Compared with conventional radio systems, short time domain pulses are able to propagate without the need for an additional RF mixing stage, which means less complexity in the system design. Also, UWB systems can be made nearly "all-digital", with minimal RF or microwave electronics, thus, low cost [39], [42].

Engineering is all about tradeoffs; no single technology is good for everything. There are always solutions that may be better suited to some applications than others. For example, in point-to-point or point-to-multipoint applications with extremely high data rate (10 Gigabits/second and higher) applications, UWB systems cannot compete with high capacity optical fiber or optical wireless communications systems. However, the high cost associated with optical fiber installation and the property of an optical wireless signal not able to penetrate a wall limit the applicability of optically based systems for in-home or in-building applications. Also, optical wireless systems will need an extremely precise pointing alignment, which make optical wireless systems not suitable for mobile environments. The dispersive Light-Emitting-Diode (LED) optical wireless communication systems will not need the extremely precise pointing alignment; thus, in-room high-data-rate based systems are achievable, but not in mobile environments [39].

2.2 Development of Ultra-Wideband Technology and Antennas

2.2.1 History

Staring in 1962, the transient characteristics of a certain class of microwave networks

could be fully described through their characteristic impulse response. At this point in time, ultra wideband (UWB) technology branches out from the field of time-domain electromagnetics [43], [44]. Conventionally, to characterize a linear, time-invariant (LTI) system, a full frequency sweep of magnitude and phase response is required. However, an LTI system can also be fully described by a different method, the so-called *impulse response* h(t). This method takes the output response of a LTI system with respect to an impulsive excitation. With the use of a convolution integral, the output response, y(t), of the LTI system can be uniquely resolved from any arbitrary input, x(t). The convolution integral of the LTI system is written as:

$$y(t) = \int_{-\infty}^{\infty} h(u)x(t-u)du \tag{2.1}$$

With the invention of the sampling oscilloscope (Hewlett-Packard, ca.1962) and pulse generation techniques of sub-nanosecond (baseband) pulses, an appropriate simulation of an impulse excitation could be generated. Thus, the impulse response of microwave networks could be examined and measured [43].

The design of wideband and radiating antenna elements was implemented using the

impulse response method [45]. The same method could be used to design short pulse radar and communication system. Different radar and communication applications were implemented using the impulse response method used by Ross at the Sperry Research Center of Sperry Rand Corporation [46]. In the year of 1972, Robbins developed a sensitive and short pulse receiver, which takes the place of the bulky time-domain sampling oscilloscope. With this new type of receiver, the development of UWB systems was rapidly increased. By the year of 1973, the first UWB communication patent was awarded to Sperry Rand Corporation [43]. The approach was first called the baseband, the carrier-free or the impulse technology in the late 1980's. Not until approximately 1989, the U.S. Department of Defense assigned a new name called "ultra wideband". With nearly 30 years, wide-ranging developments of UWB theory, techniques and hardware designs were implemented. Based on fields of UWB pulse generation and reception methods, and applications such as communications, radar, automobile collision avoidance, positioning systems, liquid level sensing and altimetry, Sperry Rand Corporation had been awarded with more than 50 patents by the year of 1989 [43].

Before 1994, many developments in the UWB area, mainly related to impulse communications, were restricted by the U.S. Government. By the year 1994, the

technology of UWB had rapidly developed due to extensive research carried out without government restriction [43].

2.2.2 History of Ultra-Wideband Antennas

The original “spark-gap” transmitter, which broke new grounds in radio technology, was starting UWB technology. The design was not first realized as UWB technology, but then later dug up by investigators. Also, even some of the ideas, which start out as designs for narrowband frequency radio, reveal some of the first concepts of UWB antennas. The concept of “syntony”, i.e. the received signal can be maximized when both transmitter and receiver are tuned to the same frequency, was presented by Oliver Lodge in 1898 [47]. With his new concept, Lodge developed many different types of “capacity areas,” or so called antennas. Those antenna designs include spherical dipoles, square plate dipoles, bi-conical dipoles, and triangular or “bow-tie” dipoles. The concept of using the earth as a ground for monopole antennas was also introduced by Lodge [47]. In fact, Lodge’s design drawing of triangular or bow-tie elements reproduced in Fig. 2.2.1 clearly shows Lodge’s preference for embodied designs. Bi-conical antennas designed by Lodge and shown in Fig. 2.2.2 are obviously used as transmit and receive links [47].

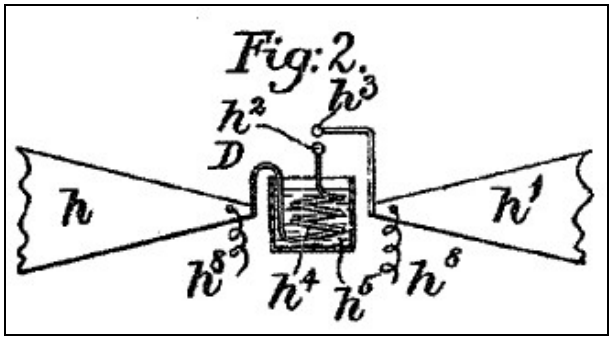

Fig. 2.2.1: Lodge's preferred antennas consisting of triangular "capacity areas," a clear precursor to the "bow tie" antenna (1898) (from [47]).

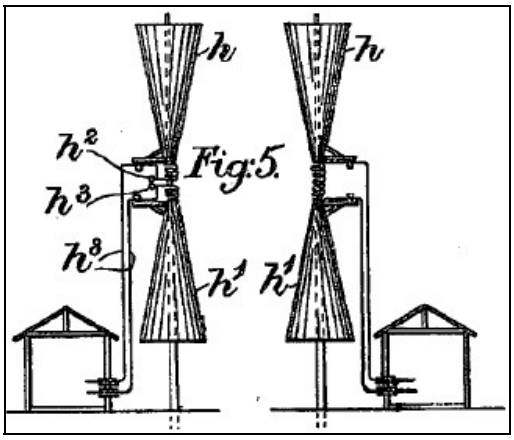

Fig. 2.2.2: Lodge's bi-conical antennas (1898) (from [47]).

Due to demands of increased frequency band and shorter waves, a "thin-wire" quarterwave antenna dominated the market with its economic advantages over the better performance of Lodge's original designs. Especially, for television antennas, much interest was focused on the ability of handling wider bandwidths due to increased video signals. In 1939, the bi-conical antenna (Fig. 2.2.3) and the conical monopole (Fig. 2.2.4) were reinvented by Carter to create wideband antennas. By adding a tapered feeding structure, Carter advanced Lodge's original designs, Fig. 2.2.5. Also, Carter was one of the first who considered adding a broadband transition as the feeding structure for a broadband antenna. This was one of the key steps towards the design of broadband antennas [47].

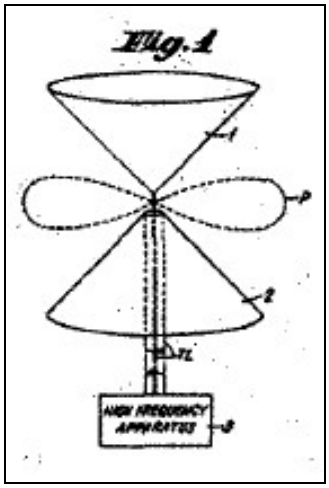

Fig. 2.2.3: Carter's bi-conical antenna (1939) (from [47]).

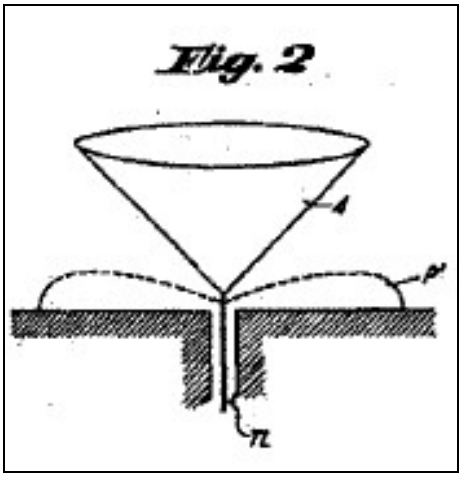

Fig. 2.2.4: Carter's conical monopole (1939) (from [47]).

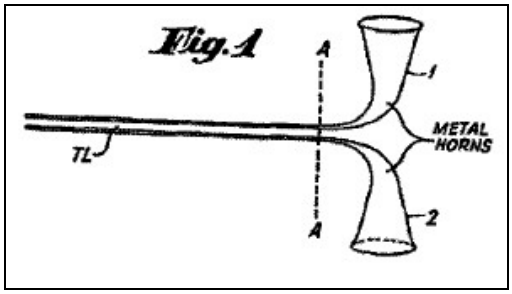

Fig. 2.2.5: Carter's improved match bi-conical antenna (1939) (from [47]).

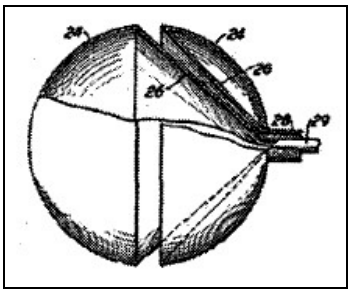

Fig. 2.2.6: Schelkunoff's spherical dipole (1940) (from [47]).

In 1940, a spherical dipole antenna combined with conical waveguides and feeding structures was presented by Schelkunoff (Fig. 2.2.6). However, his design of a spherical dipole antenna was not very useful. At that time, the most well-known UWB antenna was the coaxial horn element proposed by Lindenblad [47]. In order to make the antenna more broadband, Lindenblad took the design of a sleeve dipole element and introduced a continued impedance change. In the year of 1941, Lindenblad's elements (Fig. 2.2.7)

were used by RCA for experiments in television transmission. With the vision of broadcasting multiple channels from a single central station, the need of a wideband antenna was necessary for RCA. On the top of the Empire State Building in New York City, a turnstile array of Lindenblad's coaxial horn elements as an experimental television transmitter were placed by RCA for several years. A patent drawing of the array is shown in Fig. 2.2.8. At the top of the antenna, folded dipoles are used to carry the audio part of the television signal [47].

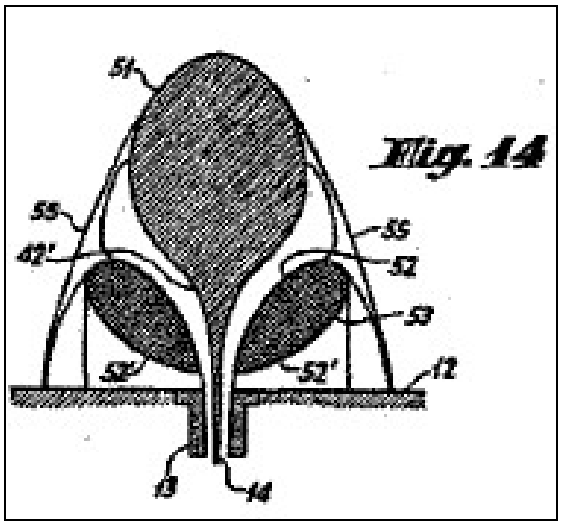

Fig. 2.2.7: Lindenblad's element in cross-section (1941) (from [47]).

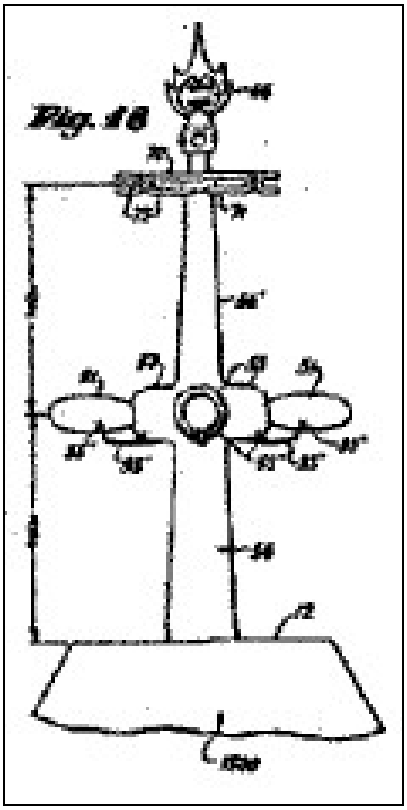

Fig. 2.2.8: A turnstile array of Lindenbald elements for television transmission (1941) (from [47]).

A similar type of Lindenblad's coaxial horn element design, called "volcano smoke antenna" and designed by Kraus, was also presented at that time [48]. Lindenblad's coaxial element played a significant roll as the cornerstone of television development. During that period, coaxial transitions became one of the design techniques for other antenna researchers and designers. By the year of 1948, two types of coaxial horn antennas were presented by Brillouin. One of them is omni-directional (Fig. 2.2.9), and the other one is directional (Fig. 2.2.10) [47].

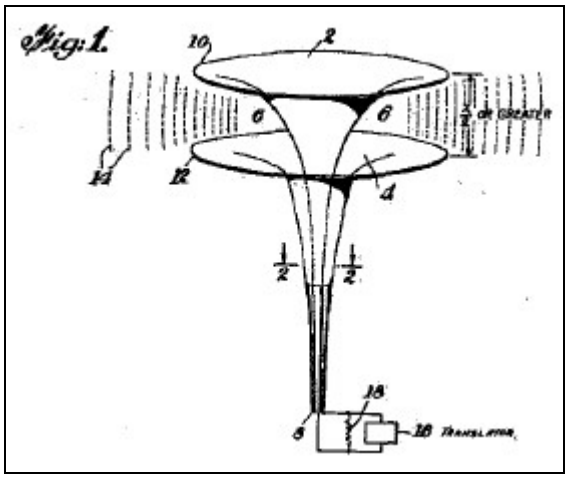

Fig. 2.2.9: Brillouin's omni-directional coaxial horn (1948) (from [47]).

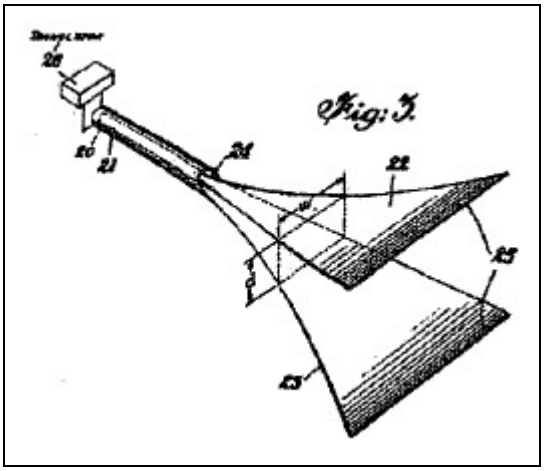

Fig. 2.2.10: Brillouin's directional coaxial horn (1948) (from [47]).

Brilliant results were offered by conventional designs, but other aspects started to grow in significance. Factors like manufacturing cost and complexity of manufacturing procedures became important considerations in the design of broadband antenna. The

well-known “bow-tie” antenna reveals those benefits. This antenna was originally suggested by Lodge and later rediscovered by Brown and Woodward. In the year of 1947, a similar type of antenna, the inverted triangular dipole, was proposed by Masters (Fig. 2.2.11). This antenna was later referred to as the “diamond antenna”. By the year of 1968, more complex electric antennas in different variety were developed. Two of those antennas were ellipsoidal monopoles and dipoles which were proposed by Stohr (Fig. 2.2.12). In Fig. 2.2.13, the broadband notch antenna is illustrated. This antenna was proposed by one of the pioneers on practical antenna design, named Lalezari. Later, a different design type of this broadband antenna with better performance was presented by Thomas. This antenna design has its advantages in terms of compact size, easier manufacturing capabilities and arrayed elements, which is the planar circular element dipole as illustrated in Fig. 2.2.14. However, better performance can be achieved by replacing the circular shaped elements with elliptical ones. Monopole antennas can also be constructed by planar elliptical elements. Beside electrical antennas, major progress on magnetic UWB antennas has also been preceded. Fig. 2.2.15 illustrates one of the magnetic UWB antennas proposed by Marié. By implementing the idea of slot antennas and varying the width of the slot line, better antenna bandwidth was achieved by Marié’s antenna [47].

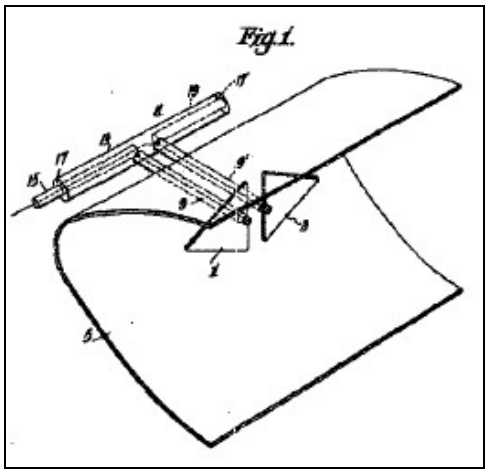

Fig. 2.2.11: Master's diamond dipole (1947) (from [47]).

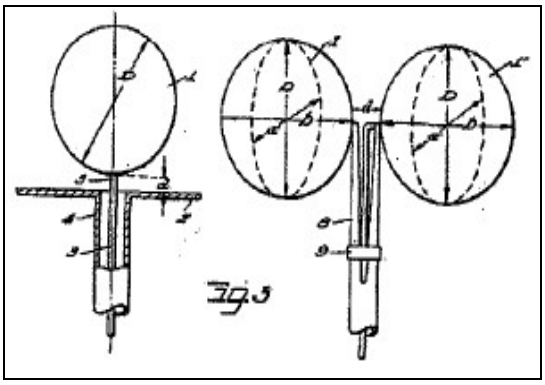

Fig. 2.2.12: (left) Stohr's ellipsoidal monopole (1968) and (right) Stohr's ellipsoidal dipole (1968) (from [47]).

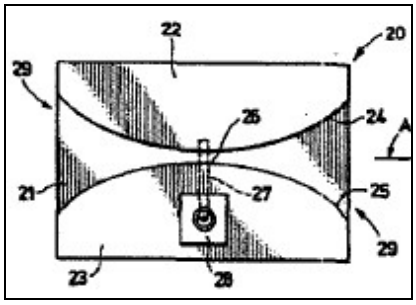

Fig. 2.2.13: Lalezari's broadband notch antenna (1989) (from [47]).

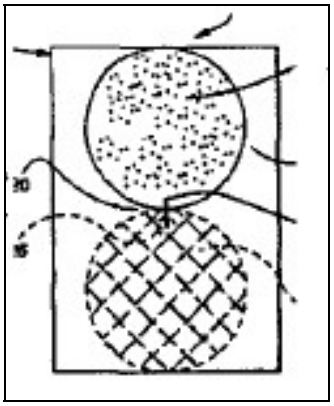

Fig. 2.2.14: Thomas's circular element dipole (1994) (from [47]).

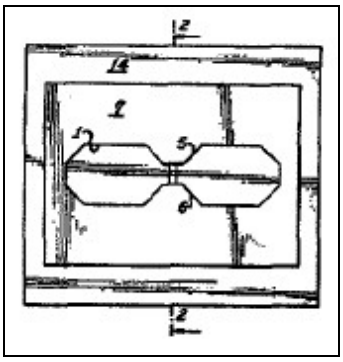

Fig. 2.2.15: Marié's wide band slot antenna (1962) (from [47]).

Another improved magnetic antenna was proposed by Harmuth as illustrated in Fig. 2.2.16. By presenting the idea of the large current radiator surface in the antenna design, the antenna performance increased. The concept of this design is to make the magnetic

antenna perform like a large current sheet. However, since both sides of the sheet radiate, a lossy ground plane was intentionally constructed to avoid any unwanted resonances and reflections. In this way, the lossy ground plane tends to cause limitations on the antenna's efficiency and performance. By the year of 2000, an innovative UWB slot antenna was proposed by Barnes, as illustrates in Fig. 2.2.17. This slot antenna maintains a continuous taper design. Therefore, with a suitable design of the slot taper, outstanding bandwidth and performance can be achieved. This UWB antenna was employed by The Time Domain Corporation as their first generation through-wall radar [47].

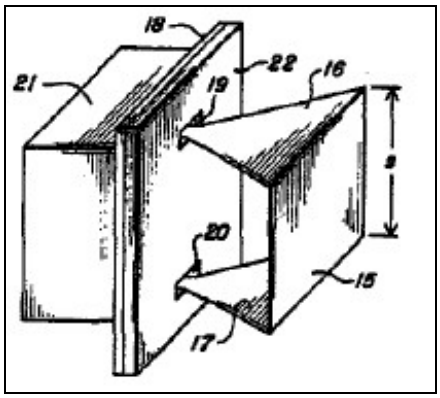

Fig. 2.2.16: Harmuth's large current radiator (1985) (from [47]).

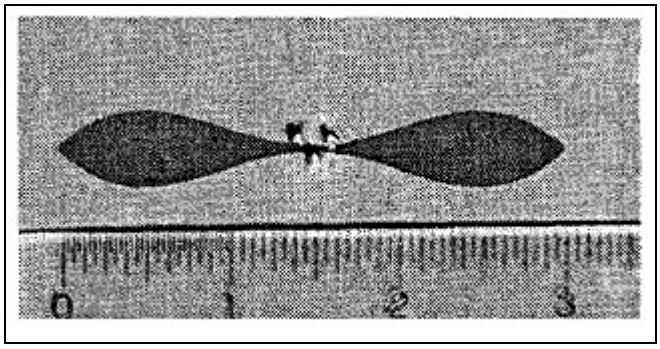

Fig. 2.2.17: Barnes's UWB slot antenna (2000) (from [47]).

2.3 Ultra-Wideband Antennas

2.3.1 Introduction to Ultra-Wideband Antennas

An antenna can be defined as a transition device that exchanges guided and radiated electromagnetic energy between transmission lines and free space. It is a device that radiates or receives radio waves. It can also be viewed as an impedance transformer between an input impedance and that of free space. A traditional radio broadcast antenna for amplitude modulation (AM) can be considered an ultra wideband antenna. The AM broadcast antenna has a fractional bandwidth of over 100 percent as the band covers a frequency range from 535 kHz to 1705 kHz. However, due to the modulation scheme, AM receivers are designed and tuned to receive individual narrowband channels of 10 kHz bandwidth. Therefore, the fractional bandwidth, over which the antenna has to operate in amplitude coherence, is only 0.6 to 1.9 percent [49].

Similar to AM broadcast antennas, traditional UWB antennas operate usually in a multi-narrowband scheme. Modern UWB antennas, however, must have abilities of transmitting and receiving a single coherent signal that covers the entire working bandwidth. A muti-band or OFDM (Orthogonal Frequency-Division Multiplexing)

modulation scheme may have its advantages over the single coherent wideband method in terms of higher dispersion tolerance over the operational bandwidth. An UWB antenna must have reliable characteristics and predicable performance over the operating band. Moreover, an UWB antenna is required to receive or transmit all required frequencies at the same time. Therefore, radiation patterns and impedance matching should be consistent across the operating bandwidth [49].

An ideal UWB antenna will have zero dispersion and a fixed phase center. Finite dispersion in real UWB antennas can be compensated if the waveform dispersion is predictable. An example of a dispersive antenna is the log-periodic antenna. The log-periodic antenna uses its small-scale parts to radiate high frequencies and its large-scale parts to radiate the low frequency range. A chirp-like and dispersive signal will be produced by this antenna. Also, along different azimuthal angles, various waveforms will be generated. A more compact and non-dispersive signal can be radiated by a planar elliptical dipole. This small element antenna radiates a Gaussian W-like waveform. Fig. 2.3.1 illustrates the time-domain behaviors of both the log-periodic antenna and the planar elliptical dipole antenna. Small element antennas are more suitable in many UWB applications because of their non-dispersive and compact characteristics

[49].

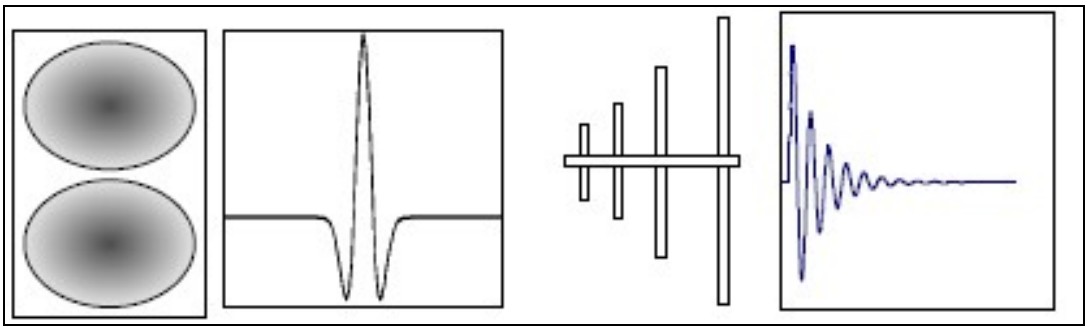

Fig. 2.3.1: A log periodic antenna (right) has a dispersive waveform, while an elliptical dipole (left) has a non-dispersive waveform (from [49]).

2.3.2 Directionality and Different Types of Antennas

Different types of antennas can be used in UWB systems. Those UWB antennas may be grouped based on their directivity being directional or non-directional. The main difference between directional and non-directional UWB antennas is that directional antennas radiate energy in preferred direction (narrow solid angle), whereas non-directional antennas radiate energy in many direction (nearly omni-directional). The directivity or the gain is defined by comparing the gain of the antenna with the isotropic model. An isotropic antenna is an ideal model which radiates energy equally in all directions (full solid angle). Therefore, an isotropic antenna is expressed in the gain of 0dBi ("dBi" means dB relative to an ideal isotropic antenna). Fig. 2.3.2 illustrates various

gain values of isotropic, dipole, and horn antennas. High gain antennas like horns or reflectors can have gain values above +10 dBi, +20 dBi, respectively. Table 2.3.1 shows a comparison between directional and omni-directional antennas based on parameters of gain, field of view, and antenna size [49].

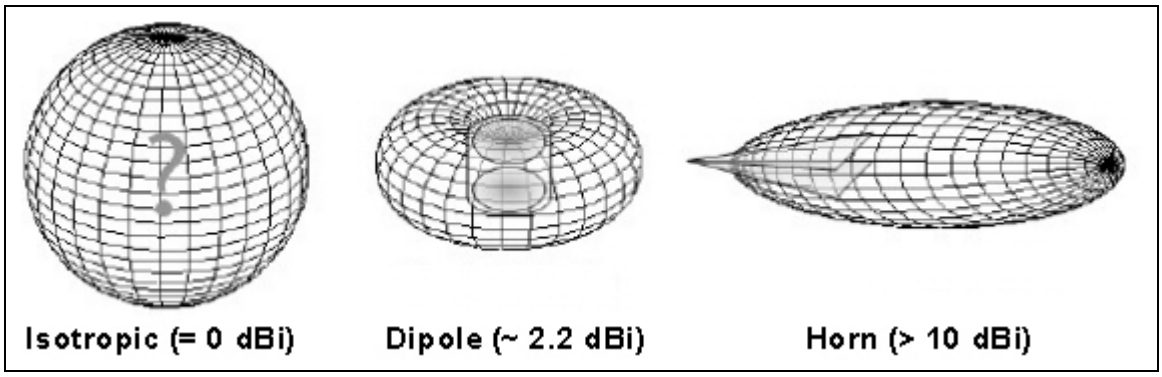

Fig. 2.3.2: An isotropic antenna (left) has a gain of 0 dBi by definition. A small dipole antenna (center) typically has a gain of about 2.2 dBi, and a horn antenna (right) may have a gain of 10 dBi or more (from [49]).

Table 2.3.1 : Trade-offs between directional and omni antennas (from [49]).

	Directional	**Omni-Directional**
Gain:	High	Low
Field of View:	Narrow	Wide
Antenna Size:	Large	Small

In order to meet the peak radiated emission limit of regulatory constraints, the transmit power of a high gain directional transmit antenna is restricted. Therefore, the link

budget is not directly affected by a high-gain transmit antenna. The only advantage of high-gain transmit antennas over low-gain transmit antennas might be lower emissions in undesired directions, which leads to less undesired signals and improved overall system performance. On the other hand, a high-gain receive antenna plays directly into the link budget. Typically, those antennas require larger size and higher tolerance of a narrower field of view [49].

Antennas can be classified as electric or magnetic types. Antennas such as dipoles and most horns, which are characterized by near-surface intense electric fields, form the group of electric antennas. In contrast, antennas with near-surface intense magnetic fields belong to the group of magnetic antennas. Typical examples are loop and slot antennas. Magnetic antennas are more suitable for embedded systems and related applications because electric antennas have a higher tendency of producing coupling effects with surrounding circuitry [49].

2.3.3 Matching and Spectral Control

To design UWB antennas, traditional narrowband methods are often used. However, modifications and adjustments are required for good designs. As the required bandwidth

increases, it becomes more difficult to design a well-matched network between the UWB antenna and the rest of the system. The purpose of a matching network is to maximize power transfer and minimize reflections [49].

To design a well-matched network for a UWB antenna, we start with a well-matched antenna. To obtain a particular impedance for an antenna, the method and the concept are well understood. A good example would be the microstrip notch antenna designed by Nester [49]. This antenna is a planar horn antenna that has smooth transitions from a microstrip to a slotline, and with continuously variable elements. Fig. 2.3.3 illustrates Nester's antenna [49].

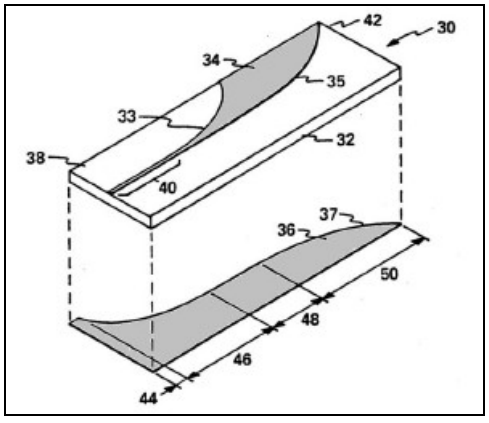

Fig. 2.3.3: The continuously tapered slot horn elements of Nester (gray colorization on elements added) (from [49]).

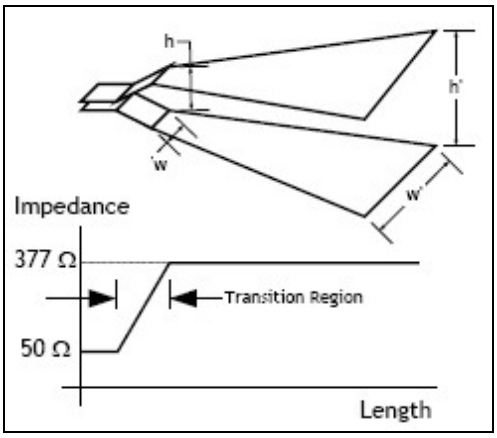

Fig. 2.3.4: A hypothetical tapered horn antenna (top) with a transition from 50 Ω to 377 Ω (bottom) (from [49]).

Complex computer algorithms are required to calculate the impedance of a slotline horn over a wide bandwidth. To demonstrate the idea, a simpler structure can be used. Consider a cross-sectional width (w) and a height (h) of a parallel-plate horn antenna. The impedance of an air gap between two plates can be approximated by (c.f. Fig. 2.3.4):

$$Z = Z_0 \frac{h}{w} \tag{2.2}$$

It is important to know that this result is only exact for $w >> 10\ h$, but it is used here to give an idea of the order of magnitudes. A 50 Ω match requires $h/w \approx 0.133$ while a 377 Ω match requires $h/w \approx 1.00$. Another example would be a hypothetical horn antenna matched to a 50 Ω feed line. The linear transition from 50 Ω to 377 Ω produces a well-matched network. Then, the long 377 Ω section is tapered to cover ultra-wideband frequencies. This antenna is illustrated in Fig. 2.3.4 [49].

Desired frequency ranges can be designed into an antenna. One of the simplest ways is to modify the scale of the same antenna. For example, across a 3:1 frequency range, a planar elliptical dipole antenna has a value of $|S_{11}|$ in the order of -20 dB. Also, the minor axis of a planar elliptical dipole antenna is approximately 0.14 λ at the lower end of the

frequency band. Therefore, the antenna with the frequency band of 1-3 GHz will have elements of approximately 1.67-inch in its minor axis. A 2-6 GHz antenna will have half the size (one fourth of the area) of the 1-3 GHz antenna with about 0.83-inch elements; and a 3-9 GHz antenna has approximately 0.56-inch elements, which will be one third the size (one ninth of the area) of the original one [49].

By applying more sophisticated methods, an UWB antenna can be made relatively insensitive to selective frequencies by using frequency notch implementations. Also, to some extent, the roll-off of he spectral rate at the edges of an operational band can be controlled. When designing an ultra-wideband system, considerations in all different angles must be taken into account. In order to make contribution to the whole system, an UWB antenna must be customized in both its impedance and frequency responses [49].

2.3.4 Directivity and System Performance

Friis Transmission Equation regulates the link characteristic of a narrowband antenna in free space. It assumes impedance-matched and polarization-matched conditions.

$$P_{RX} = P_{TX} \frac{G_{TX} G_{RX} \lambda^2}{(4\pi r)^2} = P_{TX} \frac{G_{TX} G_{RX} c^2}{(4\pi r)^2 f^2} \tag{2.3}$$

P_{RX} is the received power, P_{TX} is the transmitted power, G_{TX} is the transmit antenna gain, G_{RX} is the receive antenna gain, λ is the wavelength, f is the frequency, c is the speed of light, and r is the distance between the transmit and receive antennas. In the case of an UWB antenna, Friis Transmission Equation needs to be expressed in terms of spectral power density; power and gain will be functions of frequency:

$$dP_{RX}(f) = \frac{c^2}{(4\pi r)^2} P_{TX}(f) \frac{G_{TX}(f) G_{RX}(f)}{f^2} \tag{2.4}$$

The total received power can be obtained by taking the integration over frequency:

$$P_{RX} = \int_0^\infty dP_{RX}(f) df \tag{2.5}$$

The effective isotropic radiated power (EIRP) is:

$$EIRP(f) = P_{TX}(f) G_{TX}(f) \tag{2.6}$$

$G_{TX}(f)$ is the peak gain of the antenna in any orientation. The term *EIRP* is defined by regulatory limits. System designers intend to get the constant product of $P_{TX}(f)$ $G_{TX}(f)$ as near to the limit of 3 dB safety margin. In order for the transmit signal to fall within the limit of the permitted spectral mask, the power gain product will usually need to be reduced [49].

From equation 2.3, the path loss can be referred to as $(\lambda/4\pi r)^2$ or as $(c/(4\pi rf))^2$ variation of the signal power. The longer the distance r (the larger the $4\pi r^2$ surface area), the greater is the spread of the transmit signal, and the smaller is the signal captured by the receive antenna. In another way, the signal energy is diffused rather than lost. The $\frac{1}{f^2}$ dependence in the path loss does not suggest that signals in free space are attenuated inversely proportional to the square of the frequency. Actually, the definition of antenna gain and antenna aperture presents the $\frac{1}{f^2}$ dependence. Antenna gain $G(f)$ is defined in terms of antenna aperture $A(f)$ as:

$$G(f) = \frac{4\pi A(f)}{\lambda^2} = \frac{4\pi A(f) f^2}{c^2} \tag{2.7}$$

The antenna aperture is defined by a measure of how large a part of an incoming wave

front an antenna can capture. The antenna aperture can be also expressed as the effective area of the antenna. The antenna aperture tends to be roughly equal to the physical area of the antenna for electrically large directive antennas. As for small elements and omni-directional antennas, the antenna's physical area may actually be significantly smaller than the antenna aperture. With the ability of electromagnetic waves to couple to objects within a range of about $\lambda/2\pi$, even a thin wire or a planar antenna can still be an effective receiver or radiator of electromagnetic radiation [49].

A constant gain antenna has constant aperture in term of wavelength. For example, the aperture of a dipole antenna is approximately $0.132\,\lambda^2$. The constant gain antenna aperture decreases with $\frac{1}{f^2}$ as the frequency increases, or as λ decreases. Omni-directional antennas are typically modeled to have constant gain and pattern behavior. On the other hand, an antenna aperture, which remains fixed with frequency, is described as a constant aperture antenna. Typically, a horn antenna will have a fixed aperture. The size of the aperture in term of wavelength increases proportional to f^2, which narrows the pattern and increases the antenna gain by f^2. Typically, directive antennas reveal this characteristic [49].

Fig. 2.3.5 illustrates free space transmission behaviors of different types of transmit and receive antennas. For the link of omni to omni, both transmit and receive antennas are constant gain antennas; this results in a roll-off of $\frac{1}{f^2}$ within the band for the received power. As for the omni to directional link, the $\frac{1}{f^2}$ roll-off is canceled by the gain variation of f^2 from the constant aperture receive antenna, which yields a flat received power in the band. Depending on the receive antenna gain, the received power can be significantly larger than the omni antenna transmit power. However, this advantage is balanced out by a narrower pattern and field-of-view that comes with the increasing gain of a typical directional antenna. Due to the fact that the transmit power needs to be made to roll-off as $\frac{1}{f^2}$ in order to meet the limit of a flat *EIRP* spectral mask, a directional antenna, whose gain varies as f^2 on the transmit side of the link, does not improve the system performance [49].

One of the possible advantages of directive antennas over omni-directional antennas is that directive antennas have the ability to separate signals coming from specific directions. With this ability, angles of arrival signals can be known. Further, by implementing spatial processing techniques to incoming multi-path signal components, unwanted interfering signals can be eliminated [49].

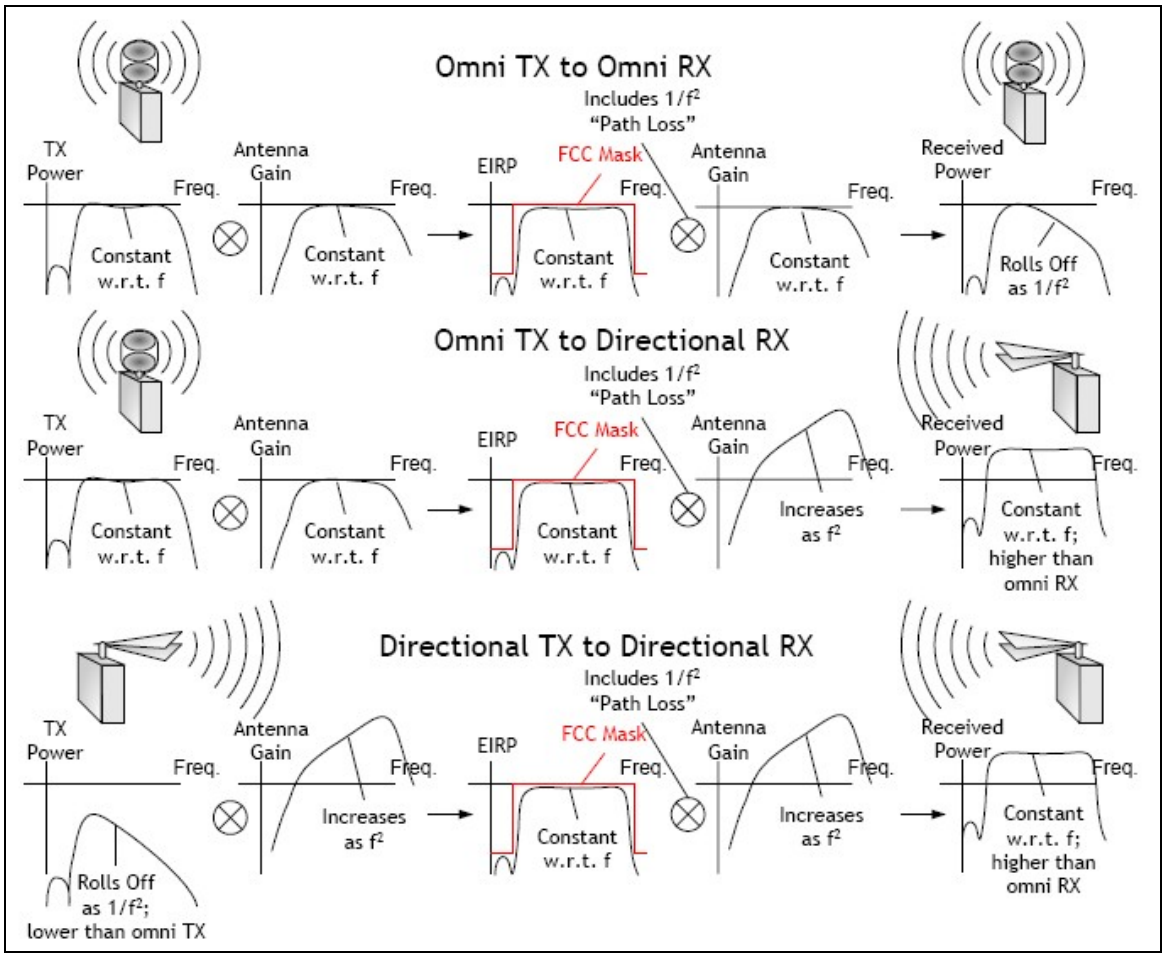

Fig. 2.3.5: The relationship between antenna directivity and link performance for an omni TX to omni RX (top), an omni TX to directional RX (middle) and a directional TX to directional RX (bottom) (from [49]).

2.3.5 Antenna Dispersion

Conventionally, gain and return loss (matching) are two fundamental parameters engineers use when evaluating antennas. Only little variation is permitted over the operating band for conventional narrowband antennas. Therefore, those parameters are assumed to be constant. For broadband antennas such as UWB antennas, however, gain

and return loss are defined as functions of frequency since they largely vary over a wide frequency range. Moreover, gain is just a scalar quantity and contains no phase information. But the performance of UWB antennas does heavily depend on their phase variation. An UWB antenna will radiate a dispersive and twisted waveform, even though the gain of the UWB antenna may appear well performed. The reason is that the phase center of an antenna varies with respect to frequency, or even moves as function of the observation angle [50].

For those systems, in which the entire operational band is utilized by a single radiated signal, or even multi-band systems, dispersion is a significant concern. Compensation is usually required for UWB systems when dispersion problems occur within the UWB antenna; even though it may be complex and costly. Conventionally, broadband characteristics can be obtained through physical geometry's variation for classical frequency independent antennas. Lower frequency parts of a signal can be produced by the larger scale portion of the antenna, and high frequency parts by the smaller portions. Frequency independent antennas will radiate dispersive waveforms, though, since the phase center varies with respect to the frequency [50].

For example, the following Fig. 2.3.6 illustrates a 1 to 11 GHz log spiral antenna. The antenna is fed at the tip of the cone where the center of the feeding coaxial line is connected. The smaller scale part of the spiral generates high frequency signals. At the base of the spiral antenna, where the larger scale part is placed, lower frequency components radiate. Fig. 2.3.7 illustrates the transmitted and the received signals of this log spiral antenna. The left side of the figure shows the transmitted impulse voltage signal detected at the feeding terminal of the transmitted antenna. The right side of the figure shows the received impulse voltage signal detected at the feeding terminal of the receiving antenna. From the received signal, the effect of dispersion is clearly revealed. Two very distinctive behaviors of the received signal expose the dispersive effect. First, the dispersive characteristic of the antenna causes the received signal to have over twice the signal length compared to the transmitted signal. Secondly, the dispersive effect is obvious from the “chirp” in the received signal waveform. Higher frequency components with narrower zero crossing time periods appear at the beginning part of the received signal. While lower frequency components with wider zero crossing time periods arrive later [50].

There is another downside from the dispersive effect, which is not clearly revealed in

Fig. 2.3.7. The received signal will change with respect to the observation angle as the phase center varies with frequency. With non-dispersive UWB antenna elements, much better system performance can be easier obtained. Therefore, the focus in recent years has been on small UWB antennas due to their many advantages over the conventional wideband antennas.

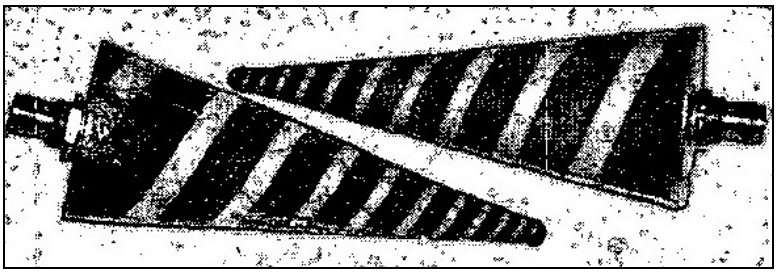

Fig. 2.3.6: Log conical spiral antennas (from [50]).

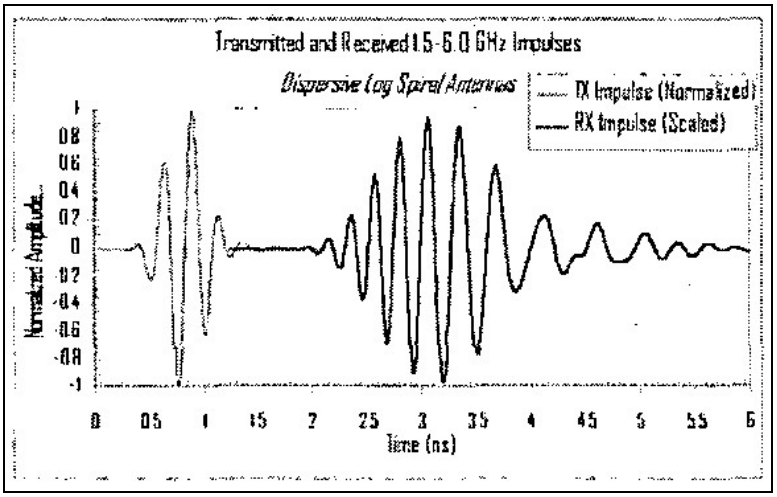

Fig. 2.3.7: Transmitted (left) and received (right) voltage waveform from a pair of conical log spiral antennas (from [50]).

Planar elliptical dipole antennas are one of the most common small element dipole antennas used. Flat dipole-like patterns and 3:1 frequency span gains are some of the featured characteristics of planar elliptical dipole antennas; also, broad bandwidths with typical return losses of 20 dB or better are obtained. Finally, non-dispersive and compact radiated waveforms will generally be produced by planar elliptical dipole antennas. A pair of identical planar elliptical dipole antennas is illustrated in Fig. 2.3.8. The planar elliptical dipole antenna has a minor axis of 3.8 cm and a major axis of 4.8 cm resulting in an axial ratio of 1.25:1.

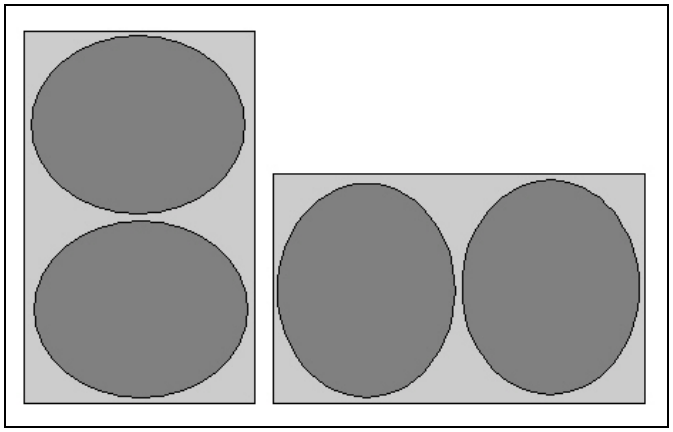

Fig. 2.3.8: 1.25:1 axial ratio planar elliptical dipoles with 4.8x3.8 cm elements [50].

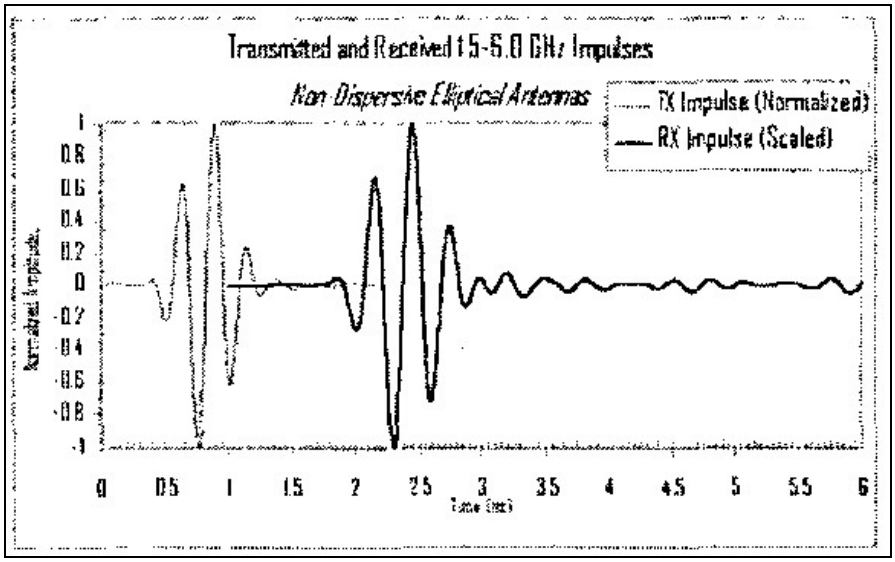

Fig. 2.3.9: Transmitted (left) and received (right) voltage waveform from a pair of planar elliptical dipole antennas (from [50]).

Fig. 2.3.9 displays the transmitted (left) and received (right) voltage signals from a pair of planar elliptical dipole antennas. It is obvious that both signals look very similar. This reveals the non-dispersive behavior of planar elliptical dipole antennas. With minimum variation in the relative delay between paths of various frequency components, UWB antennas with very low dispersion are achievable [50].

3.0 UWB Printed-Circuit-Board (PCB) Antennas

3.1 Introduction to UWB PCB Antennas

In the recent rapid research of ultra-wideband (UWB) technology, the UWB antenna is one of the most essential components for an UWB system. Many applications such as local network, imaging radar, and communication employ UWB technology. Therefore, developments of UWB antennas become important and complex for system and antenna designers. In conventional UWB systems, the antenna radiates in the preferred direction with high gain performance and operates over a broad impedance-matched bandwidth.

One of the examples would be log-periodic antennas; they have broadband impedance matching and reasonable gain in the desired direction. However, due to their dispersive properties on broadband waveform radiation, extra compensations and complexities are required. Another type of broadband antenna would be the TEM horn. To have lower dispersive rating, bi-conical antennas are a good choice for broadband systems. Bi-conical antennas have a broadband impedance match and tend to generate non-dispersive waveforms. However, when applying UWB systems to portable devices, conventional UWB antennas are not suitable. This is mainly due to their bulky size and

directional properties. Monopole and dipole antennas are good options for portable UWB devices. They have great features such as broadband impedance matching, small size and omni-directional radiation. However, from a system design point of view, fabrication may not be easy because those antennas require a perpendicular ground plane. Therefore, planar or printed-circuit board (PCB) antennas are much more suitable in terms of manufacturing complexities. Also, when designing UWB antennas, designers must make new considerations based on new UWB standards.

As for portable applications, PCB antennas are the most suited compared to other types of UWB antennas. Therefore, different types of planar UWB antennas have been developed. UWB PCB antennas are usually compact in design and small in size. Also, planar antennas can be easily designed to have broad bandwidth and omni-directional radiation. Relatively small planar antennas will tend to generate low-dispersive waveforms. Most of the planar antennas developed so far are in microstrip or coplanar waveguide (CPW) technology. Future UWB systems in mobile devices will operate at high data rate and in short-range applications. Planar antennas are widely used in wireless communications due to their low cost and light-weight properties as well as their ease of

fabrication. Therefore, the realization of UWB antennas in printed-circuit technologies within relatively small substrate areas is of primary importance.

In the following sections, two primary types of PCB antennas will be compared. They are designed in microstrip and CPW feeding technologies. Several examples from both technologies will be selected and compared. The comparison will be based on antenna performances in five different areas: voltage standing wave ratio (VSWR) or return loss (S_{11}), gain, radiation patterns, polarization, and group delay or phase center variation. The first parameter, VSWR, should be less or equal to 2 for the required bandwidth or the return loss should be less or equal to -10 dB. Those parameters indicate how well the impedance is matched over the operational bandwidth. The second parameter is the gain of a UWB antenna. Typically, the gain refers to the maximum gain for each frequency of the operating band, independent of the varying direction. The third parameter is the radiation pattern, where directionalities of radiation are determined. Most of the time, omni-directional radiation patterns are preferable for portable UWB antennas.

The fourth parameter is the polarization of the antenna. Two different and perpendicular polarizations are defined, both vertical polarization E_θ (co-polarization)

and horizontal polarization E_ϕ (cross-polarization). If an antenna's radiating elements are parallel located in the y-z plane, perpendicular to the x-axis and facing the positive x-axis direction, then both polarizations will be oriented as illustrated in Fig. 3.1.1. In order to completely observe radiation patterns and polarization of an UWB antenna, two primary perpendicular radiation planes need to be defined, both E-plane and H-plane. For each plane, both polarizations need to be plotted for selected frequencies. Typically, four radiation plots will be required, two plots for each plane, and one for each polarization. With respect to the orientation of Fig. 3.1.1, the x-y plane is defined as H-plane and y-z plane or x-z plane is defined as E-plane.

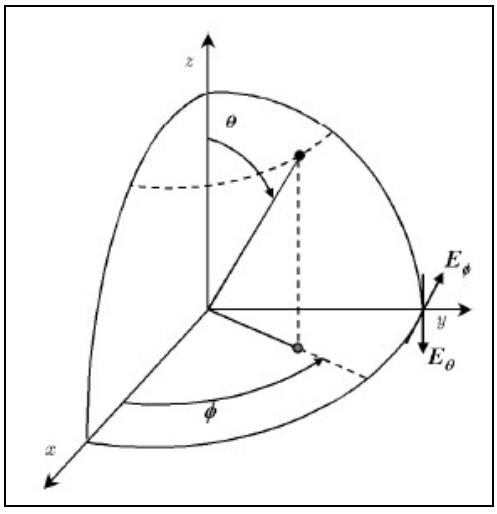

Fig. 3.1.1: Orientation of field components, both polarizations.

The final parameter is the group delay or the phase center variation. Both the group delay and the phase center variation are ways of measuring the dispersive property of UWB antennas. In the time domain, a transient analysis is performed which leads to the group delay. A pulse, whose frequency spectrum covers the bandwidth of the antenna, is generated, applied at the antenna input and its radiated pulse detected. Both pulses are Fourier transformed and their phase response recorded. The group delay is obtained from the derivative of the phase variation with respect to angular frequency. As for the phase center variation, in the frequency domain, the spherical wave front in the far field is detected for each frequency, from which the apparent phase center along the antenna surface or axis can be calculated. Alternatively, the phase variation in the near field over the main beam is computed for different phase center points moved from a reference point on the surface of the antenna. Then a valid phase center location is detected if the phase variation over the main beam is within a few degrees. These methods are complicated and time-consuming. The following Fig. 3.1.2 illustrates a simple layout of phase center measurements. At one frequency, three points with equal phase ϕ_0 are detected and tracked back to phase center C_1. The points of equal phase response will move with frequency, so that at a different frequency, an equal phase ϕ_0' appears to be generated from phase center C_2.

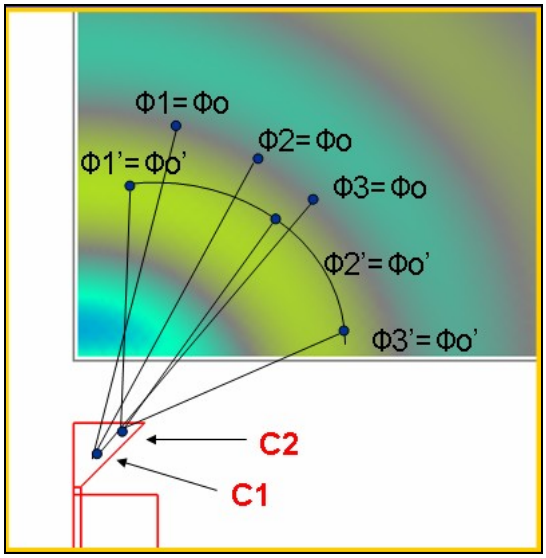

Fig. 3.1.2: Simple phase center variation measurement layout (antenna at the bottom).

3.2 Microstrip UWB Antennas

Microstrip technology is one of the most common techniques used to design planar antennas. However, when microstrip technology is applied to planar UWB antennas, fabrication on both sides of the substrate is required. This means that microstrip UWB antennas must have ground planes on the opposite side of the substrate material to support the feeding microstrip line. Two different designs of microstrip UWB antennas from other published papers are presented here for comparisons. Those antennas will be illustrated in terms of those five performance parameters mentioned in the previous section.

Example 1: A New Ultra-Wideband Antenna for UWB Applications [10]

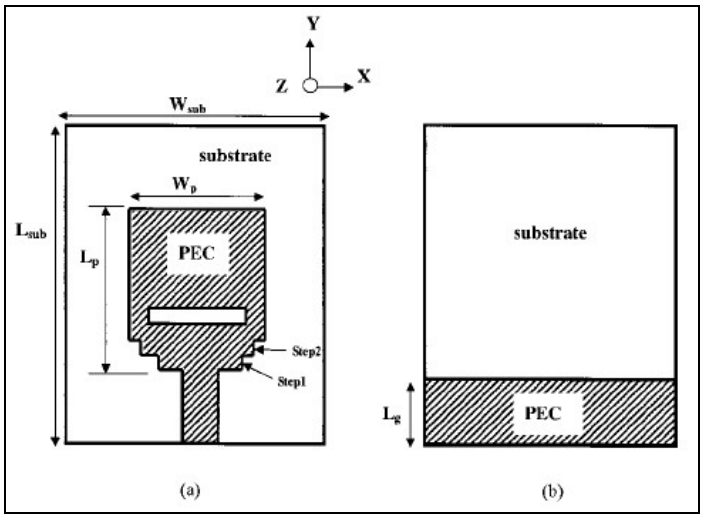

Fig. 3.2.1: Top view (a) and bottom view (b) of the proposed UWB antenna from [10].

This antenna, which has compact dimensions of 15 x 14.5 mm^2, is printed on one side of an FR4 substrate of thickness 1.6 mm and relative permittivity 4.4 (Fig. 3.2.1). In this design, a 3.2-12 GHz frequency range for return loss (S_{11}) < -10 dB is obtained. Fig. 3.2.2 illustrates the return loss obtained by measurement and simulation. Fig. 3.2.3 shows the measured antenna gain in a frequency range between 3 and 10 GHz. The gain variations are less than 5 dBi. The lowest gain is about -0.2 dBi [10].

Fig. 3.2.4 illustrates the measured radiation pattern at 3 GHz for both co-polarized

and cross-polarized fields. From Fig. 3.2.4, nearly omni-directional radiation pattern is obtained for the co-polarized radiation in the xz-plane. However, there is too much variation between the co-polarized and cross-polarized radiation and, therefore wideband operation in dual polarization is not possible.

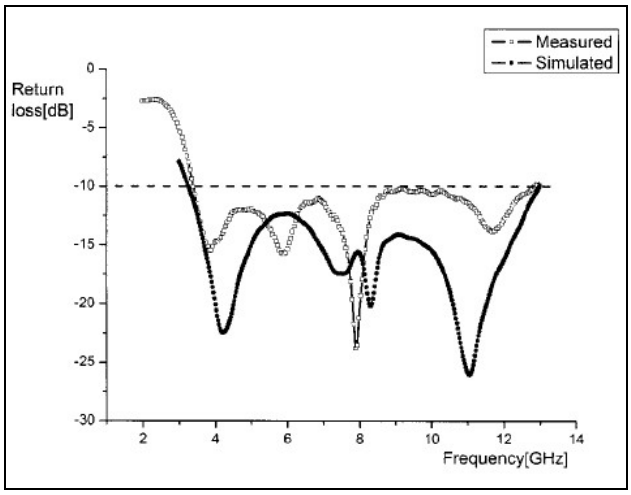

Fig. 3.2.2: Return loss in both simulation and measurement from [10].

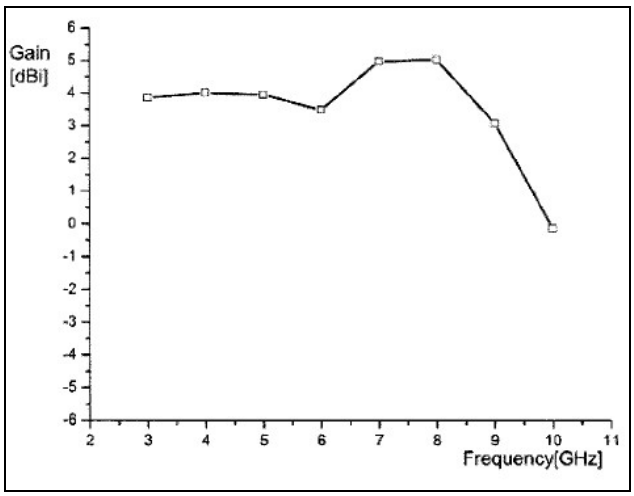

Fig. 3.2.3: Measured antenna gain from [10].

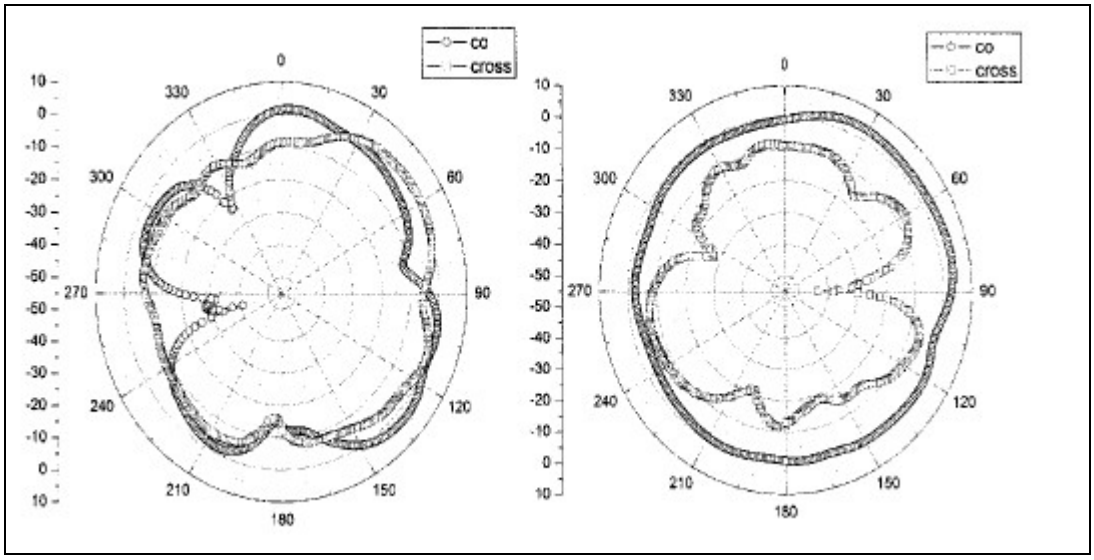

Fig. 3.2.4: Measured radiation patterns at 3 GHz, xy-plane (left) and xz-plane (right) from [10].

Fig. 3.2.5 illustrates the measured group delay. From the figure, group delay variations of up to 0.5 ns can be observed within the operating bandwidth (2-12 GHz) [10].

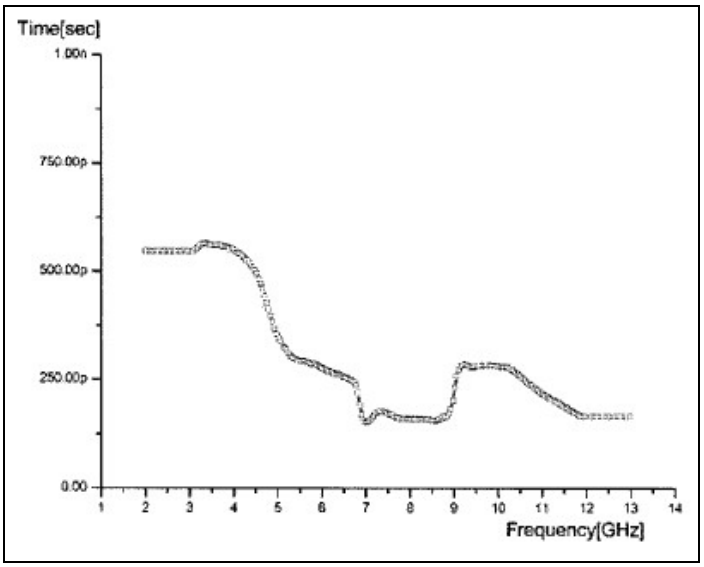

Fig. 3.2.5: Measured group delay from [10].

Example 2: Low-Cost PCB Antenna for UWB applications [12]

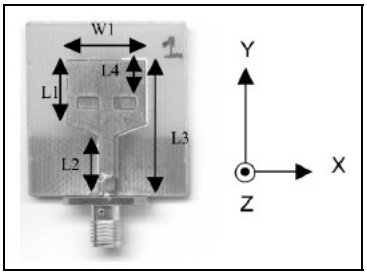

Fig. 3.2.6: Layout of the proposed antenna from [12].

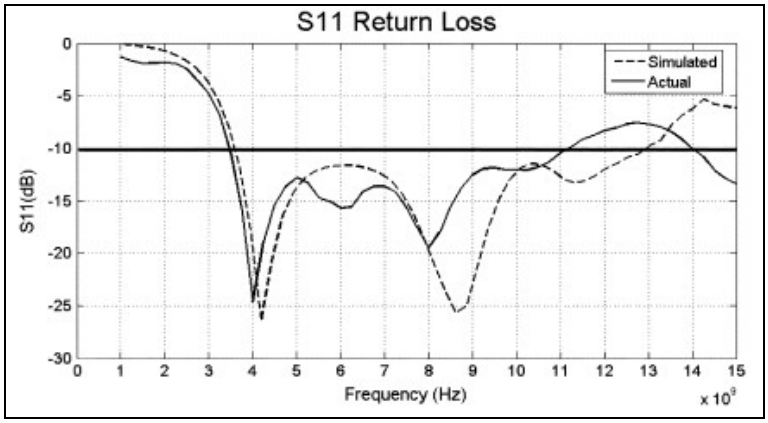

Fig. 3.2.7: Return loss of both simulation and measurement from [12].

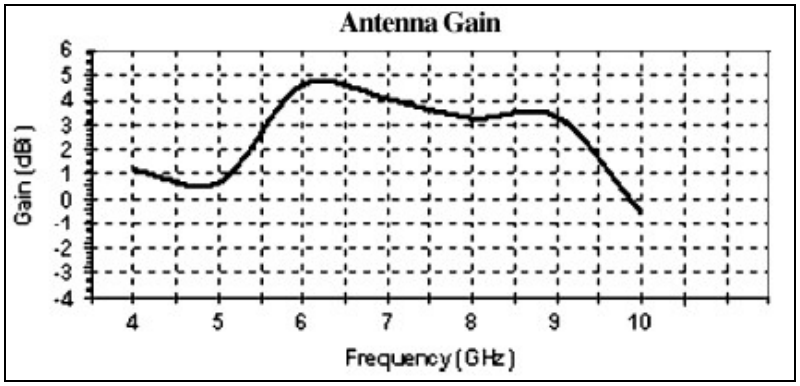

Fig. 3.2.8: Measured gain from [12].

This UWB antenna is fabricated on a 3 x 3 cm^2, 1.6-mm-thick FR4 board (Fig.

3.2.6). Fig. 3.2.7 illustrates the return loss obtained from both simulation and measurement. The bandwidth covers a frequency range from 3.4 GHz to 11 GHz. Gain results are displayed in Fig. 3.2.8 between 4 GHz and 10 GHz. The gain variation is about 5 dBi. The lowest gain is about -0.5 dBi at 10 GHz [12] and demonstrates that this antenna is a very poor radiator at high frequencies.

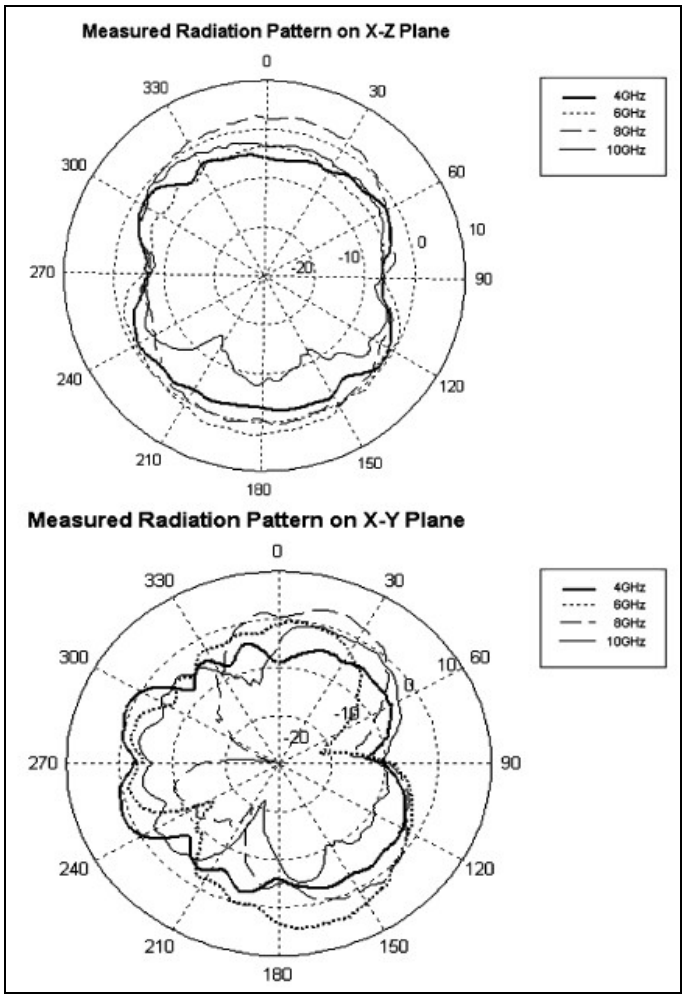

Fig. 3.2.9: Measured radiation patterns in xz-plane and xy-plane from [12].

Fig. 3.2.9 illustrates measured radiation patterns in both the xz- and xy-planes for various frequencies. Nearly omni-directional radiation patterns are obtained in the xz-plane. However, no information about polarization is provided in the paper. Fig. 3.2.10 displays the measured group delay. Its variation is less than 100 ps from 3 GHz to 12 GHz [12].

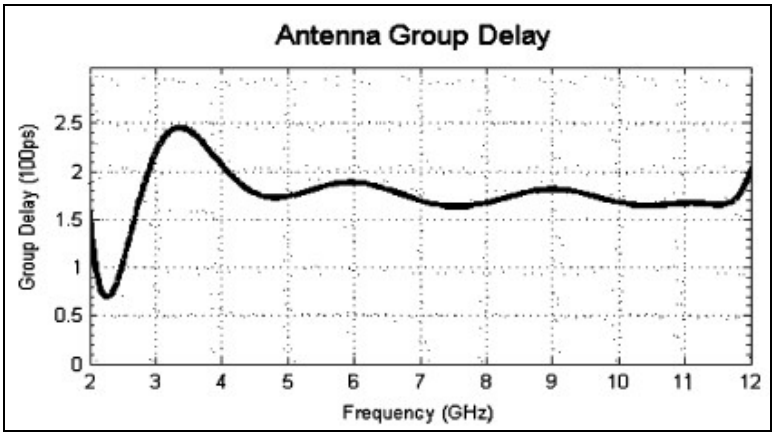

Fig. 3.2.10: Measured group delay from [12].

3.3 Coplanar Waveguide (CPW) UWB Antennas

Most of the PCB antennas are microstrip-type antenna. They will need a ground plane on the opposite side of the substrate for electromagnetic waves to travel along the feed line. However, by applying CPW feed technology, only one side of the substrate needs to be processed. Both radiating elements and ground planes are on the same side of the substrate. Therefore, most of the electromagnetic wave travels in the slots on the

surface of the substrate, and less energy is lost in the substrate. Thus, this provides a possibility for a wider impedance matching bandwidth. Also, the CPW feeding technique requires an easier fabrication process. Two different designs of CPW-fed UWB antennas from other published papers are presented here to showcase the state-of-the-art. Those antennas will be illustrated in terms of those five performance areas mentioned in section 3.1.

Example 1: An Ultrawideband Coplanar Waveguide-Fed Tapered Ring Slot Antenna [23]

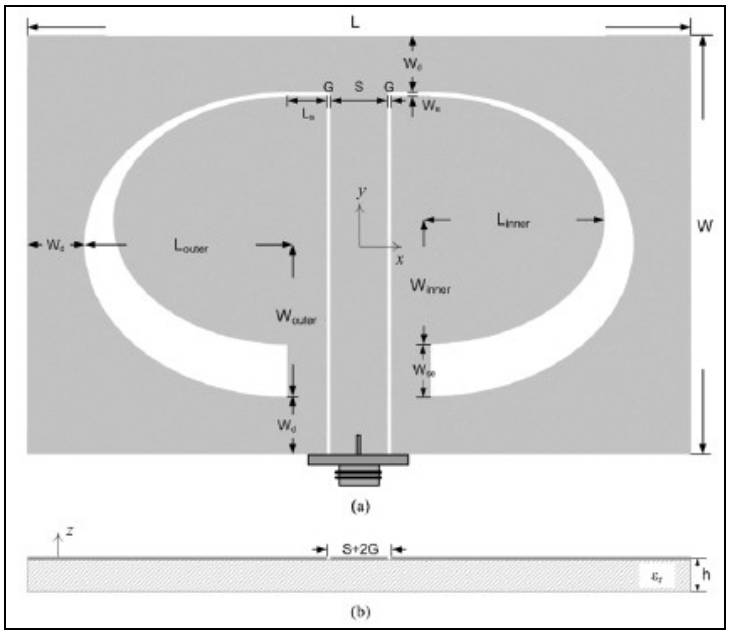

Fig. 3.3.1: Layout of the proposed UWB antenna, (a) top view and (b) cross-section view from [23].

This CPW-fed UWB antenna (Fig. 3.3.1) is fabricated on a 66.1 x 44 x 0.762 mm^3 Rogers RO4003 substrate with dielectric constant of 3.38. Fig. 3.3.2 illustrates the return loss obtained from both simulation and measurement. The return loss is less than -10 dB from 3.1 GHz to 12 GHz.

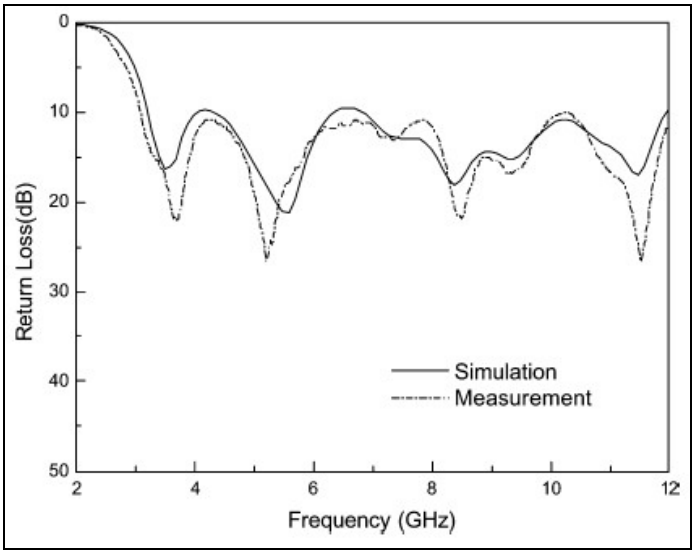

Fig. 3.3.2: Simulated and measured return loss from [23].

Fig. 3.3.3 displays the gain of the proposed antenna; however, this does not show the peak gain but the gain in different angles at both E-plane (yz-plane) and H-plane (xz-plane) (c.f. Fig. 3.3.1). Radiation patterns displayed in Fig. 3.3.4 show both simulation and measurement results in both E-plane and H-plane at various frequencies. Nearly omni-directional radiation patterns are obtained in the H-plane. Polarization

properties are not displayed in these radiation patterns. Fig. 3.3.5 illustrates various group delays at different angles in the E-plane. The maximum group delay variation is about 0.5 ns [23].

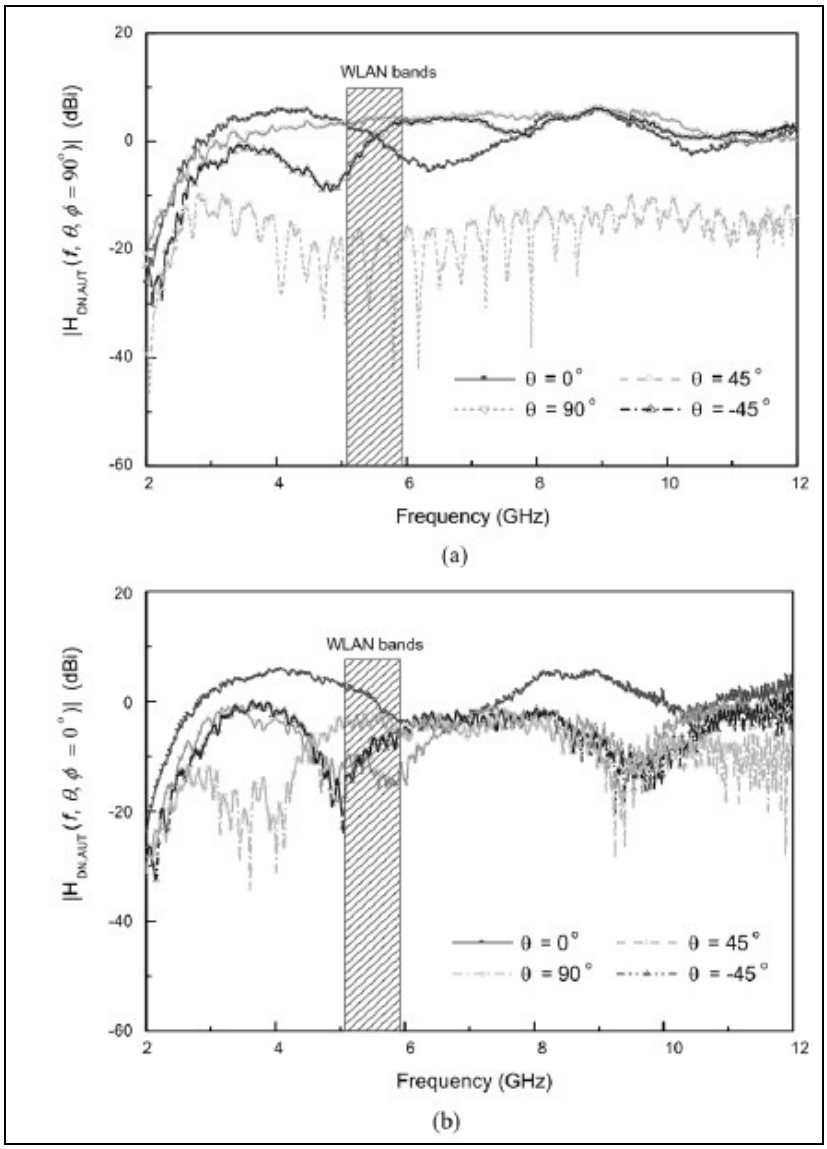

Fig. 3.3.3: Measured gain responses of the proposed UWB antenna at θ = -45°, 0°, 45° and 90° in (a) E-plane and (b) H-plane from [23].

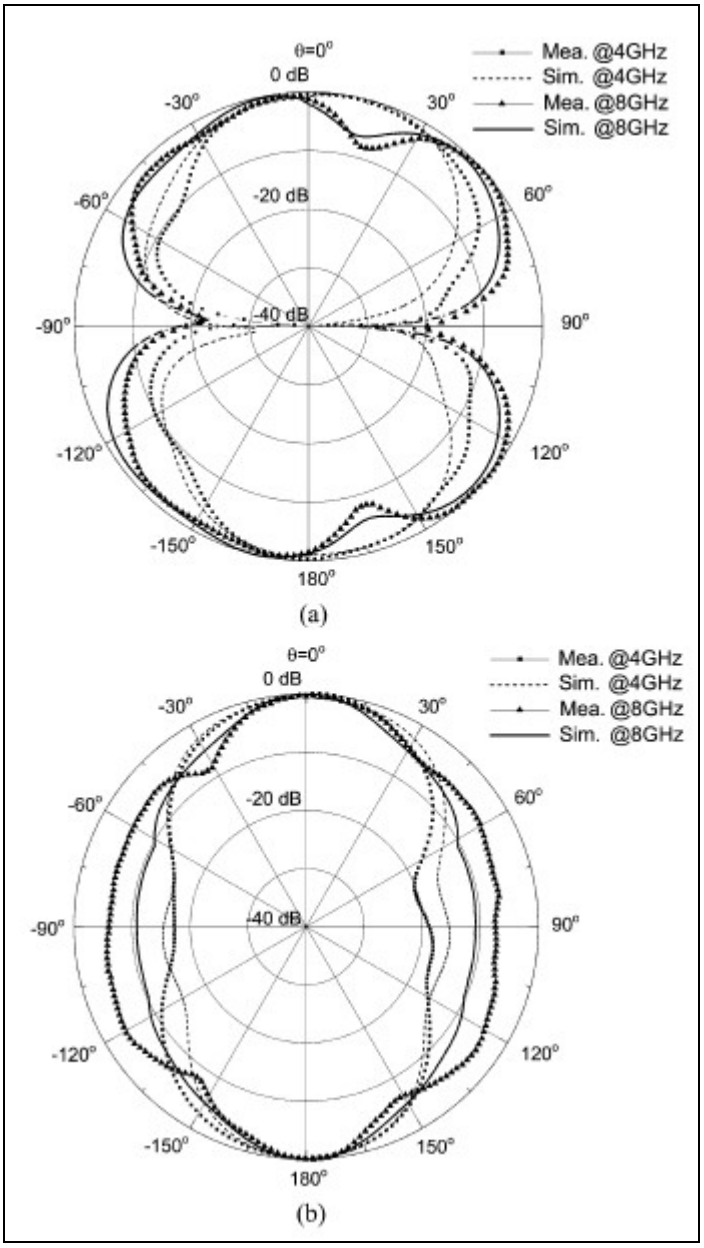

Fig. 3.3.4: Measured and simulated radiation patterns of the CPW-fed antenna. (a) E (yz) - plane and (b) H (xz) - plane from [23].

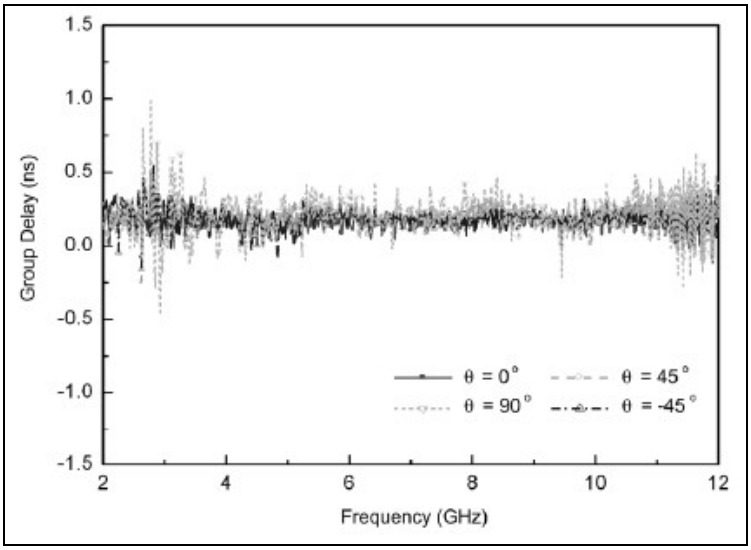

Fig. 3.3.5: Measured group delay at θ = -45°, 0°, 45° and 90° in E-plane from [23].

Example 2: A Compact UWB Antenna with CPW-Feed [29]

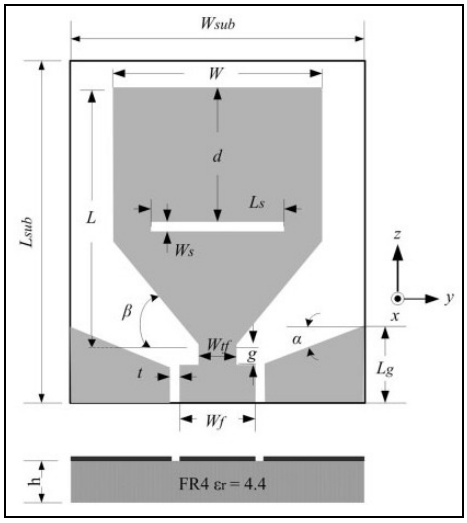

Fig. 3.3.6: Layout of the proposed UWB antenna, top view and cross-section view from [29].

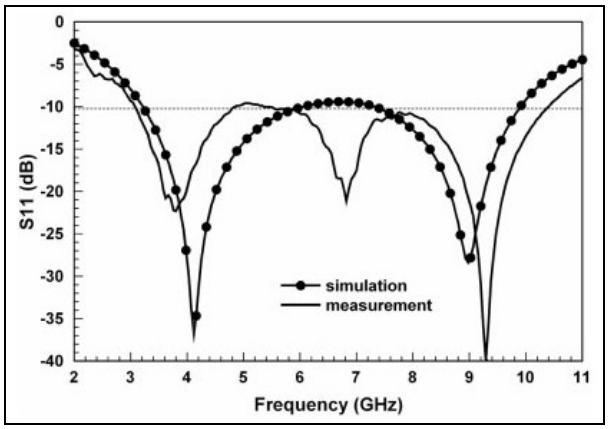

Fig. 3.3.7: Simulated and measured return loss from [29].

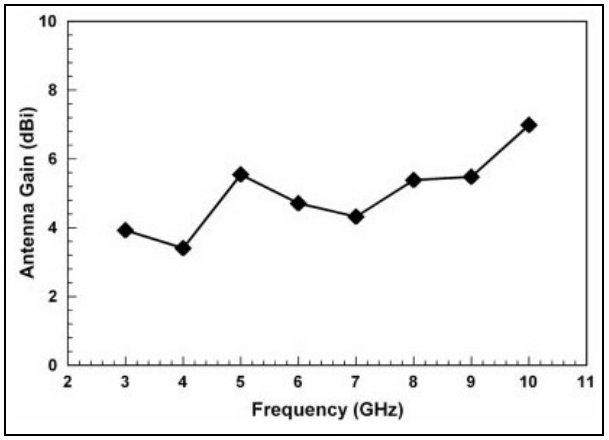

Fig. 3.3.8: Measured antenna peak gain from [29].

This antenna has a size of 15.5 x 17 mm^2 (W_{sub} x L_{sub}) and is printed on one side of a FR4 substrate with thickness of 1.6 mm and relative permittivity of 4.4 (Fig. 3.3.6). Fig. 3.3.7 illustrates the return loss obtained from both simulation and measurement. This antenna has a return loss of less or equal to -10 dB from 3.08 GHz to 10.3 GHz. Fig. 3.3.8 displays the measured peak gain. Gain variations are about 4 dBi, and the lowest gain is about 2.6 dBi. Radiation patterns are illustrated in Fig. 3.3.9. Both polarizations at various frequencies are displayed in the xy-, xz- and yz-planes. Nearly omni-directional

co-polarized radiation patterns are obtained in the xy-plane. However, too much variation between the co-polarized and cross-polarized fields occur; therefore, dual-polarization cannot be utilized. Also, group delay results are not available in this paper [29].

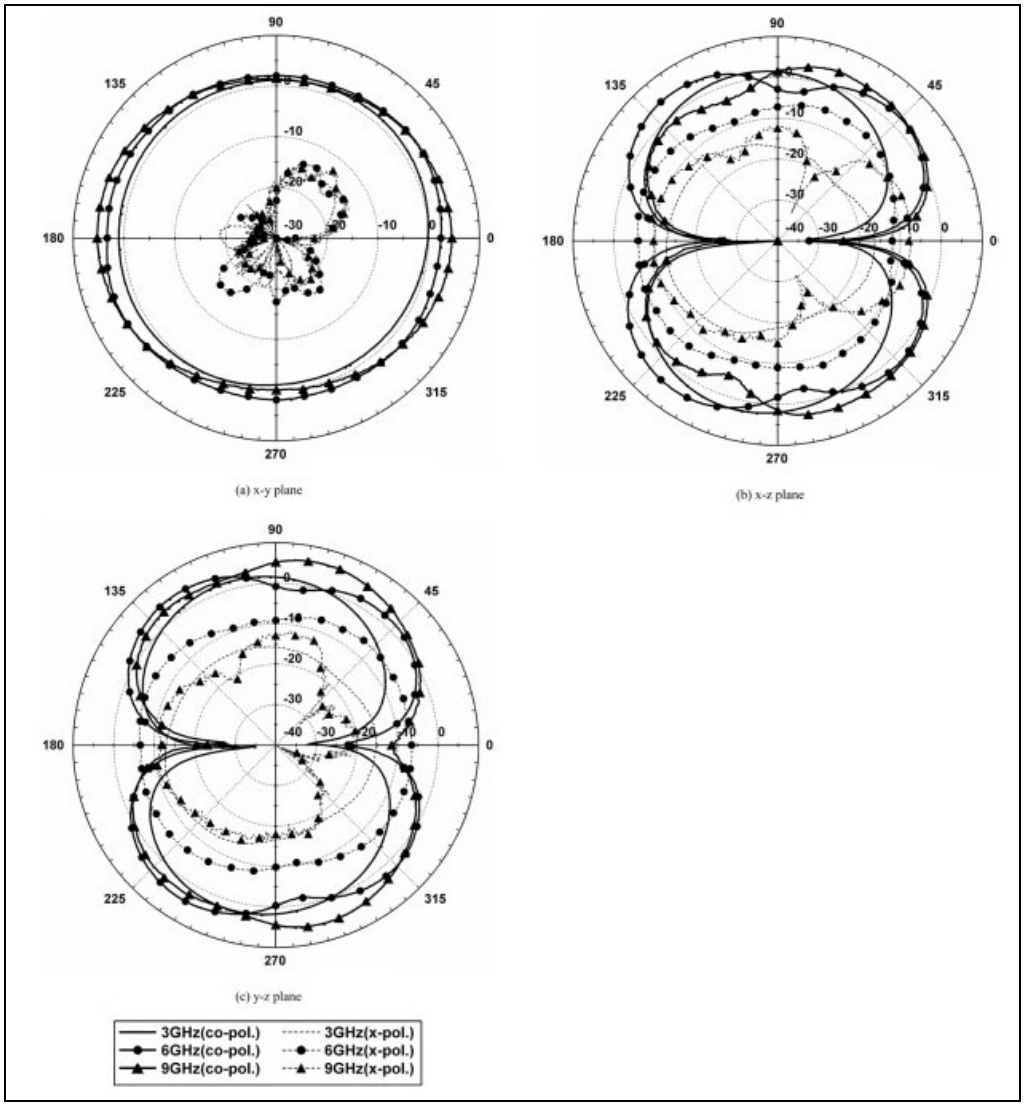

Fig. 3.3.9: Measured radiation patterns of the proposed UWB antenna from [29].

3.4 Comparison between Mirostrip and CPW UWB Antennas

From the previous two sections, different designs in both microstrip and CPW-fed technologies are compared based on the five performance areas of each example. The following Table 3.1 illustrates the summary of comparison between each of the two microstrip and CPW-fed UWB antenna examples.

Table 3.4.1: Summary of comparison between microstrip and CPW-fed UWB antenna examples.

	Return Loss (≤ -10 dB)	**Peak Gain Variation/Minimum peak gain**	**Radiation Patterns**	**Polarization**	**Group Delay (ps)**	**Substrate Area (mm^2)**
Microstrip Example 1	3.2 - 12 GHz	5 dBi/-0.2dBi	Omni-directional in co-polarization	Single polarization	< 500	15 x 14.5 mm^2
Microstrip Example 2	3.4 – 11 GHz	5 dBi/-0.2dBi	Omni-directional radiation	Not available	< 100	30 x 30 mm^2
CPW-fed Example 1	3.1 - 12 GHz	Cannot compare	Omni-directional radiation	Not available	< 500	66.1 x 44 mm^2
CPW-fed Example 2	3.08 – 10.3 GHz	4 dBi/2.6dBi	Omni-directional in co-polarization	Single polarization	Not available	15.5 x 17 mm^2

From Table 3.1, it can be concluded that the CPW-fed technique will give a slightly better bandwidth depending on the design. Moreover, less peak gain variation and higher minimum peak gain are achievable.

4.0 UWB Coplanar Waveguide Antennas

4.1 The First Design

A new printed-circuit antenna in coplanar waveguide technology for ultra-wideband applications is introduced in this thesis. Since design guidelines for UWB antennas are nonexistent, the design of this new CPW UWB PCB antenna starts from the design of [14]. The layout of this antenna is presented in Fig. 4.1.1, and Fig. 4.1.2 displays its dimensions. This planar triangular monopole antenna has a VSWR of less than 2.5 from 4 GHz to 10 GHz. Fig. 4.1.3 illustrates the VSWR results. Radiation patterns in the H-plane (xy-plane) between 4 GHz to 7 GHz are displayed in Fig. 4.1.4. Both polarizations, E_θ (co-polarization) and E_Φ (cross-polarization), are presented. Omni-directional radiation patterns are obtained the in co-polarization [14].

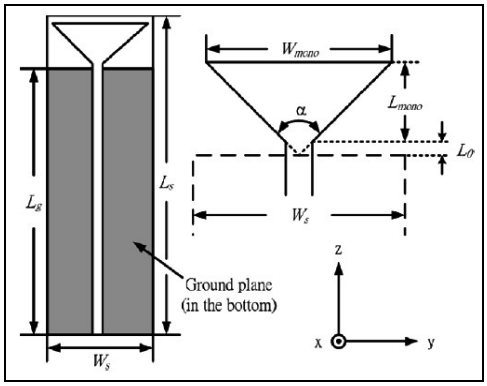

Fig. 4.1.1: Layout of the antenna from [14].

PARAMETERS OF THE PRINTED PTMA

Parameters	Values
W_{mono}	17 mm
L_{mono}	7.6 mm
L_0	1 mm
c	90°
L_s	60 mm
W_s	20 mm
L_g	50 mm
T	1 mm
PCB substrate (ε_r tanδ)	(4.7, 0.018)

Fig. 4.1.2: Dimensions of the antenna from [14].

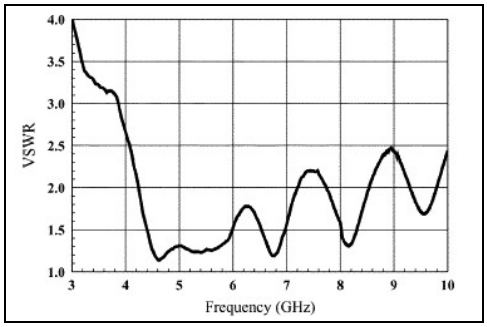

Fig. 4.1.3: VSWR of the antenna from [14].

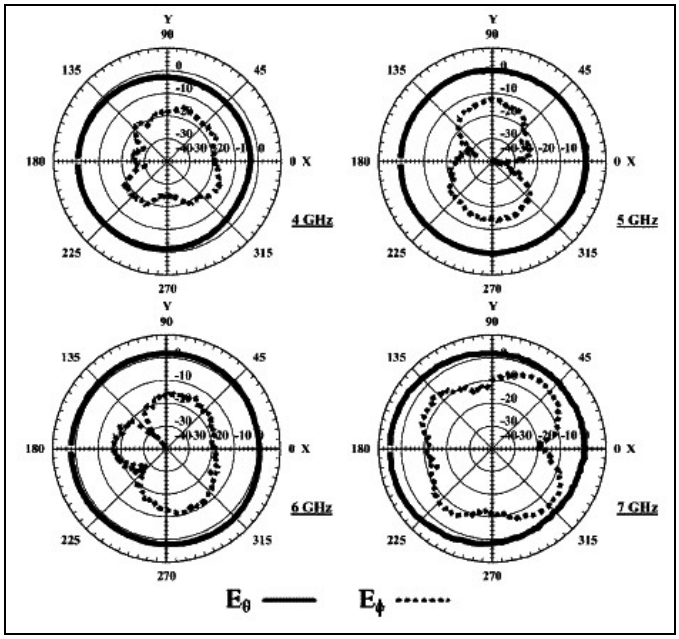

Fig. 4.1.4: H-plane (xy-plane) radiation patterns, 4 - 7 GHz from [14].

With some investigations and simulations performed on the antenna of [14], suggestions for improvement become apparent. First, the original microstrip feed is replaced by a CPW feed. The ground plane at the back of the substrate is moved to the front, thus placing the radiating element and ground planes on the same side of the substrate. Fig. 4.1.5 shows the layout of the CPW-fed antenna. All other dimensions

remain as in [14]. The gaps between each ground plane and the transmission line are 1 mm. Fig. 4.1.6 illustrates the VSWR of the CPW-fed antenna as obtains from a simulation with HFSS.

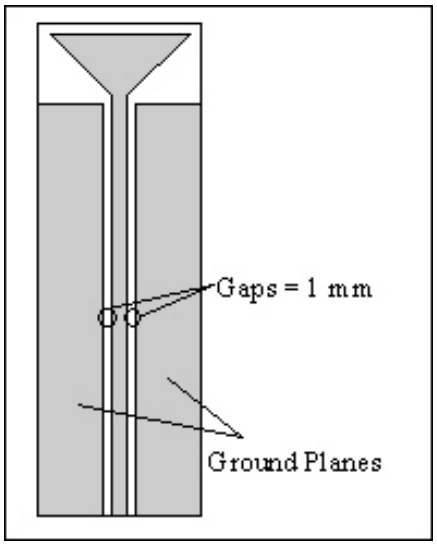

Fig. 4.1.5: The layout of the CPW-fed antenna.

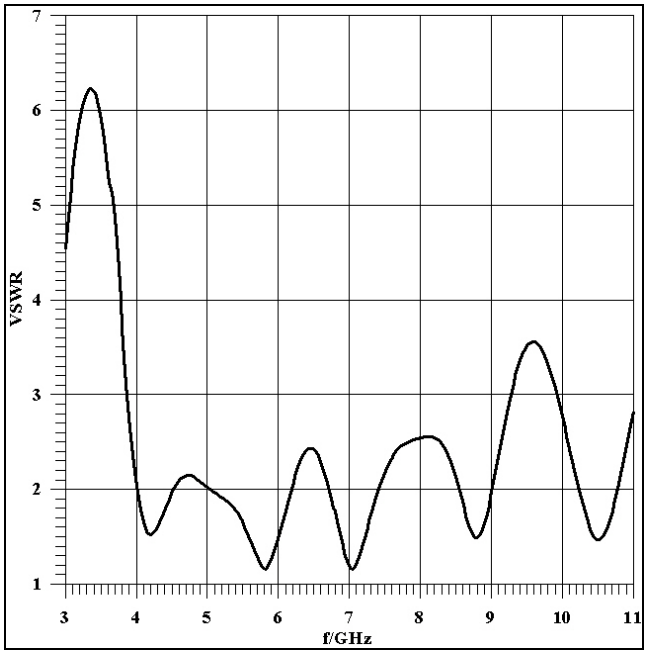

Fig. 4.1.6: VSWR performance of the CPW-fed antenna.

From the VSWR result of Fig. 4.1.6 and compared with that of Fig. 4.1.3, it is obvious that the bandwidth performance rather deteriorated than improved. The lower frequency range displays a slightly better match as the VSWR equals two at 4 GHz; however, the VSWR performance in the upper frequency range is worse than in the original design [14]. Therefore, different approaches must be applied to improve the

VSWR performance of the CPW-fed antenna. This can include a change in the physical size of the antenna or in the configuration of the radiating element and the ground planes.

4.2 Different Design Approaches

In order to obtain the operational UWB frequency band (3.1 GHz to 10.6 GHz) proposed by the FCC, changes must be made to increase the bandwidth. A first approach is to change the physical size of the antenna. The original antenna dimensions [14] are 20 x 60 mm^2 (W x L) (c.f. Fig. 4.1.2). To bring the VSWR down to a value of two for the lower frequency band (3 GHz to 4 GHz), the physical size of the new antenna design is adjusted to 30 x 40 mm^2 (W x L). Wider width increases the performance in the lower frequency band. Next, a stepped configuration is introduced to both the radiating patch and ground planes. Those steps can be viewed as individual resonating elements which create multiple interacting resonances in the operating band. This follows from basic principles outlined in [37]. Fig. 4.2.1 illustrates the first design approach. The VSWR performance of Fig. 4.2.1 as computed by HFSS is displayed in Fig. 4.2.2.

From the VSWR result of Fig. 4.2.2, it is apparent that changing the physical size of the antenna extends the bandwidth to the lower frequency range.

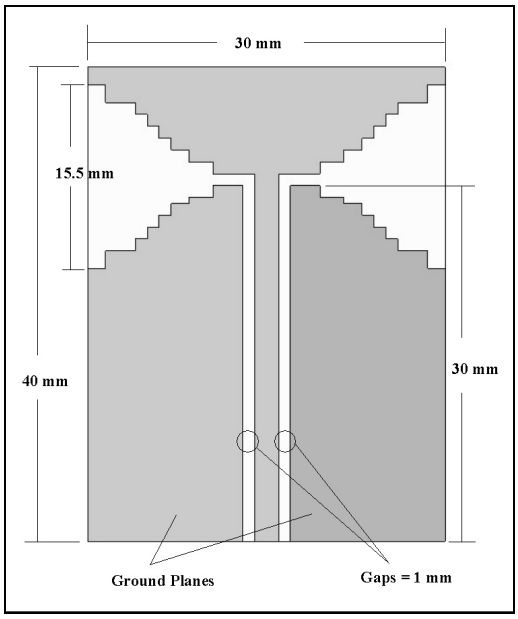

Fig. 4.2.1: Layout of the first design approach.

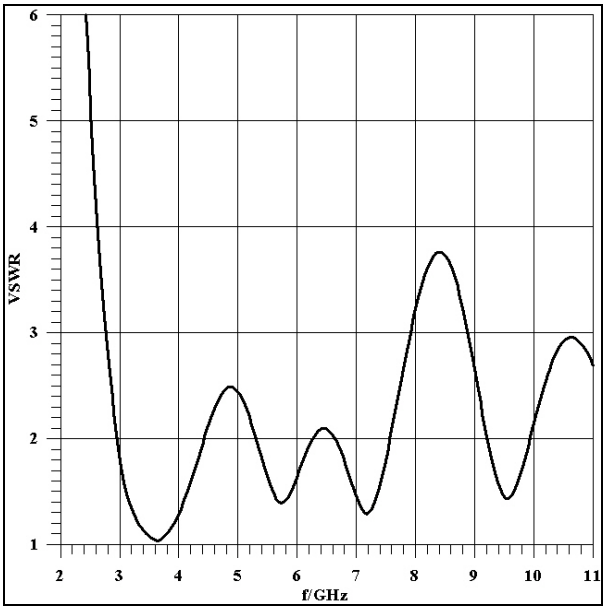

Fig. 4.2.2: VSWR performance of the first design approach.

In this case, between 3 GHz to 4.4 GHz, VSWR values are now less than two. However, the stepped configuration in both the radiating patch and ground planes has not yet improved the overall VSWR performance. Therefore, different stepped configurations need to be investigated. Fig. 4.2.3 illustrates the second design approach; the only change made is on the stepped configuration. This time, the opening edges between the radiating patch and ground planes are increased from 15.5 mm to 17 mm. This produces better resonances in the lower frequency range. As a result, the stepped configuration of the radiating patch and ground planes appear somewhat like a conical shape profile. The VSWR performance for the second design approach is displayed in Fig. 4.2.4. The lower

frequency band is improved. A VSWR value ≤ 2 is obtained from 2.9 GHz to 5.9 GHz. By applying the idea of wider opening edges, further investigations can be made to extend the operating bandwidth.

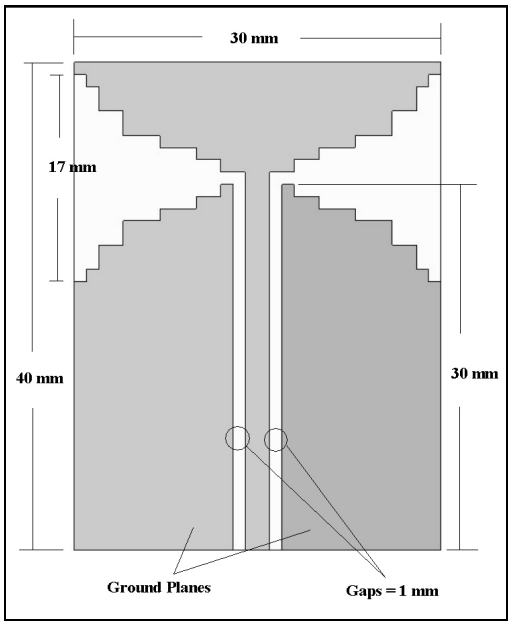

Fig. 4.2.3: Layout of the second design approach.

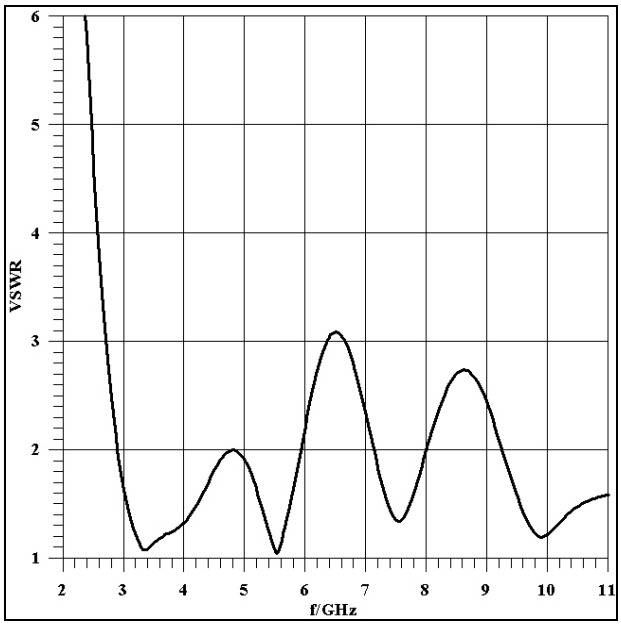

Fig. 4.2.4: VSWR performance of the second design approach.

In order to make the opening edges wider, the lengths of ground planes are decreased from 30 mm to 25 mm. In this way, the distances of the opening edges increase from 17 mm to 27 mm, and the new stepped configuration is applied to resemble a more conical profile. This third design approach is illustrated in Fig. 4.2.5. Fig. 4.2.6 displays its VSWR performance. It is obvious that the VSWR improved significantly. It is larger than

two only in two narrow ranges, 6.8 GHz to 7.6 GHz and 9.3 GHz to 10.4 GHz.

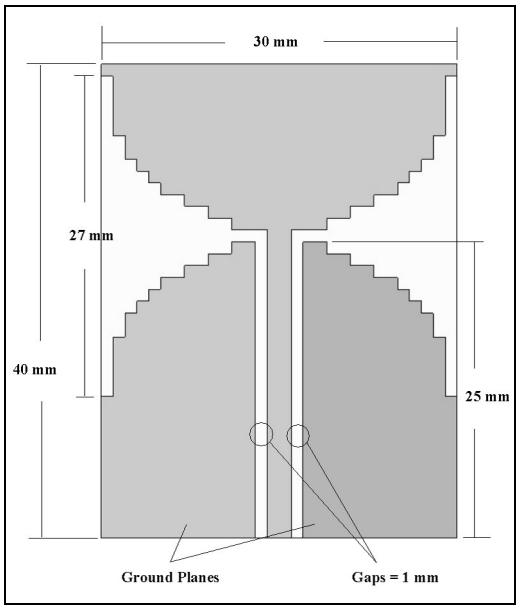

Fig. 4.2.5: Layout of the third design approach.

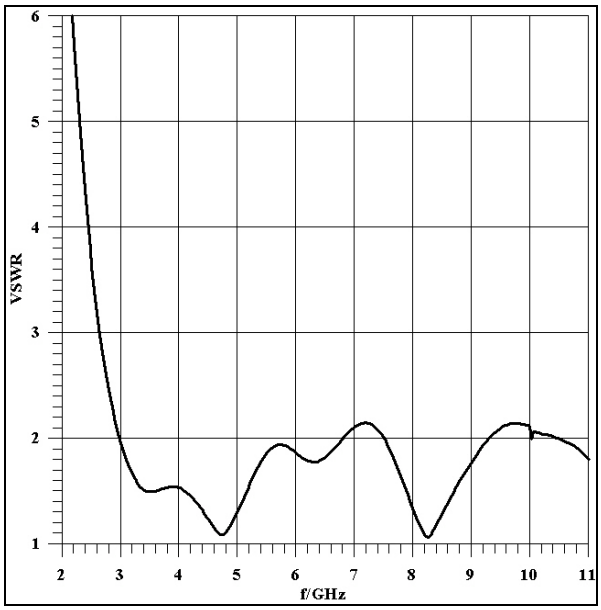

Fig. 4.2.6: VSWR performance of the third design approach.

By adjusting the lengths of the opening edges and the step size of each step, further increases in bandwidth can be achieved. Fig. 4.2.7 illustrates the fourth design approach with opening edge lengths equal to 24 mm and with larger step size. The VSWR performance is displayed in Fig. 4.2.8. This time, the higher frequency range, up to 10.3 GHz has a VSWR value of less than two. The design of a new UWB printed-circuit antenna in coplanar technology is getting closer. Fig. 4.2.9 shows comparisons of VSWR performance from the first design approach to the fourth design approach.

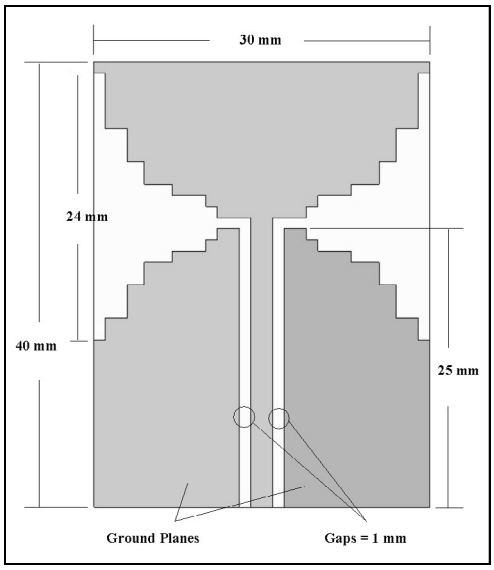

Fig. 4.2.7: Layout of the fourth design approach.

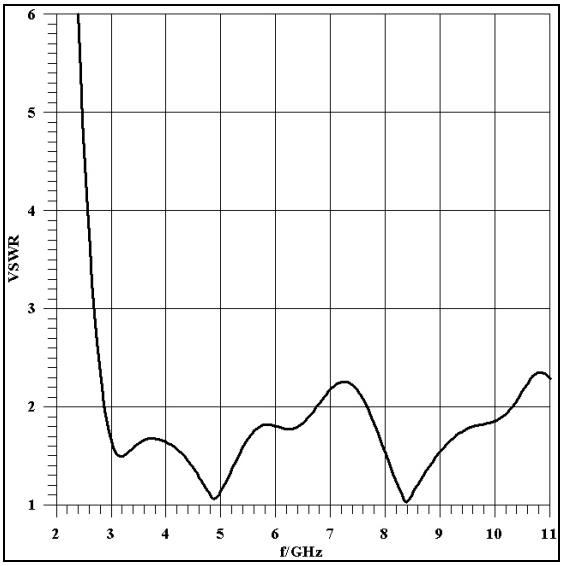

Fig. 4.2.8: VSWR performance of the fourth design approach.

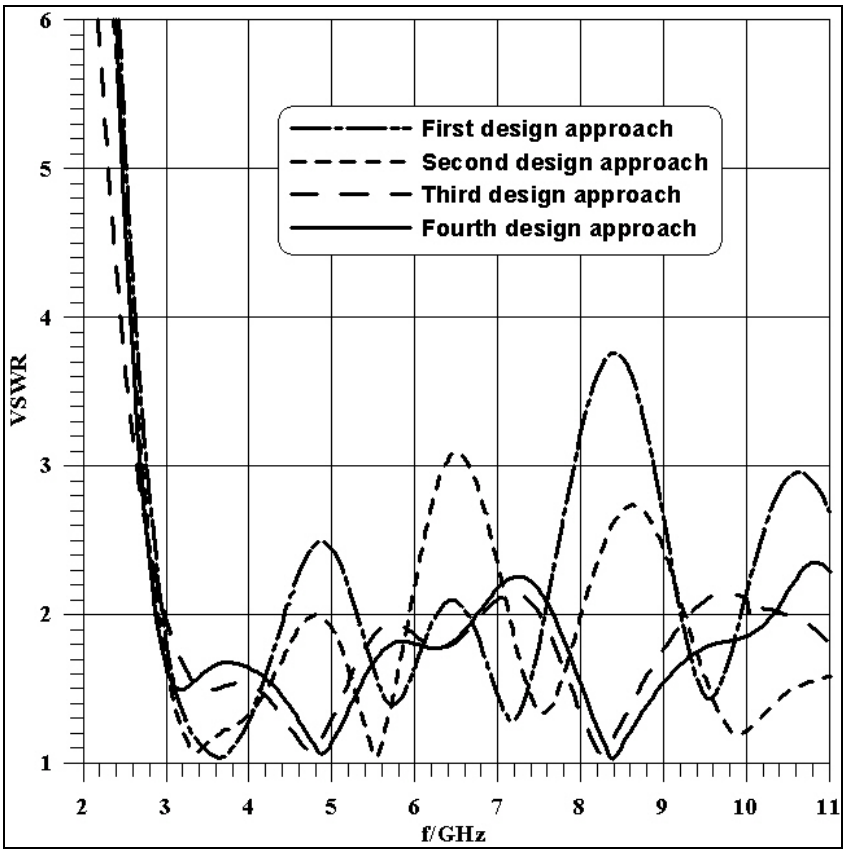

Fig. 4.2.9: Comparisons of VSWR performances from the first to the fourth design approaches.

4.3 The Final Design

After a variety of design approaches, with some optimization on different step sizes, a new printed-circuit antenna in coplanar waveguide technology for UWB is introduced. The frequency of operation is 3.1 GHz to 10.6 GHz with a VSWR < 2. Fig. 4.3.1 illustrates the layout of the new UWB antenna with detailed dimensions, and Table 4.1 displays the dimensional values. This UWB antenna uses an FR4 substrate of 1mm thickness and 30mm x 40mm (W x L) substrate area. The permittivity parameters are ε_r = 4.7 and tanδ = 0.018.

Table 4.3.1: Dimensional values of the proposed UWB antenna.

Symbol	Distance (mm)	Symbol	Distance (mm)	Symbol	Distance (mm)
W	30	***W8***	2	***H8***	1
L	40	***W9***	3	***L1***	2
W1	1	***H1***	1	***L2***	3
W2	2	***H2***	5	***L3***	2
W3	1.5	***H3***	3	***L4***	1
W4	1.5	***H4***	2	***L5***	1
W5	1	***H5***	1	***L6***	1
W6	1	***H6***	1		
W7	2	***H7***	1		

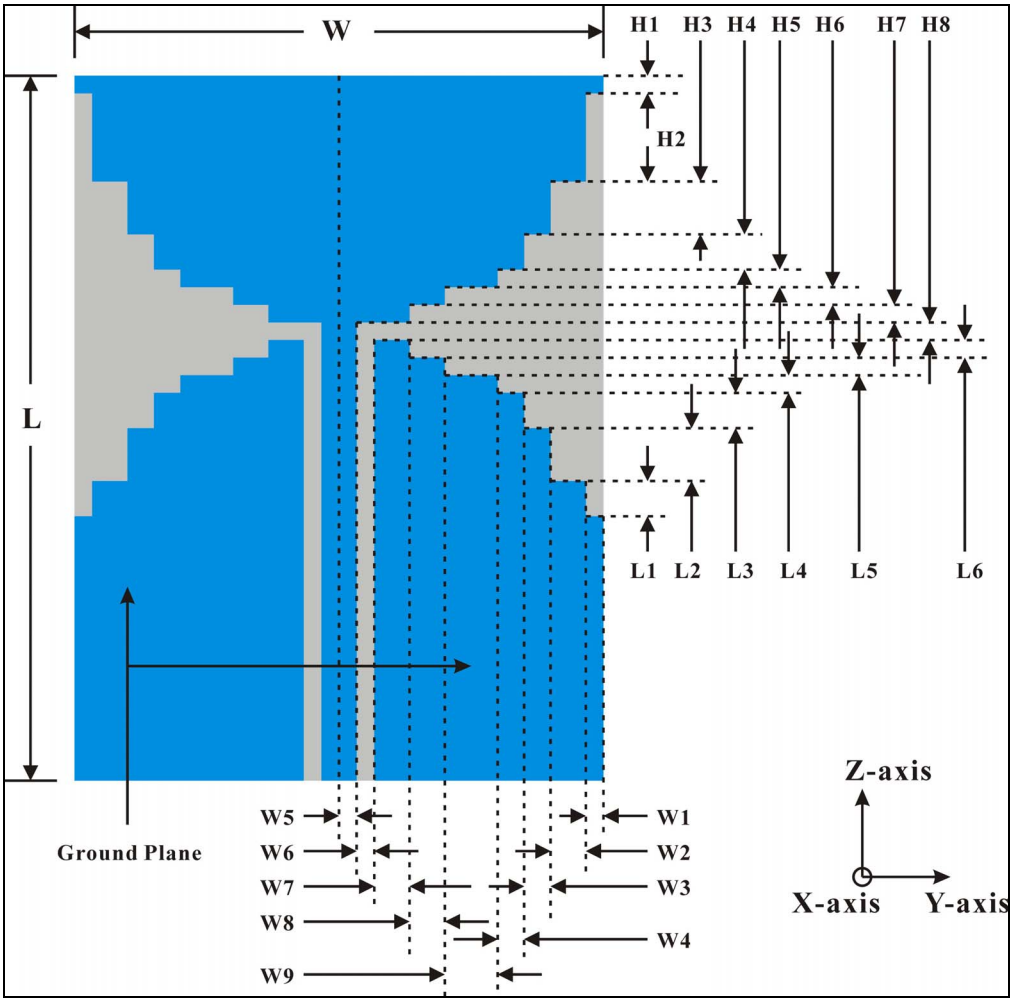

Fig. 4.3.1: Detailed layout of the proposed UWB antenna in CPW technology.

The design of the coplanar UWB antenna follows basic principles outlined in [37] as far as the stepped configuration in Fig. 4.3.1 is concerned. The slots have been inserted on a rough trial-and-error basis. Also, the width of the antenna is designed to increase the lower frequency band. The design of the antenna appears to be a stepped version of a similar antenna presented in [26]. However, there are two fundamental differences. First of all, the antenna in [26] is a slot radiator, which maintains metallic strips at the left and

right edges of the substrate. Such metallic strips are missing in Fig. 4.3.1 and thus result in a somewhat conical shape of the radiating profile – similar to a tapered slot antenna. Secondly, the stepping is chosen such that the smallest dimension is 0.5mm. This contributes to low manufacturing sensitivity. However, it also influences the characteristic impedance of the feeding coplanar waveguide, which is significantly higher than the 50Ω coaxial line to be connected at the input. (Note that the coaxial line is also used to physically connect the two ground planes.) As we will show later, this mismatch is not to the detriment of the antenna performance. The entire antenna has then been fine optimized with respect to the input voltage standing wave ratio (VSWR) and pattern performances.

4.4 Final Design Results

4.4.1 HFSS Simulation Model

The coplanar UWB antenna was designed using the finite-element full-field solver software HFSS®. Since a major concern with using professional software packages such as HFSS is validation of the results, Fig. 4.4.1 and Fig. 4.4.2 present performance comparisons with existing UWB antennas. Fig. 4.4.1 shows the VSWR (both simulated

and measured) of the triangular monopole antenna presented in [14]. Although the agreement between theory and measurements is not ideal, the simulations agree well with measurements over the entire 3-10 GHz bandwidth. A similar comparison for the multiple-resonance UWB antenna presented in [37] is shown in Fig. 4.4.2 for the VSWR performance and in Fig. 4.4.3 for radiation patterns. Note that this design operates over a much larger bandwidth than that of Fig. 4.4.1. Nonetheless, the simulated performances agree well with measurements, thus validating the simulations with HFSS. The differences between simulated and measured results are attributed by the measurement setup, which cannot be included in the simulation model. As far as Fig. 4.4.2 is concerned, both simulated and measured results satisfy the design specification of VSWR ≤ 2.

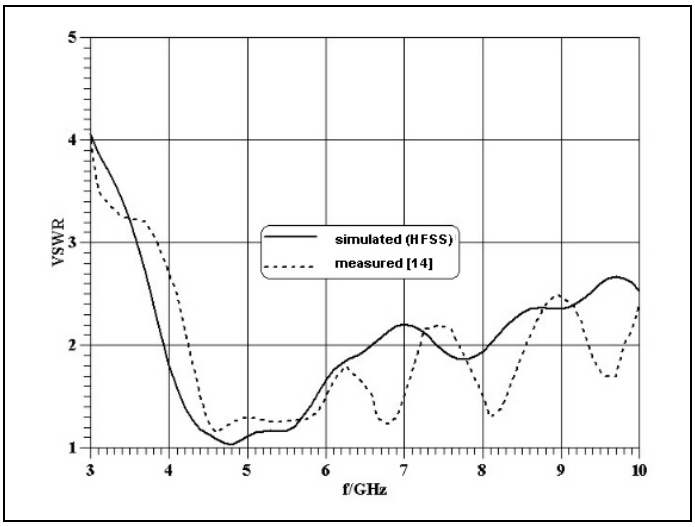

Fig. 4.4.1: VSWR performance (simulated and measured) of the UWB antenna presented in [14].

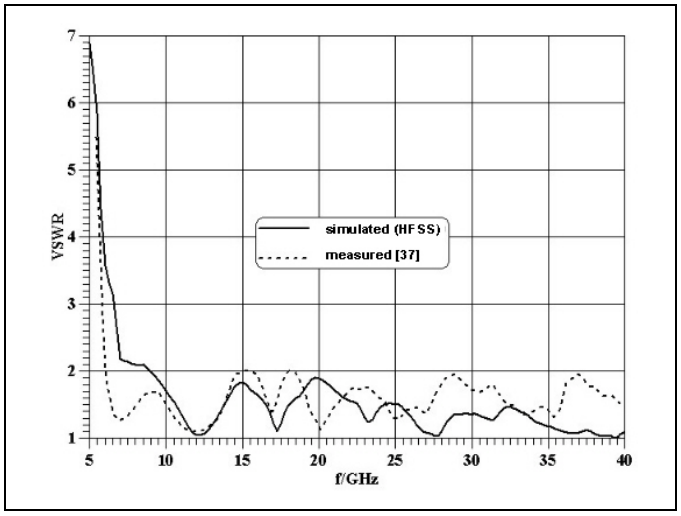

Fig. 4.4.2: VSWR performance (simulated and measured) of the UWB antenna presented in [37].

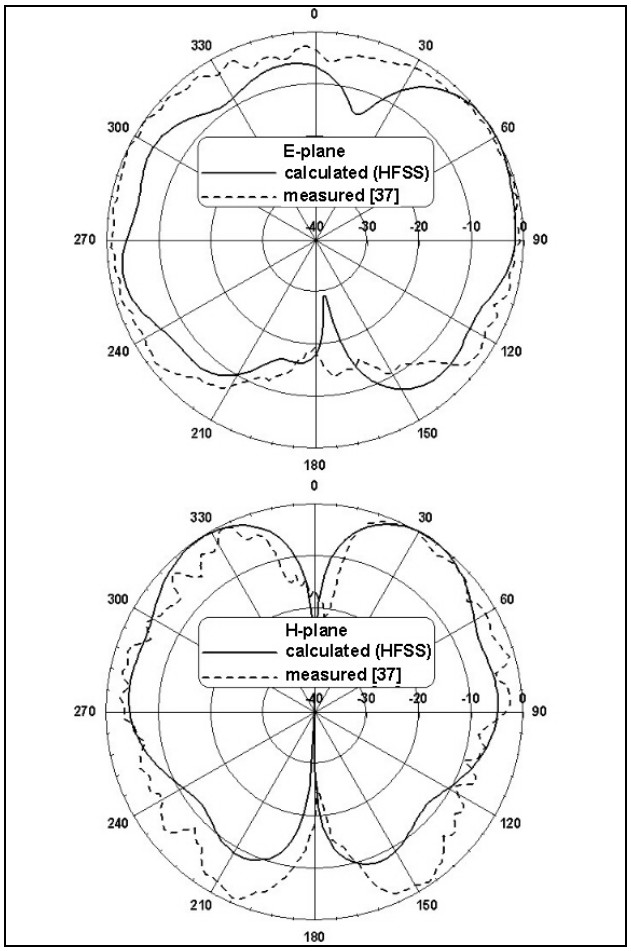

Fig. 4.4.3: E- and H-plane radiation patterns at 10 GHz (simulated and measured) of the UWB antenna presented in [37].

Fig. 4.4.4 illustrates the final design model created in HFSS. It has three main parts: UWB antenna, coax cable, and radiation boundary. The UWB antenna consists of the printed-circuit board, one radiating patch and two ground planes. In the simulation model, the radiating patch and the two ground planes are just surfaces without thickness; they are set up to be perfect electric boundaries in HFSS. In order to obtain more accurate simulation results, finer mesh operations such as surface approximations are applied on the radiating patch and the two ground planes. The setting for all those surfaces is: surface deviation = 0.1 mm, normal deviation = 5 deg, and aspect ratio = 4.

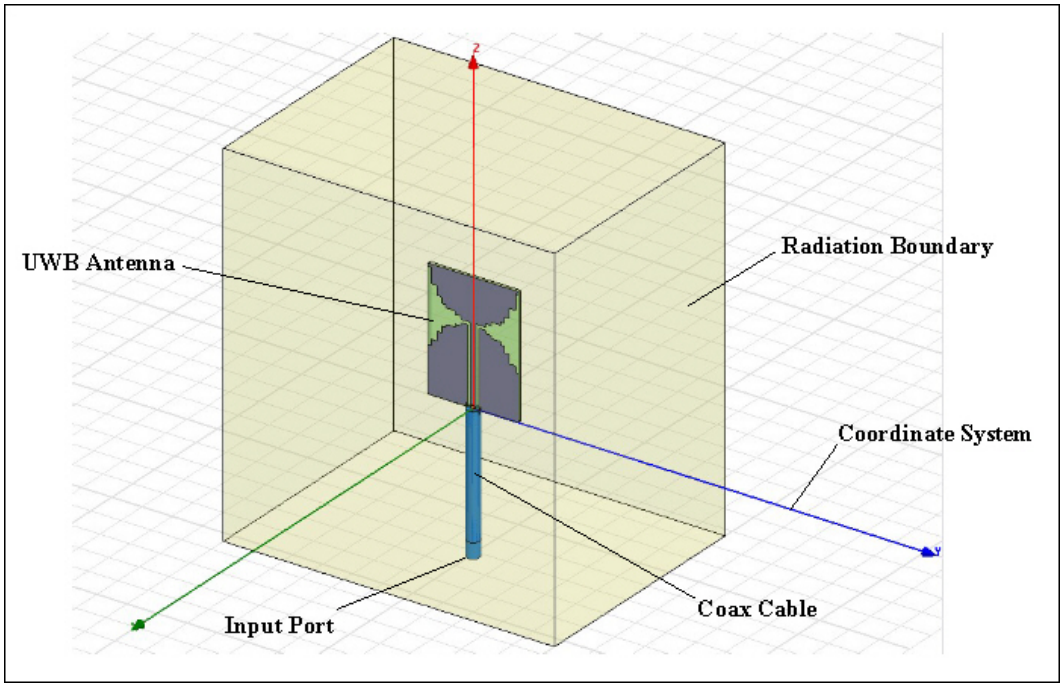

Fig. 4.4.4: Final design model of proposed UWB antenna in HFSS.

The coax cable part consists of the inner conductor, the dielectric gap and the outer ground shielding. The inner conductor is modeled as a perfect electric conductor (pec) material, and has a radius of 0.6 mm. The dielectric gap material is polyethylene and has $\varepsilon_r = 2.25$ and $\tan\delta = 0.018$. The outer ground shielding is modeled as perfect electric boundary surface around the dielectric gap. It has a radius of 2.094 mm. Three small connecting pins are created in the simulation model to connect the inner conductor of the coax cable to the center conductor of the radiating patch and the outer ground shielding of the coax cable to the ground planes of the UWB antenna. The length of the coax cable in the simulation model is set up to be 45 mm. This allows the input port of the coax cable to be located outside of the radiation boundary. This coax cable essentially models a 50Ω coaxial (SMA) connector.

As for the last part of the simulation model, the radiation boundary is a tool in HFSS to simulate far-field radiation patterns. According to setup procedures in HFSS, the radiation boundary has to be at least a quarter of a wavelength away from the antenna. Unlike conventional narrow band antenna designs, UWB antennas have very wide bandwidths; for simulation simplicities, the wavelength at the lowest frequency of the operating band is selected as it gives the largest radiation boundary. By selecting the

wavelength at the lowest frequency, this radiation boundary can fulfill the condition over the entire operating band. For the final design simulation model, the wavelength at 2 GHz is selected. A quarter wavelength at 2 GHz is 37.5 mm. The simulation model uses 40 mm as the distance from the antenna to the radiation boundary.

The solution type of this final design model is set up in the driven mode category. Under the HFSS simulating environment, a solution frequency is specified which usually is the center frequency within the operating band (sweep band). During the simulation, HFSS will perform an accurate calculation based on this solution frequency for the entire antenna model. For all other frequencies within the operating band, solutions will be calculated from matrix manipulations and transformations of the result obtained at the solution frequency. For traditional narrow band antenna designs, the solution frequency can be selected as the center frequency of the operating band. However, the operating band of a UWB antenna is very wide; thus the guidelines for narrow band systems do not apply. Inaccurate simulation results will occur if the solution frequency is not carefully chosen. Ideally, in order to get accurate results for UWB components, the entire operating band should be subdivided into many narrow sub-bands. With different solution frequency setups for different narrow sub-bands, accurate results can be obtained for each

narrow sub-band. This is a good approach for getting an accurate simulation result for an existing UWB antenna. However, it is not a very practical method when designing an UWB antenna. In order to speed up the design process, only approximated results are used when designing an UWB antenna.

The problem that causes inaccurate results is related to the mesh cell size of the simulation model. Due to the wide operating band, wavelengths of propagating modes can vary significantly. In HFSS, different solution frequencies will give different mesh sizes; thus longer wavelengths give larger mesh cell sizes and vice versa. A smaller mesh cell size means finer meshing, which will model the antenna more accurately. For the proposed final design of the UWB antenna in coplanar waveguide technology, the operating band is from 3.1 GHz to 10.6 GHz. Therefore, the frequency of 11 GHz is selected as the solution frequency, and the band is swept between 2 GHz to 11 GHz. The antenna simulation is modeled based on the 11 GHz mesh cell size, and the simulation calculates accurately for the frequency of 11 GHz. Any frequency lower than 11 GHz will have larger mesh cell sizes; thus the mesh cell size at 11 GHz models the antenna accurately for any lower frequency. Also, additional mesh operations such as surface approximations are applied on parts which require finer meshing such as the center patch

and the ground planes. With those setups, faster design processes and more accurate solutions of the simulation models are achieved.

Once a reasonable result for the VSWR is obtained for the proposed UWB antenna, different solution frequencies are applied for conformation tests. The operating band is divided into different sub-bands with different solution frequencies such as 3 GHz, 4 GHz, 5 GHz, and up to 10 GHz. Each solution frequency setup has a bandwidth of 2 GHz, thus using sub-bands overlapping by 1 GHz. From those sub-band simulations, the VSWR result of the proposed UWB antenna in CPW technology under the 11 GHz solution frequency setup is confirmed to be accurate. Radiation patterns and gains at different frequencies are obtained from each sub-band simulation result for the purpose of better accuracy. The average time for each simulation is about 1 hour and 20 minutes, and the average memory usage is about 1.5 gigabytes for each simulation.

4.4.2 HFSS Simulation Results

Fig. 4.2.5 demonstrates that the VSWR is below 2 between 3 GHz and 5.7 GHz, and between 6 GHz and 10.7 GHz. The maximum VSWR of 2.03 occurs at 5.83 GHz. Note that this result includes effects of a coaxial (SMA) connector attached to the input of the

coplanar waveguide. Therefore, compared to other UWB printed-circuit designs, this performance is excellent. Fig. 4.2.6 shows the maximum gain in the frequency range from 3 GHz to 10 GHz. The variation over the frequency range is about 3.6 dBi. This is significant but compares well with other UWB antennas operating over similar frequency ranges.

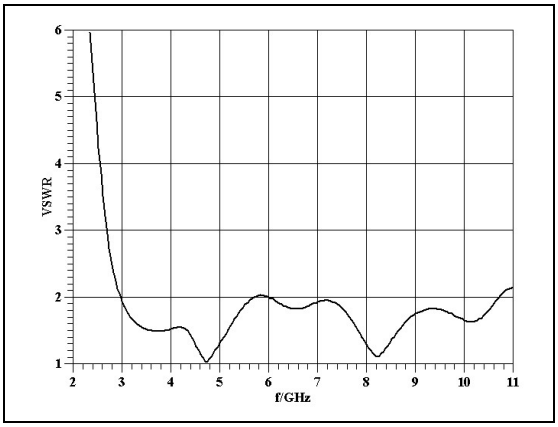

Fig. 4.4.5: VSWR performance of the proposed final design UWB antenna in coplanar waveguide technology.

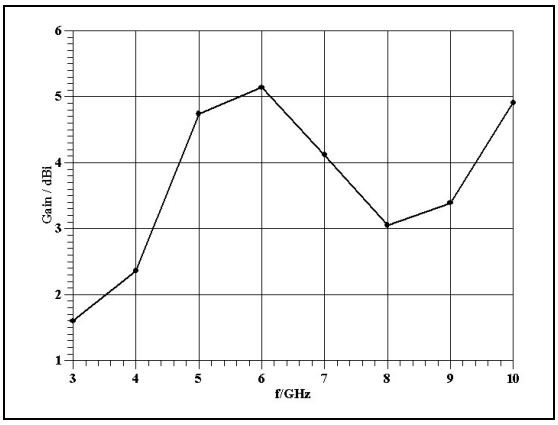

Fig. 4.4.6: Maximum gain of the proposed final design UWB antenna in coplanar waveguide technology.

In order to display the radiation patterns, the conventional definition of angles θ and ϕ with respect to coordinates x, y, z ($\frac{x}{r} = \sin\theta\cos\phi$, $\frac{y}{r} = \sin\theta\sin\phi$, $\frac{z}{r} = \cos\theta$) is used (c.f. Fig. 4.4.4). The normalized H-plane radiation patterns in the x-y plane are shown in Fig. 4.4.7 and Fig. 4.4.8. The vertical polarization (Fig. 4.4.7) is mostly omni-directional up to 8 GHz and starts to deteriorate slightly at 10 GHz. The reception in horizontal polarization, which is shown in Fig. 4.4.8 and normalized to the same values as in Fig. 4.4.7, is due to the direction of the field in the coplanar feed line. Therefore, these patterns are almost zero at ϕ = 0 degrees and ϕ = 180 degrees. Such property can be used in polarization sensitive measurements. The co-polarized patterns in the E-plane are shown in Fig. 4.4.9 (y-z plane) and in Fig. 4.4.10 (x-z plane). It is demonstrated that the basic shapes of the patterns do not significantly change over the frequency band of operation and that – as expected – variation is larger towards the upper frequency limit. Also, those radiation patterns behave like those of dipole antennas. These results compare well with those of other printed-circuit UWB antennas. Note that in presenting these normalized radiation patterns, different normalization constants have been used. For example, the 90-degree values in Fig. 4.4.7 and Fig. 4.4.9 should be identical, but they differ by a few dB due to different normalization.

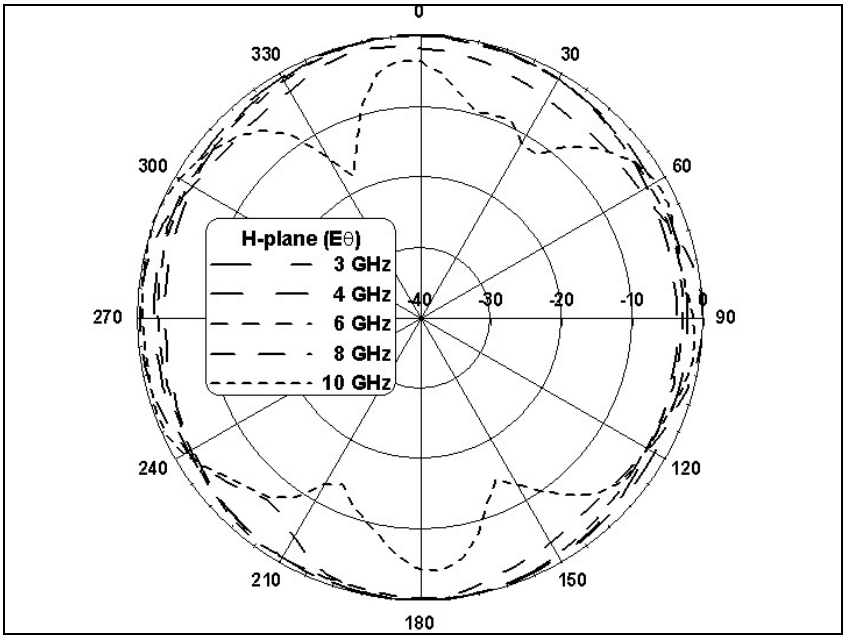

Fig. 4.4.7: Normalized co-polarized H-plane (x-y plane) radiation patterns $E_\theta(\pi/2, \phi)$ of the coplanar UWB antenna for various frequencies.

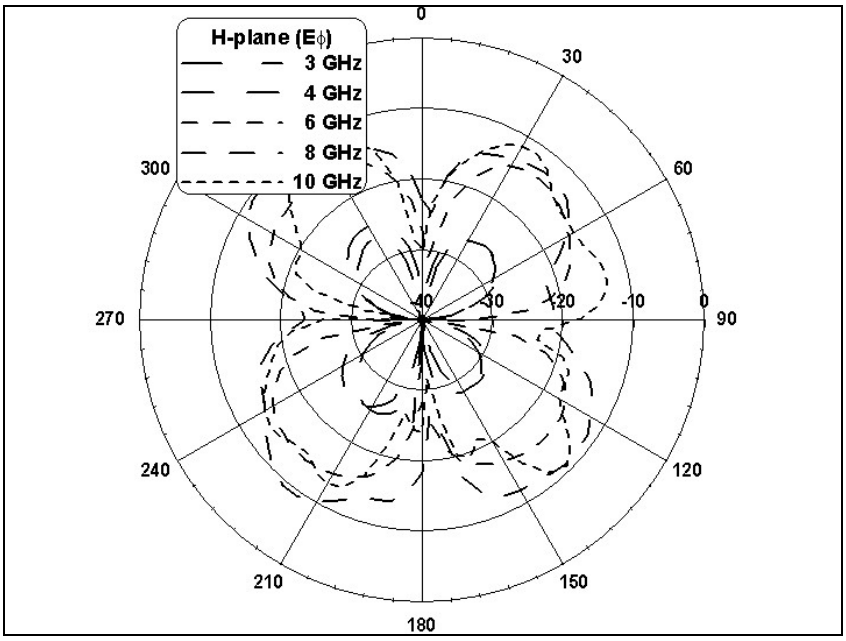

Fig. 4.4.8: Normalized cross-polarized H-plane (x-y plane) radiation patterns $E_\Phi(\pi/2, \phi)$ of the coplanar UWB antenna for various frequencies.

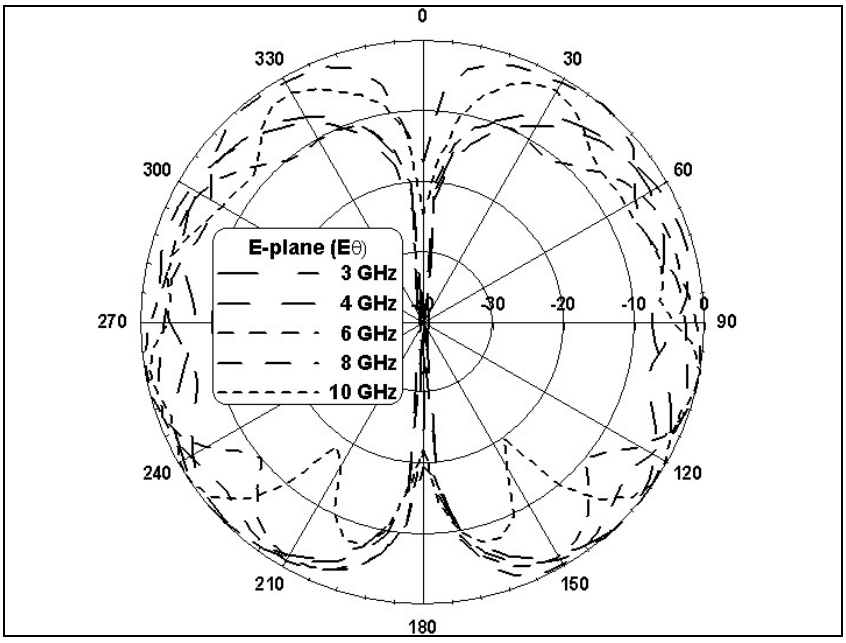

Fig. 4.4.9: Normalized co-polarized E-plane (y-z plane) radiation patterns $E_\theta(\theta,\pi/2)$) of the coplanar UWB antenna for various frequencies.

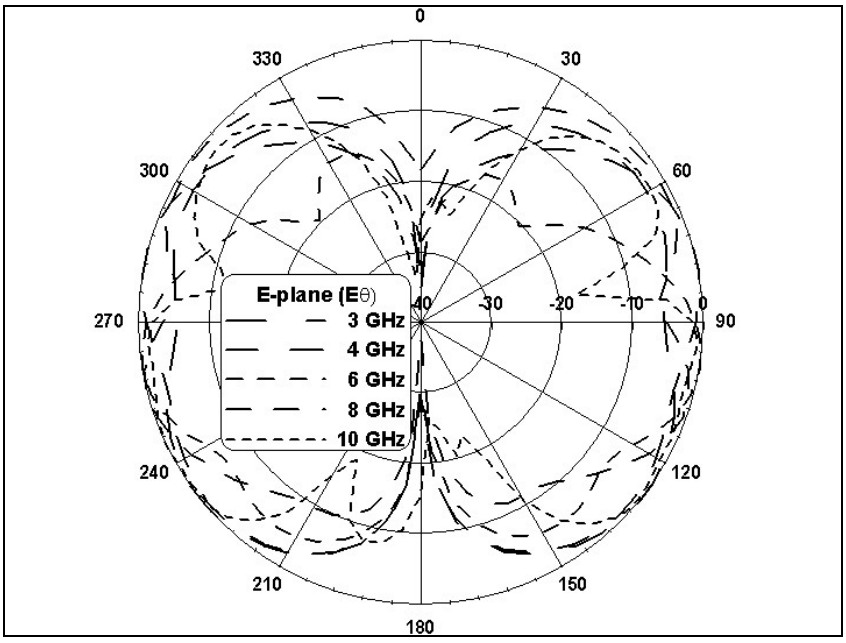

Fig. 4.4.10: Normalized co-polarized E-plane (x-z plane) radiation patterns $E_\theta(\theta,0)$ of the coplanar UWB antenna for various frequencies.

The proposed UWB antenna in CPW technology uses an FR4 substrate, which is one of the most common materials used for printed-circuit boards. Thus manufacturing complexities and costs are reduced. However, cheaper substrate material comes with varying permittivity parameters when the operating frequency changes. Therefore, a sensitivity test based on variations of relative dielectric constant is performed. From the manufacturer's specifications, the relative dielectric constant can vary from 4.0 to 4.7. Three different values (ε_r = 4.0, 4.4 or 4.7) are selected for the sensitivity test. Fig. 4.4.11 illustrates the related VSWR results.

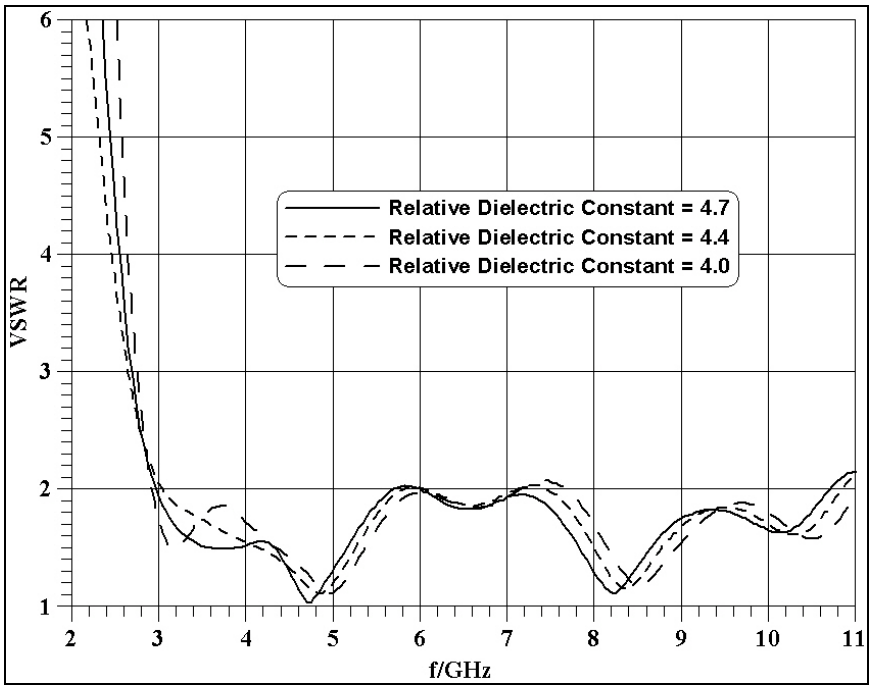

Fig. 4.4.11: Comparisons of VSWR performance for different relative dielectric constants.

Variations of VSWR with respect to different relative dielectric constants are limited. For the operating band from 3.1 GHz to 10.6 GHz, the VSWR values from the three different relative dielectric constants are mostly below two. The highest VSWR value of 2.1 occurs around 7.4 GHz for the relative dielectric constant of 4.0. Again, note that those results include effects of a coaxial (SMA) connector attached to the input of the coplanar waveguide. Therefore, compared to other UWB printed-circuit designs, those performances are still excellent.

4.4.3 MEFiSTo-3D Simulation Model

The Transmission-Line Matrix (TLM) method in the time domain is utilized to determine the group delay of this UWB antenna. In order to compare results obtained for the proposed coplanar UWB antenna with those of different antennas, the above time-domain method is also applied to the microstrip UWB antenna presented in [15]. The TLM time-domain field solver MEFiSTo-3D® is used for this task. Fig. 4.4.12 shows VSWR results of the proposed UWB antenna obtained from both simulation packages, HFSS and MEFiSTo-3D. Note that the connection of the input of the antenna to a coaxial cable is included in both simulation models. Good agreement is observed, thus verifying the antenna's performance at its input terminal. The only difference is in the higher

frequency range, 8.5 GHz to 10.6 GHz, where the VSWR values from MEFiSTo-3D are slightly higher than two. This is caused by the size limitation of the absorbing boundary in MEFiSTo-3D. A more detailed description will be presented later in this section.

Fig. 4.4.13 shows VSWR results of the UWB antenna in [15] from both simulation packages, HFSS and MEFiSTo-3D, and also from the measurements in [15]. The data from HFSS is in reasonable agreement with measurements. Note that the HFSS model includes the connection to a coaxial cable. In order to reduce the computational domain, i.e., shorten the long microstrip feed line shown in [15], the coaxial connector could not be modeled in MEFiSTo-3D. Therefore, and especially in the higher frequency range, the agreement between measurements and MEFiSTo-3D is not as good as that with HFSS. However, the basic shape and the reasonably small discrepancies validate numerical computations.

Fig. 4.4.14 shows the setup of the simulation model of the proposed UWB antenna in MEFiSTo-3D. Since the problem is symmetric with respect to a magnetic wall in the x-z plane (all other walls are absorbing boundaries), only half of the computational space is required.

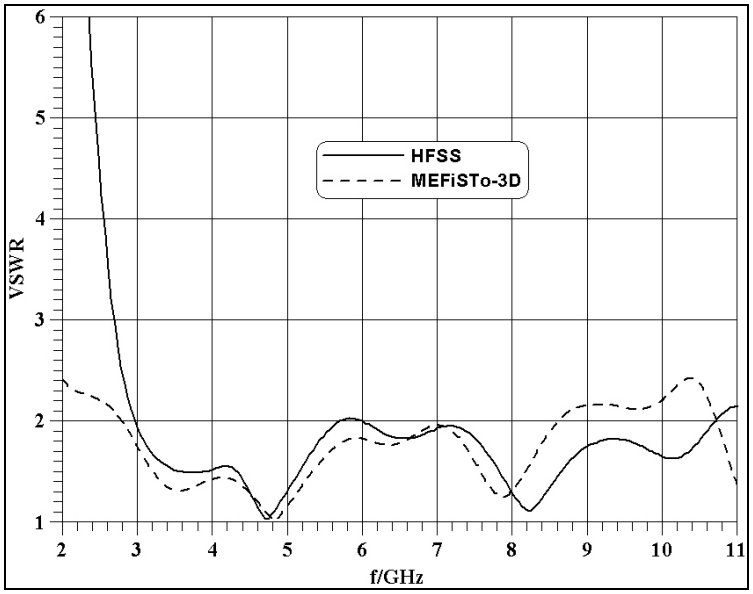

Fig. 4.4.12: Comparison of VSWR performance between HFSS and MEFiSTo-3D for the proposed coplanar UWB antenna.

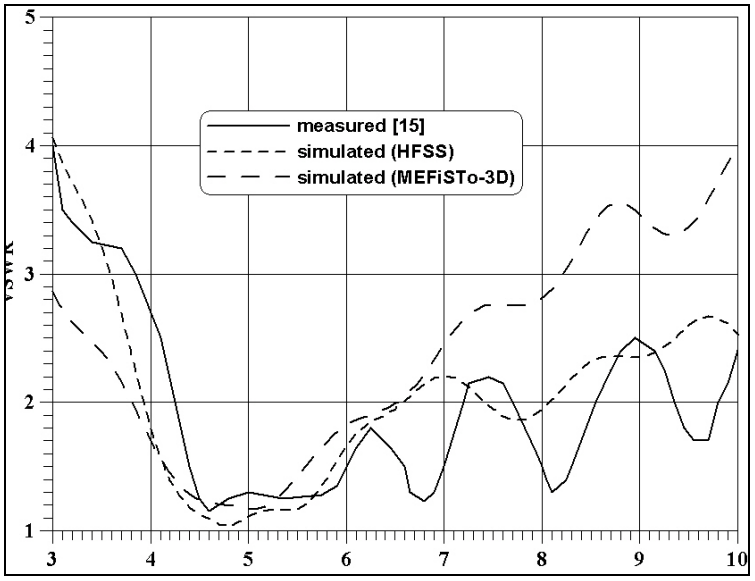

Fig. 4.4.13: Comparison of VSWR performance between measurements, HFSS and MEFiSTo-3D for the UWB antenna in [15].

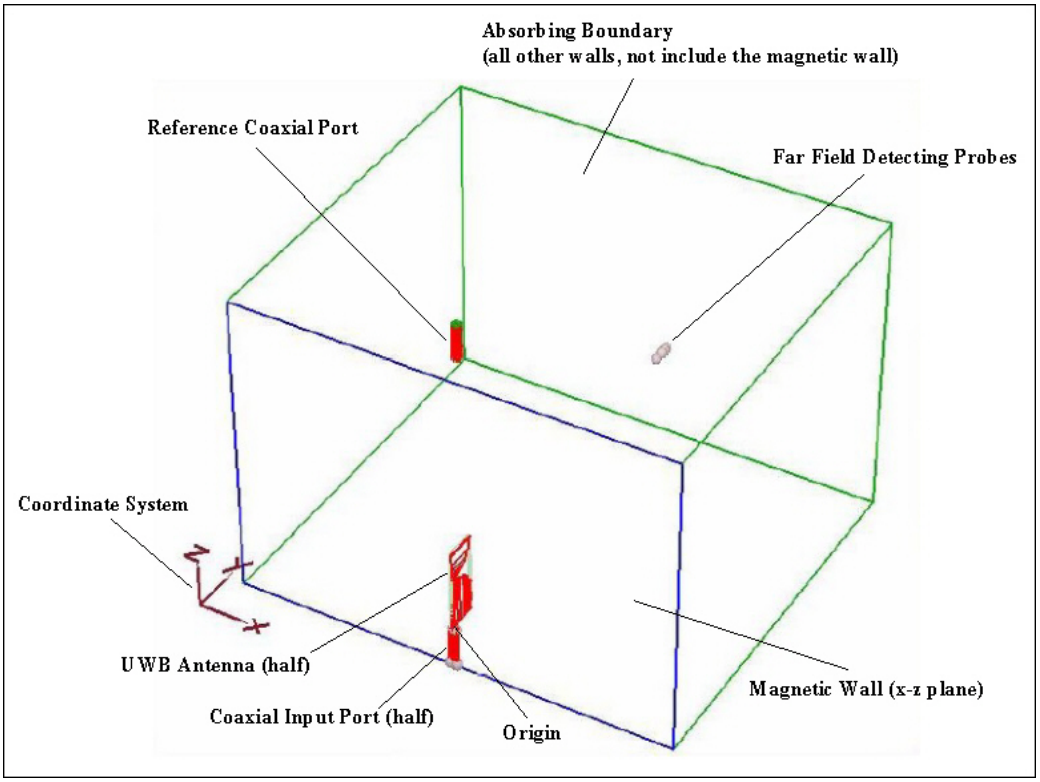

Fig. 4.4.14: Final design model of proposed UWB antenna in MEFiSTo-3D.

In order to observe proper radiating time domain signals, radiating signals need to be sampled at a distance in the far field. Equation (4.1) presents the minimum distance of the far field for conventional narrow band antennas. R is the minimum distance from the center of the radiating source to the far field region at a specific wavelength λ. D is the largest dimension of the antenna.

$$R = \frac{2D^2}{\lambda} \tag{4.1}$$

However, unlike conventional narrow band antennas, UWB antennas radiate a wide band of frequencies (wavelengths). Therefore, in order to satisfy the far field condition for the entire operating band, the longest distance according to equation (4.1) must be used.

For the proposed UWB antenna, the largest dimension is 50 mm (diagonal distance of a 30 x 40 mm^2 PCB). The frequency of 11 GHz is selected as the highest operating frequency and gives a wavelength of 27.3 mm. By using equation (4.1), the longest far field distance is about 183.2 mm. Under the environment of MEFiSTo-3D, an absorbing boundary is required to surround any radiating source, such as an antenna. However, the absorbing boundary model provided by MEFiSTo-3D is not perfect and thus, some small reflections will occur. In order to limit the amount of reflections from the absorbing boundary, the absorbing boundary needs to be in the far field region.

Even though the simulation model makes use of the magnetic wall to half the computational space, lack of computer memory (RAM – Random Access Memory) is still a big issue. Microsoft Window XP (32-bit) limits each of its application memory usage to about 2 gigabytes of RAM. MEFiSTo-3D is a 32-bit application software, which can use up to 4 gigabytes of RAM. In order to use the full potential of MEFiSTo-3D, Microsoft

Window XP (64-bit) is used as the operating system. During the setup of the simulation model under MEFiSTo-3D, the mesh cell size needs to be selected properly. For the proposed UWB antenna in CPW technology, the smallest dimension is 0.5 mm. Thus the selected mesh cell has the volume of 0.5 x 0.5 x 0.5 mm^3. Different mesh cell sizes will require different amounts of computational memory and time; a smaller mesh cell requires larger RAM and longer simulation time. Even with the amount of RAM available for the simulation (up to 4 gigabytes), memory is still not sufficient for the full far field simulation (including the magnetic wall). Only one direction (y-axis) of the absorbing boundary reaches the far field region, where detecting probes are placed. The origin of the coordinate system for the simulation model in Fig. 4.4.14 is positioned at the top of the coaxial input port, which is 20 mm long. The absorbing boundary has the following dimensions: Δx = 210 mm (from -105 to 105 mm), Δy = 185 mm (from 0 to 185 mm) and Δz = 150 mm (from -20 to 130 mm).

The input of the UWB antenna is excited with a pulse covering the entire frequency spectrum of the application (3.1 GHz to 10.6 GHz). At a point in the far field, probes detect the vertical polarization E_θ and the horizontal polarization E_ϕ. Several detecting probes are placed closed to the far field boundary (c.f. Fig. 4.4.14). They have the same x

and z position (x = 0 mm and z = 26 mm) and along the y direction from 176 mm to 185mm. Some are in positions slightly below the far field boundary and some are in the far field region. Note that a reference port is included and positioned outside the absorbing boundary (c.f. Fig. 4.4.14). The purpose of having an extra identical coaxial input port such as a reference port is to observe undistorted input signals and obtain proper VSWR performance of the proposed UWB antenna.

With only one direction of the computational boundary actually extending into the far field region, the VSWR performance of the UWB antenna modeled by MEFiSTo-3D shows slightly worse results in the higher frequency region. More reflections occur at higher frequencies due to the size limitation of the absorbing boundary. Higher frequencies require larger absorbing boundaries in order to reach far field conditions. Also, due to the mesh cell size, the coaxial input port and the reference port are modeled differently. The 50 Ohm coax cable has an inner core radius of 0.6 mm and an outer core radius of 2.094 mm. Due to the mesh cell size, it has to be remodeled to have inner and outer core radii of 0.5 mm and 2 mm, respectively. This changes the impedance of the original coax cable to 55 Ohms. With the mismatch at the input, the VSWR performance of the UWB antenna simulated by MEFiSTo-3D is expected to have some distortion. The

average simulation time is about 15 hours, and the average memory usage is about 3.7 gigabytes of RAM.

4.4.4 MEFiSTo-3D Simulation Results

One set of detecting probes is set up in the far field region (x =0 mm, y = 185 mm, z = 26 mm). Input and detected time domain signals are Fourier transformed to obtain amplitude and phase responses. The group delay is obtained from the derivative of the phase response (phase differences between input and detected signals) with respect to frequency. Fig. 4.4.15 shows the input time-domain signal together with its corresponding amplitude (in dB) and phase spectrum. Note that the duration of the pulse is about 0.4 ns and the phase variation is in the order of hundreds of degrees. The radiated signals E_θ (solid lines) and E_ϕ (dashed lines) as detected by far field probes in Fig. 4.4.14 and their amplitude and phase spectra are shown in Fig. 4.4.16. Figs. 4.4.16a and 4.4.16b confirm that the main polarization is vertical (E_θ) since the detected signal in horizontal polarization (E_ϕ) is at least 20 dB below its vertical component. Fig. 4.4.16c shows the phase variation now in thousands of degrees, which is a result of the ringing of the detected time signal in Fig. 4.4.16a.

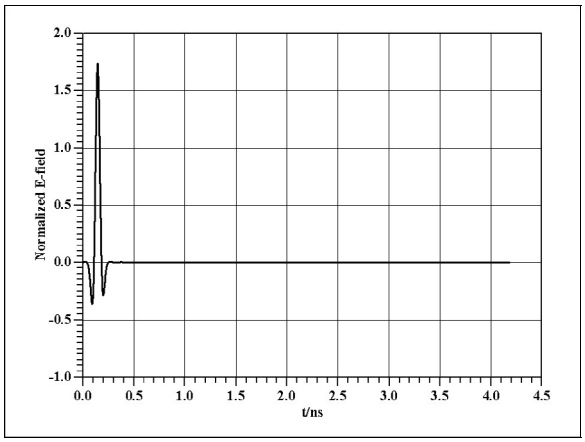

(a)

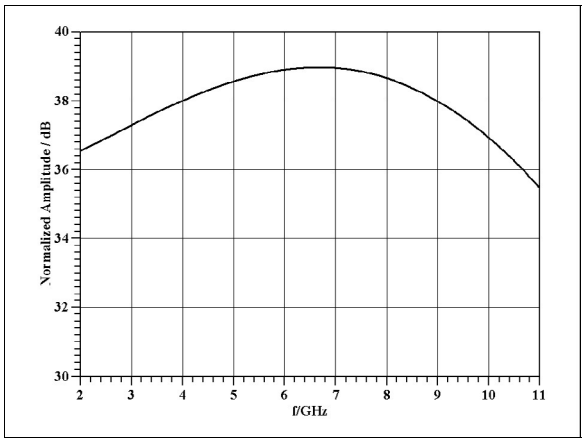

(b)

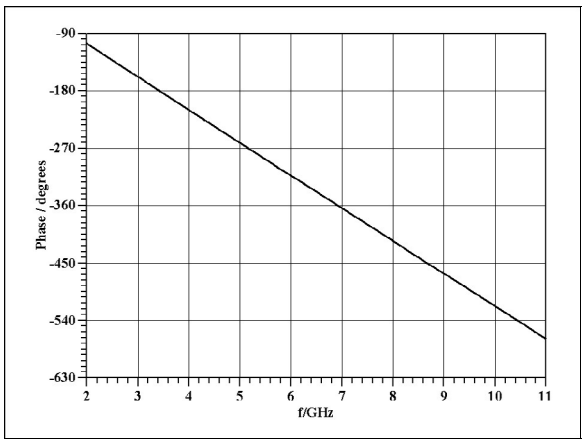

(c)

Fig. 4.4.15: Time-domain signal (a), amplitude spectrum (b) and phase spectrum (c) at the input of the coaxial cable feeding the coplanar antenna (c.f. Fig. 4.4.14)**.**

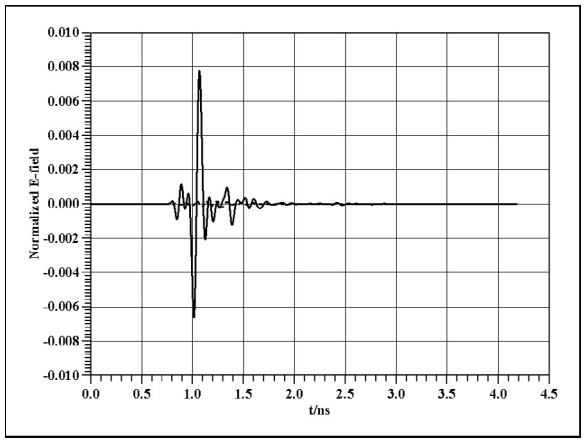

(a)

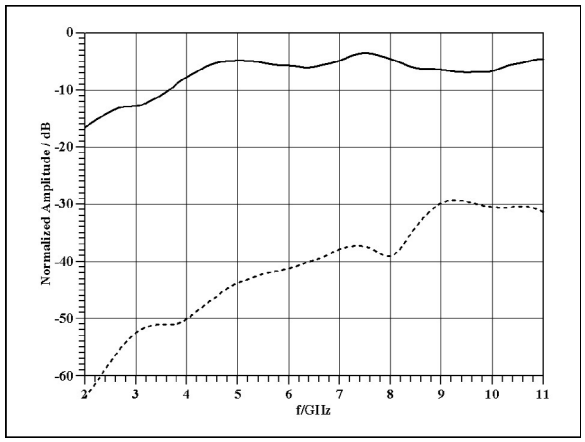

(b)

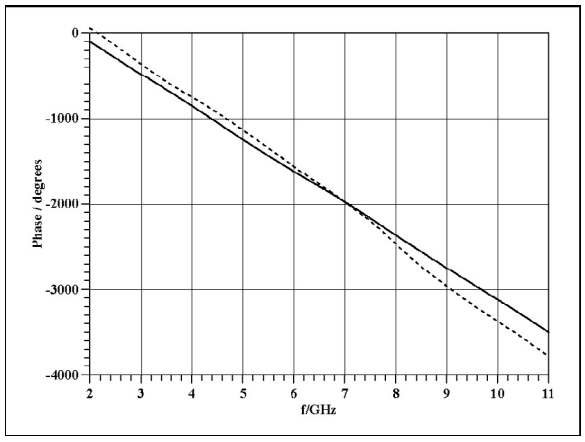

(c)

Fig. 4.4.16: Radiated time-domain signal (a), amplitude spectrum (b) and phase spectrum (c) detected by the probes; E_θ (solid lines) and E_ϕ (dashed lines).

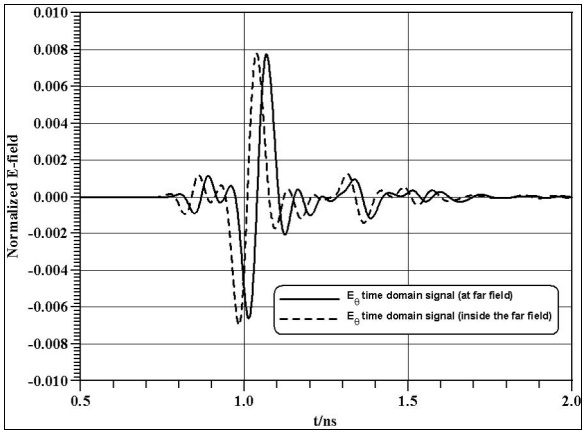

(a)

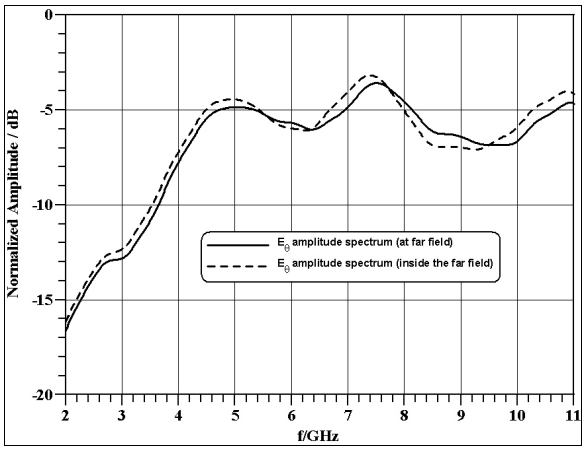

(b)

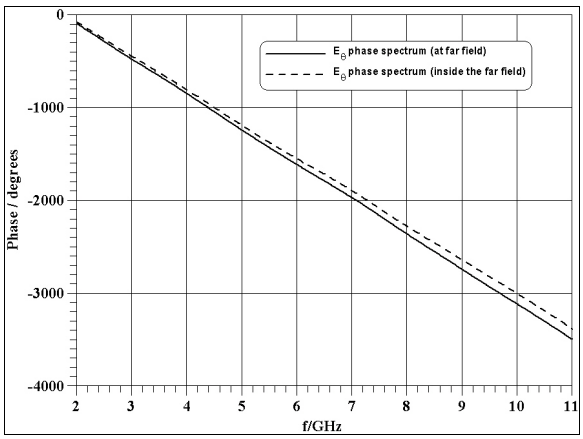

(c)

Fig. 4.4.17: Radiated E_θ time-domain signal (a), amplitude spectrum (b) and phase spectrum (c) detected by two sets of probes at the far field boundary (solid lines) and slightly within the far field boundary (dashed lines).

Moreover, notice that the main part of the received pulse in Fig. 4.4.16a looks similar to a negative derivative of the input pulse rather than the original input signal in Fig. 4.4.15a. Such behavior is common in antennas that radiate pulses covering a significant frequency spectrum, e.g. [41].

For the purpose of comparison, main polarization (E_θ) results obtained from two different sets of detecting probes are illustrated in Fig. 4.4.17. One set of detecting probes is at the far field boundary (x =0 mm, y = 185 mm, z = 26 mm), and the other set is slightly inside the far field boundary (x =0 mm, y = 176 mm, z = 26 mm). Note that the far field boundary is at y = 183.2 mm. As expected, the time domain signal inside the far field boundary leads that at the far field boundary. From Fig. 4.4.17a and Fig. 4.4.17b, only little variations between two sets of detecting probes in both amplitude and phase spectra are observed. Fig. 4.4.18a and Fig. 4.4.18b show the amplitude and group-delay responses, respectively, of the coplanar UWB antenna fed by a coaxial cable. The amplitude response in the main polarization (solid line) is between –40 to –50 dB which is due to the small effective area of the receiving probes. Since the variations in amplitude and phase (group delay) determine the distortion of the pulse transmitted by the antenna, the respective values – as read from the data plotted in Fig. 4.4.18 – are summarized

below for both vertical (VP) and horizontal (HP) polarizations.

Frequency range: 3.1 GHz – 10.6 GHz

Amplitude variation: < 8.7 db (VP); < 23 dB (HP)

Group-delay variation: < 163 ps (VP); < 620 ps (HP)

Note that the amplitude variation of 8.7 dB in vertical polarization (E_θ) is in very good agreement with the radiation patterns displayed in Fig. 4.4.9 for individual frequencies between 3 GHz and 10 GHz. Since Fig. 4.4.18 was obtained from data computed by the time-domain solver MEFiSTo-3D and Fig. 4.4.9 from that of the frequency-domain package HFSS, this agreement (together with Fig. 4.4.12) verifies the design and performance of the proposed coplanar UWB antenna. For comparison purposes, the microstrip UWB antenna in [15] is also simulated using MEFiSTo-3D to compute the group delay. After exciting the microstrip antenna with a pulse shown in Fig. 4.4.15, detecting the radiated signal and calculating amplitude and phase responses, the data presented in Fig. 4.4.19 is obtained. Between 3 GHz and 10 GHz, the amplitude variation in vertical polarization is similar to that of the coplanar UWB antenna in Fig. 4.4.18a.

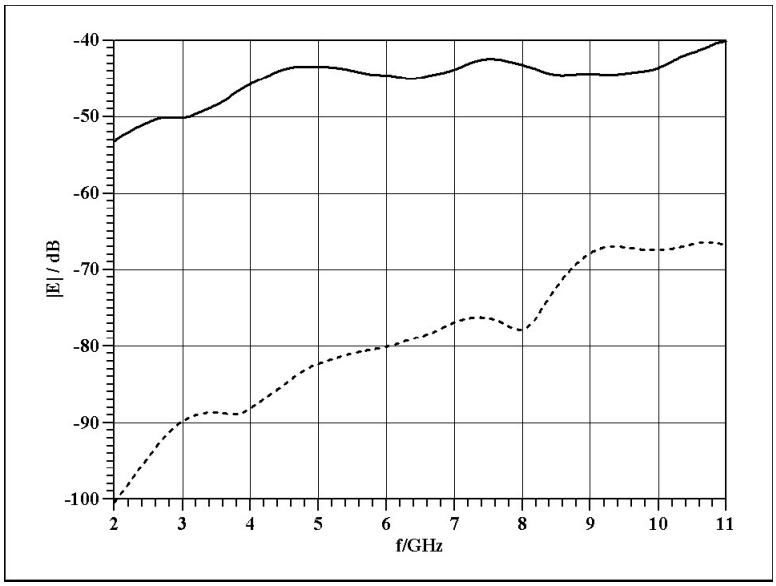

(a)

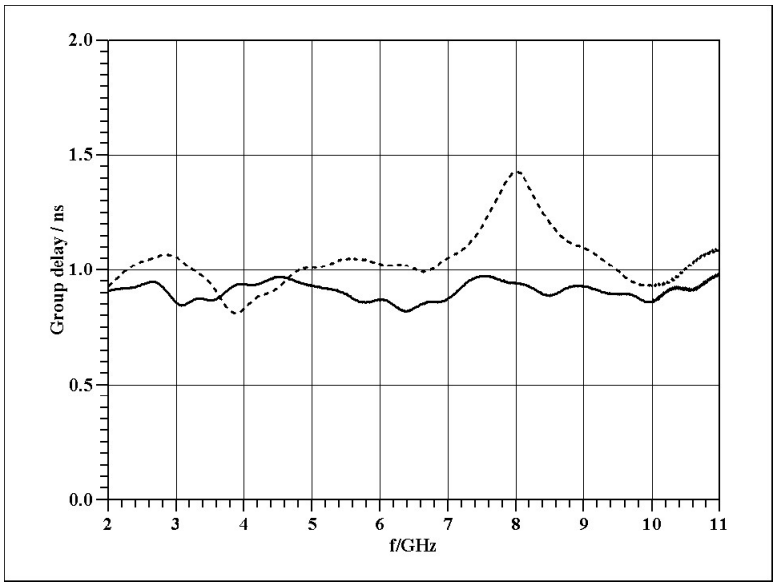

(b)

Fig. 4.4.18: Amplitude response (a) and group-delay characteristic (b) of coplanar UWB antenna; vertical polarization E_θ (solid lines,) and horizontal polarization E_ϕ (dashed lines).

The signal level difference between horizontal and vertical polarizations in Fig. 4.4.19a is smaller than that in Fig. 4.4.18a. This is due to the fact that the x-component of the

electric field represents the main polarization in a microstrip line if the antenna is oriented in the same way as the coplanar one in Fig. 4.4.14. The group delay performances of the microstrip antenna are inferior to those of the coplanar antenna in both polarizations. The following values are obtained:

Frequency range: 3.0 GHz – 10.0 GHz

Amplitude variation: < 8.8 db (VP); < 31 dB (HP)

Group-delay variation: < 239 ps (VP); < 1.9 ns (HP)

Both the coplanar and the microstrip antenna display nearly omni-directional radiation patterns with characteristics slightly distorting towards 10 GHz (c.f. [14] and [15] for details). Over the 3.1 – 10.6 GHz range, the VSWR performance of the coplanar antenna is superior to that of the microstrip antenna. The amplitude variations in vertical polarization are comparable; in horizontal polarization, however, it is 8 dB in favour of the coplanar antenna. The group-delay variations of the coplanar antenna are much smaller than those of the microstrip antenna and, therefore, the coplanar structure of Fig. 4.3.1 is better suited for UWB applications.

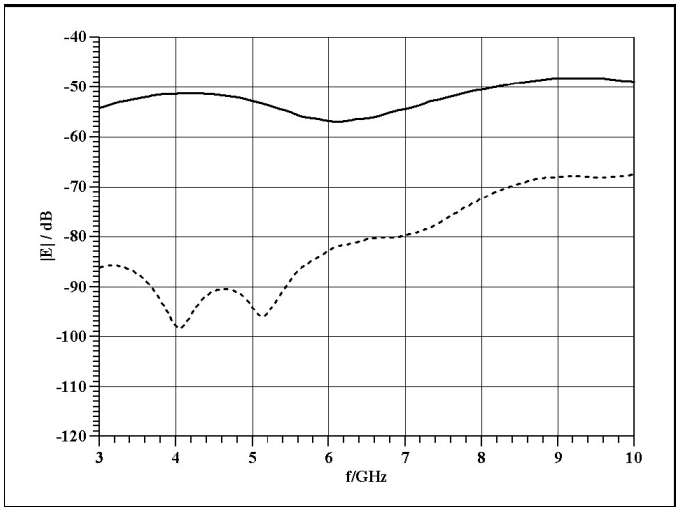

(a)

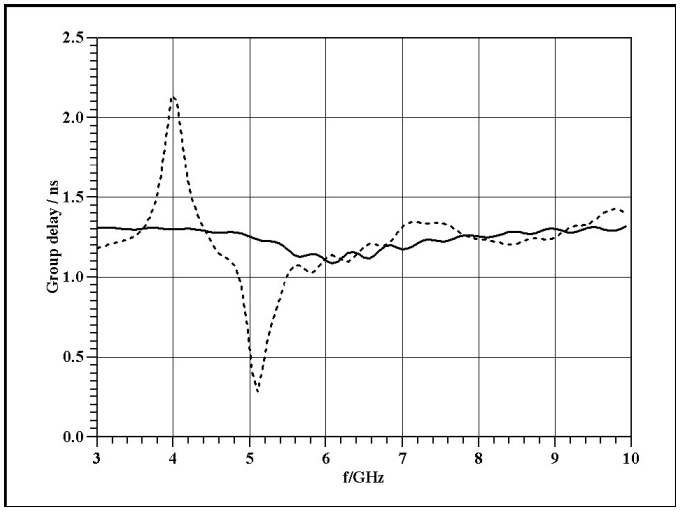

(b)

Fig. 4.4.19: Amplitude response (a) and group-delay characteristic (b) of the microstrip UWB antenna in [15]; vertical polarization E_θ (solid lines,) and horizontal polarization E_ϕ (dashed lines).

It is noted that a smaller group-delay variation (< 100 ps) is reported in [12] for a microstrip UWB antenna with two slots in the radiating patch. However, the gain of that antenna is lower than the one reported in Fig. 4.4.6 and even drops below 0 dB above 9.8 GHz [12].

4.5 The Improved Final Design

Further improvement can be made on the proposed final design of the UWB antenna in CPW technology. The coplanar waveguide at the input of the proposed UWB antenna has an input impedance about 75 Ohm. As mention in Section 4.3, even with the mismatch between the input of the antenna and the 50 Ohm coaxial line, good VSWR performance is still obtained. Recall that this relates to the assumed manufacturing sensitivity which dictates a minimum slot width of 0.5 mm. If higher manufacturing sensitivity is allowed, a 50 Ohm CPW feed can be designed to match the 50 Ohm coaxial cable. This section presents an improved UWB antenna design with a 50 Ohm CPW feed. Only a few changes are made to the originally proposed UWB antenna. Referring to Fig. 4.3.1, *W6* is reduced to 0.25 mm and *W7* is extended to 2.75 mm. For manufacturing simplicity, the thickness of the PCB is changed to 1.575 mm instead of 1 mm. The remaining dimensions are the same. This improved UWB antenna still uses an FR4 substrate PCB and 30mm x 40mm (W x L) substrate area. The permittivity parameters are $\varepsilon_r = 4.7$ and $\tan\delta = 0.018$.

Fig. 4.5.1 displays VSWR performances obtained from both HFSS and MEFiSTo-3D, and both simulation results agree well. The values of the improved design

are much better than those of the original proposed design (at least a drop of 0.4 in VSWR in the operating band). The results of the sensitivity test from different relative dielectric constants are illustrated in the Fig. 4.5.2. Again, only very little variation is observed. Fig. 4.5.3 shows the gain results of the improved UWB antenna. The variation is about 3 dBi, which is slightly better than the original design. Radiation patterns are illustrated from Fig. 4.5.4 to Fig. 4.5.7. Behaviors and characteristics are very similar to those of the original one, which is due to the fact that the shape and size of the radiating elements are the same and that only the feed and substrate thickness are altered.

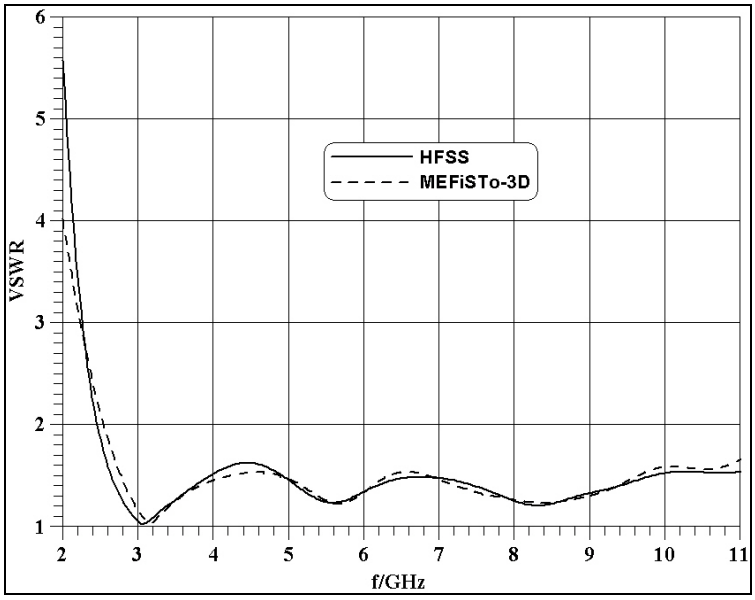

Fig. 4.5.1: Comparison of VSWR performances obtained with HFSS and MEFiSTo-3D for the improved coplanar UWB antenna.

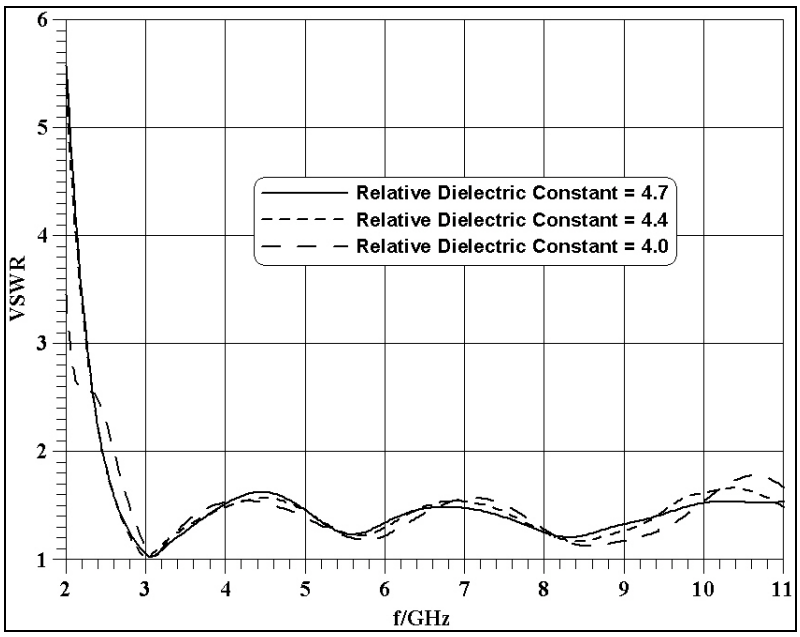

Fig. 4.5.2: Comparison of VSWR performances for different relative dielectric constants of the improved UWB antenna design.

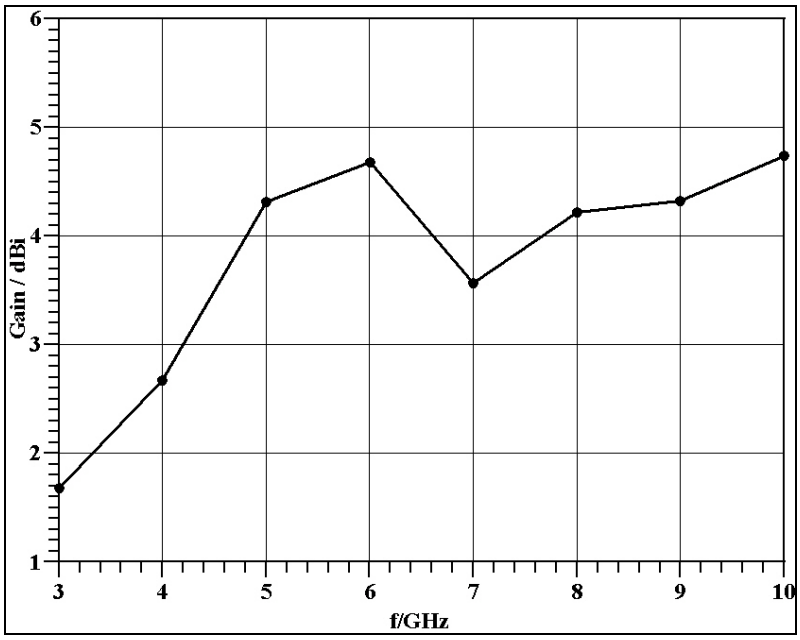

Fig. 4.5.3: Maximum gain of the improved UWB antenna in coplanar waveguide technology.

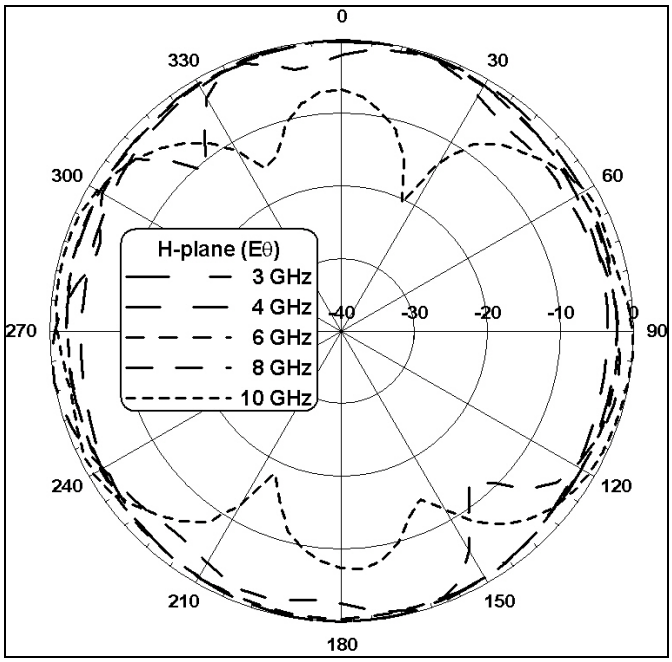

Fig. 4.5.4: Normalized co-polarized H-plane (x-y plane) radiation patterns $E_\theta(\pi/2, \phi)$ of the improved coplanar UWB antenna for various frequencies.

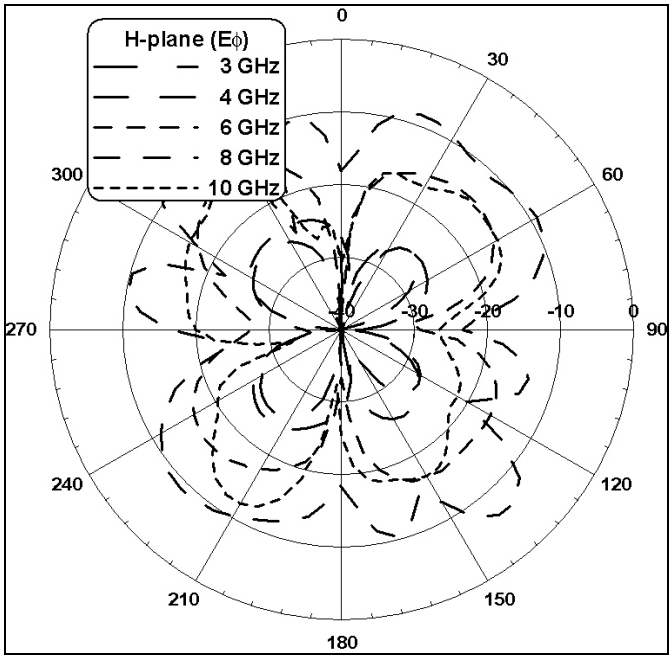

Fig. 4.5.5: Normalized cross-polarized H-plane (x-y plane) radiation patterns E_ϕ $(\pi/2, \phi)$ of the improved coplanar UWB antenna for various frequencies.

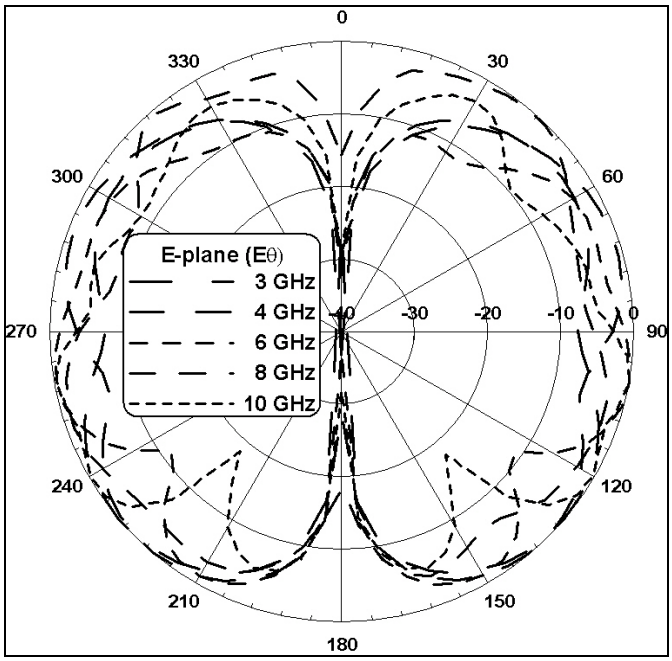

Fig. 4.5.6: Normalized co-polarized E-plane (y-z plane) radiation patterns $E_\theta(\theta,\pi/2)$) of the improved coplanar UWB antenna for various frequencies.

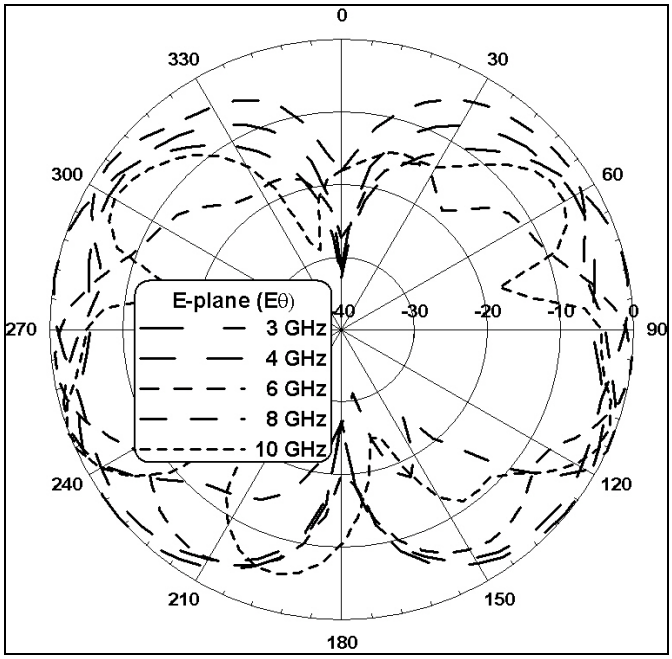

Fig. 4.5.7: Normalized co-polarized E-plane (x-z plane) radiation patterns $E_\theta(\theta,0)$ of the improved coplanar UWB antenna for various frequencies.

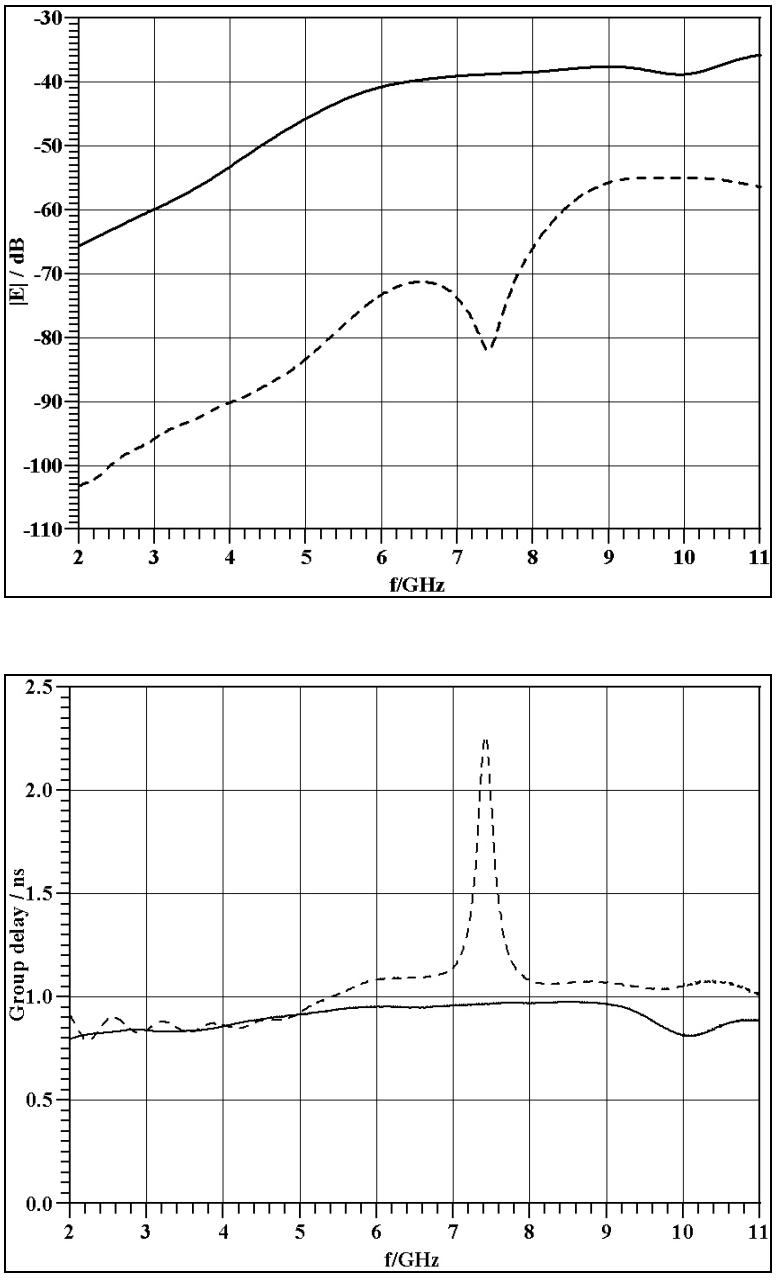

Fig. 4.5.8: Amplitude response (a) and group-delay characteristic (b) of the improved coplanar UWB antenna; vertical polarization E_θ (solid lines,) and horizontal polarization E_ϕ (dashed lines).

Fig. 4.5.8a and Fig. 4.5.8b show the amplitude and group-delay responses,

respectively, of the improved coplanar UWB antenna fed by a coaxial cable. In order to simulate the improved UWB antenna design in MEFiSTo-3D, 0.25 x 0.25 x 0.25 mm^3 mesh cells must be used. Due to the memory (RAM) limitation, a much smaller absorbing boundary is used. This affects both amplitude and group-delay responses. Therefore, worse results are obtained for both amplitude and group delay variations. However, the group-delay variation of the principal polarization is only 16 ps above that of the original design. Compared to Fig. 4.4.18, the results for vertical (VP) and horizontal (HP) polarizations are:

Frequency range: 3.1 GHz – 10.6 GHz

Amplitude variation: < 22.5 db (VP); < 40.1 dB (HP)

Group-delay variation: < 179 ps (VP); < 1.5 ns (HP)

5.0 Conclusions and Further Work

5.1 Conclusions

In the recent rapid research of ultra-wideband (UWB) technology, the UWB antenna is one of the most essential components. As for mobile applications, printed-circuit antennas are more suited than other types of UWB antennas. Therefore, different types of planar UWB antennas have been presented. In this thesis, two types of printed-circuit antennas in microstrip and coplanar technology are compared based on different design parameters. Designs in microstrip technology require processing on both substrate sides for fabrication. However, by applying coplanar technology, a number of advantages for the fabrication and better antenna performance can be offered.

As the result of the research, the proposed ultra-wideband printed-circuit antenna in coplanar waveguide technology presents a viable option for communication and measurements in the 3.1 - 10.6 GHz frequency range. Nearly omni-directional characteristic is obtained for vertical polarization while the horizontal polarization shows possible applications for direction finding (nulling). The antenna shows excellent VSWR characteristics, and the radiation patterns vary within acceptable margins over the entire

frequency range. Also, due to variations of the relative dielectric constant in the PCB, VSWR performances of antennas using different relative dielectric constants are compared and are found to show little variation. The antenna is designed using a commercially available electromagnetic field solver, HFSS, which is verified through measurements at similar ultra-wideband antennas.

Time-domain techniques, applied here in form of the TLM solver MEFiSTo-3D, present a viable option for the analysis and modeling of UWB printed-circuit antennas. Amplitude characteristics and VSWR performances extracted from the time-domain solution agree well with frequency-domain methods, which are used for the design of UWB antennas. The computation of group-delay data in an actual application of pulsed transmission is one of the clear advantages of time-domain over frequency-domain techniques. Even with the computer memory (RAM) limitations encountered, reasonable group delay results are obtainable. This is considered a simpler way of obtaining group delay characteristics for UWB antennas than the computation of a varying phase center. The time-domain modeling procedure presented here is applied to two different printed-circuit UWB antennas, and agreement with frequency domain computations and measurements is demonstrated. Comparing different design parameter results, the

proposed coplanar UWB antenna not only offers advantages in fabrication over the microstrip UWB antenna [14], but also has overall better antenna performances. This makes the proposed coplanar UWB antenna more suitable for UWB applications.

Finally, an improved design of the proposed coplanar UWB antenna is presented. By changing the input impedance of the CPW feed to 50 Ohm, which matches the 50 Ohm coaxial cable, better VSWR performance is obtained. Moreover, the maximum gain variation decreases. While the radiation patterns for various frequencies remain similar to those of the previous design. Group delay characteristics and amplitude variations slightly degrade. However, this appears to be mainly due to the much smaller absorbing boundary used in MEFiSTo-3D, which affects greatly the group delay and amplitude responses.

5.2 Further Work

The proposed coplanar UWB antenna presented in this thesis is not truly ideal for mobile applications like cellular phones. Ideal cellular phone antennas should be able to transmit and receive in dual polarizations. In order to be fully operational in any position or orientation of cellular phones, antennas should have omni-directional radiation patters in both polarizations. Therefore, the objective for future work is to develop an

omni-directional UWB antenna operating in dual polarization. This can be accomplished, for instance by using two coplanar UWB antennas presented in this thesis and combining them perpendicularly at their feeds. In this way, the new UWB antenna can produce omni-directional vertical polarization radiation patterns in the H-plane and omni-directional horizontal polarization radiation patterns in the E-plane.

Another goal is to reduce the size of the new UWB antenna, which will fit better on cellular phones considering the limitations of available space. UWB systems have to coexist with current narrowband applications. Rather than using additional filters to eliminate such frequencies from the UWB signal, an evolving trend is to investigate UWB trend antennas with notch characteristics in the respective frequency band. This might be accomplished by using resonating slots in the radiating patches in order to develop frequency-dependent mismatches within the feed lines. For future designs utilizing optimization, a sensitivity analysis of all parameters should be performed in order to identify those parameters which show the highest influence on the design. This will reduce design time frames and optimization complexity. Moreover, it will define manufacturing tolerances.

References

[1] R.T. Johnk, D.R. Novotny, C.M. Weil, M. Taylor and T.J. O'Hara, "Efficient and accurate testing of an EMC compliance chamber using an ultrawideband measurement system," 2001 IEEE EMC-S Int. EMC Symp. Dig., Vol. 1, pp. 302-307, Aug. 2001.

[2] K.W. Jin, T.J. Huat, T.Y.K. Roland, K.C.H. Ernest, "Time-domain measurements of transient field coupling through slots," Proc. 17th Int. Zurich Symp. EMC, pp. 642-645, Feb./Mar. 2006.

[3] R.F. Martin, "Ultra-wideband (UWB) rules and design compliance issues," 2003 IEEE EMC-S Int. EMC Symp. Dig., Vol. 1, pp. 92-96, Aug. 2003.

[4] J.D. Brunett, R.M. Ringler and V.V. Liepa, "On measurements for EIRP compliance of UWB devices," 2005 IEEE EMC-S Int. EMC Symp. Dig., Vol. 2. pp. 473-476, Aug. 2005.

[5] K. Chung, S. Pyun and J. Choi, "Design of an ultrawide-band TEM horn antenna with a microstrip-type balun," IEEE Trans. Antennas Propogat, Vol. 53, pp. 3410-3413, Oct. 2005.

[6] L. Yang and G.B. Giannakis, "Ultra-wideband communications: an idea whose time has come," IEEE Signal Proc. Mag., Vol. 21, pp.26-54, Nov. 2004.

[7] International Telecommunication Union, Radiocommunication Study Groups, "Framework for the introduction of devices using ultra-wideband technology," Document 1/85(Rev.1)-E, 09 Nov. 2005.

[8] K. Kiminami, A. Hirata and T. Shiozawa, "Double-sided printed bow-tie antenna for UWB communications," IEEE Antennas Wireless Propagat. Lett., Vol. 3, pp. 152-153, 2004.

[9] J. Liang, C.C. Chiau, X. Chen and C.G. Parini, "Printed circular disc monopole antenna for ultra-wideband applications," IEE Electronics Lett., Vol. 40, No. 20, pp.

1246- 1247, Sep. 2004.

[10] S.H. Choi, J.K. Park, S.K. Kim and J.Y. Park, "A new ultra-wideband antenna for UWB applications," Microwave Opt. Technol. Lett., Vol. 40, No. 5, pp. 399-401, Mar. 2004.

[11] J. Liang, C.C. Chiau, X. Chen and C.G. Parini, "Study of a printed circular disc monopole antenna for UWB systems," IEEE Trans Antennas Propagat., Vol. 53, pp. 3500-3504, Nov. 2005.

[12] Z.N. Low, J.H. Cheong and C.L. Law, "Low-cost PCB antenna for UWB applications," IEEE Antennas Wireless Propagat. Lett., Vol. 4, pp. 237-239, 2005.

[13] J. Liang, C.C. Chiau, X. Chen, and C.G. Parini, "Printed circular ring monopole antennas," Microwave Opt. Technol. Lett., Vol. 45, No. 5, pp. 372-375, June 2005.

[14] C.-C. Lin, Y.-C. Kan, L.-C. Kuo and H.-R. Chuang, "A planar triangular monopole antenna for UWB communication," IEEE Microwave Wireless Comp. Lett., Vol. 15, pp. 624-626, Oct 2005.

[15] H.R. Chuang, C.C. Lin and Y.C. Kan, "A printed UWB triangular monopole antenna," Microwave J., Vol. 49, pp. 108-120, Jan. 2006.

[16] K. Rambabu, M.Z. Alam and J. Bornemann, "Design of compact dual-polarized printed-circuit antenna for ultra-wideband applications," Proc. 36th European Microwave Conf., pp. 626-629, Manchester, UK, Sep. 2006.

[17] D.-C. Chang, J.-C. Liu, and M.-Y. Liu, "A novel tulip-shaped monopole antenna for UWB applications," Microwave Opt. Technol. Lett., Vol. 48, No. 2, pp. 307-312, Feb. 2006.

[18] C.-F. Tseng and C.-L. Huang, "Ultrawideband planar microstrip-fed monopole antenna," Microwave Opt. Technol. Lett., Vol. 49, No. 1, pp. 183-185, Jan. 2007.

[19] A. M. Abbosh, M.E. Bialkowski, M.V. Jacob and J. Mazierska, "Investigations into an LTCC based ultra wideband antenna," Proc. Asia-Pacific Microwave Conf., 4p.,

Suzhou, China, Dec. 2005.

[20] C.T.H. Lim, "A GCPW-fed printed antenna for UWB applications," Proc. Asia-Pacific Microwave Conf., 3p., Suzhou, China, Dec. 2005.

[21] X. Chen, J. Liang, P. Li, L. Guo, C.C. Chiau and C.G. Parini, "Planar UWB monopole antennas," Proc. Asia-Pacific Microwave Conf., 4p., Suzhou, China, Dec. 2005.

[22] H.K. Lee, J.K. Park and J.N. Lee, "Design of a planar half-circle shaped UWB notch antenna," Microwave Opt. Technol. Lett., Vol 47, No. 1, pp. 9-11, Oct. 2005.

[23] T.-G. Ma and C.-H. Tseng, "An ultrawideband coplanar waveguide-fed tapered ring slot antenna," IEEE Trans. Antennas Propagat., Vol. 54, pp. 1105-1110, Apr. 2006.

[24] Y.-C. Lee, S.-C. Lin and J.-S. Sun, "CPW-fed UWB slot antenna," Proc. Asia-Pacific Microwave Conf., 4p., Yokohama, Japan, Dec. 2006.

[25] S. Nikolaou, D.E. Anagnostou, G.E. Ponchak, M.M. Tentzeris and J. Papapolymerou, "Compact Ultra Wide-Band (UWB) CPW-fed elliptical monopole on Liquid Crystal Polymer (LCP)," IEEE AP-S Int. Symp. Dig., pp. 4657-4660, Albuquerque, USA, July 2006.

[26] E.S. Angelopoulos, A.Z. Anastopoulos and D.I. Kaklamani, "Ultra-wideband bow-tie slot antenna fed by a cpw-to-cpw transition loaded with inductively coupled slots," Microwave Opt. Technol. Lett., Vol. 48, No. 9, pp. 1816-1820, Sep. 2006.

[27] X.-L. Liang, S.-S. Zhong and W. Wang, "UWB printed circular monopole antenna," Microwave Opt. Technol. Lett., Vol. 48, No. 8, pp. 1532-1534, Aug. 2006.

[28] J.-S. Sun, Y.-C. Lee and S.-C. Lin, "New design of a CPW-fed ultrawideband slot antenna," Microwave Opt. Technol. Lett., Vol. 49, No. 3, pp. 561-564, Mar. 2007.

[29] D.-B. Lin, I.-T. Tang and M.-Y. Tsou, "A compact UWB antenna with CPW-feed," Microwave Opt. Technol. Lett., Vol. 49, No. 3, pp. 564-567, Mar. 2007.

[30] R. Chair, A.A. Kishk and K.F. Lee, "Ultrawide-band coplanar waveguide-fed rectangular slot antenna," IEEE Antennas Wireless Propagat. Lett., Vol. 3, pp. 227-229, No. 1, 2004.

[31] N. Fortino, G. Kossiavas, J.Y. Dauvignac and R. Staraj, "Novel antennas for ultrawideband communications," Microwave Opt. Technol. Lett., Vol 41, No. 3, pp. 166-169 , May 2004.

[32] W. Wang, S.S. Zhong and S.-B. Chen, "A novel wideband coplanar-fed monopole antenna," Microwave Opt. Technol. Lett., Vol 43, No. 1, pp. 50-52 , Oct. 2004.

[33] J.I. Kim and Y. Jee, "Design of ultrawideband coplanar waveguide-fed LI-shape planar monopole antennas," IEEE Antennas Wireless Propagat. Lett., Vol. 6, pp. 383-387, 2007.

[34] C.T.H. Lim, "A GCPW-fed printed antenna for UWB applications," Proc. Asia-Pacific Microwave Conf., 3p., Suzhou, China, Dec. 2005.

[35] Z.N. Chen and X. Qing, "Research and development of planar UWB antennas," Proc. Asia-Pacific Microwave Conf., 4p., Suzhou, China, Dec. 2005.

[36] B.L. Ooi, G. Zhao, M.S. Leong, K.M. Chua and C.W.L. Albert, "Wideband LTCC CPW-fed two-layered monopole antenna," IEE Electronics Lett., Vol. 41, No. 16, pp. 9-10, Aug. 2005.

[37] K. Rambabu, H.A. Thiart, J. Bornemann and S.Y. Yu, "Ultrawideband printed-circuit antenna," IEEE Trans. Antennas Propagat., Vol. 54, pp. 3908-3911, Dec. 2006.

[38] Z. Ying and J. Andersson, "An ultra wideband 'cobra' patch antenna," IEE Proc.-Microw. Antennas Propag., Vol. 151, pp. 486-490, Dec. 2004.

[39] Multispectral Solutions, Inc., "Ultra Wideband (UWB) Frequently Asked Questions (FAQ)," July 2003, http://www.multispectral.com/UWBFAQ.html (last visited 13 Dec. 2004).

[40] B. Pattan, “A brief Exposure to ultra-wideband signaling,” Microwave J., Vol. 46, No. 12, pp. 104-108, Dec. 2003.

[41] D. Ghosh, A. De, M.C. Taylor, T.K. Sarkar, M.C. Wicks and E.L. Mokole, “Transmission and reception by ultra-wideband (UWB) antennas”, IEEE Trans. Antennas Propagat. Mag., Vol. 48, pp. 67-99, Oct. 2006.

[42] I. Oppermann, M. Hämäläinen and J. Iinatti, *UWB Theory and Applications*. Chistester, UK: John Wiley & Sons Ltd, 2004.

[43] R.J. Fontana, “Recent Applications of Ultra Wideband Radar and Communications Systems,” http://www.multispectral.com/UWBFAQ.html (last visited 13 Dec. 2004).

[44] G.F. Ross, “The transient analysis of certain TEM mode four-port networks,” IEEE Trans. Microwave Theory Tech., Vol. MTT-14, pp. 528-542, Nov. 1966.

[45] G.F. Ross, “A time domain criterion for the design of wideband radiating elements,” IEEE Trans. Antennas Propagat., Vol. 16, pp. 355-356, May 1968.

[46] C.L. Bennett and G.F. Ross, “Time-domain electromagnetics and its applications,” Proc. IEEE, Vol. 66, No. 3, pp. 299-318, Mar. 1978.

[47] H.G. Schantz, “A brief History of UWB Antennas,” IEEE Aerospace and Electronic Systems Mag., Vol. 19, pp. 22-26, Apr. 2004.

[48] L. Paulsen, J.B. West, W.F. Perger and J. Kraus, “Recent Investigations on the Volcano Smoke Antenna,” IEEE AP-S Int. Symp. Dig., Vol. 3, pp. 845-848, June 2003.

[49] H.G. Schantz, “Introduction to Ultra Wideband Antennas,” IEEE Ultra Wideband Systems and Technologies Conf., pp. 1-9, Nov. 2003.

[50] H.G. Schantz, “Dispersion and UWB Antennas,” Proc. Conf. Ultrawideband Systems and Technologies, pp. 161-165, May 2004.